The Dissertation Committee for Kevin Anthony Stevens Certifies that this is the approved version of the following dissertation:

The Effect of Temperature on the Transport Properties of High Performance Polymers

Committee:

Benny D. Freeman, Supervisor

Donald R. Paul

Christopher J. Ellison

Isaac C. Sanchez

Judy S. Riffle

The Effect of Temperature on the Transport Properties of High Performance Polymers

by

Kevin Anthony Stevens, B.S.

Dissertation

Presented to the Faculty of the Graduate School of

The University of Texas at Austin

in Partial Fulfillment

of the Requirements

for the Degree of

Doctor of Philosophy

The University of Texas at Austin

December 2016

Dedication

To my friends, family, and loved ones: I couldn't have done it without you.

Acknowledgements

I would like to thank my advisor, Professor Benny Freeman. He gave me guidance and direction for my academic studies. His example of the pursuit of knowledge and the importance of attention to detail has given me inspiration and will influence my approach to experimentation for many years to come. I also want to thank my thesis committee: Professor Don Paul, Professor Christopher Ellison, Professor Isaac Sanchez, and Professor Judy Riffle. Thank you for your time and comments on my thesis.

Many of the previous students in the Freeman group also gave me guidance, and they never hesitated to provide advice and suggest plans of action. Dr. Dan Miller, Dr. Kevin Tung, Dr. Hee Jeung Oh, Dr. Sirirat Kasemset, Albert Lee, Dr. Grant Offord, Dr. Katrina Czenkusch, Dr. Joe Cook, Dr. Tom Murphy, Dr. Geoff Geise, and Dr. Tom Murphy: thank you for helping me out.

Several postdocs also graciously spent their time helping me with both serious discussion and learning as well as some of my at times ludicrous questions. Dr. Claudio Ribeiro, thank you for helping teach me when I first got started. Dr. Kris Gleason, your incredible contribution of both technical knowledge (both depth and breadth) has inspired me tremendously, and your automation of permeation (and sorption) equipment has saved me countless hours of sleep. Dr. Michele Galizia, your discussions were invaluable, and I will miss having them.

I already miss working with the group and the members who I saw every day, many of whom I trained in lab safety. (Seriously, everyone, safety is important. Always stay safe!) Ni Yan, Jovan Kamcev, Eui Soung Jang, Lu Wang, Amanda Paine, Jaesung Park, Michelle Dose, Melanie Merrick, Alon Kirschner, Yu-Heng Cheng, and Christina

Rodriguez, my life is richer having met you. Keep in mind that graduate school isn't a thing you have to do to get a Ph.D. It is a journey and will be a cherished part of your life.

Several of my longstanding colleagues also helped guide me over many years need special mention. Dr. David Sanders and Dr. Zach Smith: the two of you got me on my feet after I landed in Dr. Freeman's group. You taught me how to do experiments, how to think, and what it means to do research. Thank you for everything. Dr. Qiang Liu: we joined the group at the same time, worked in similar areas, and enjoyed many experiences. You have no idea how much you helped, even when it was simply listening to me ramble. Dr. Lisa He: thank you for being there (even though you bailed out of my office), thank you for helping with sanity checks, and thank you for continuing to help me even after you've moved off after graduate school. Josh Moon: thank you for sharing an office with me, being a sounding board, and keeping my wild ideas in check. You helped keep me on track for graduating. I enjoyed working with you, and I wish you the very best.

To everyone I worked with: don't be strangers! Keep in touch.

To my family and loved ones: you supported me through the hardest thing that I've done in my life. Thank you for understanding when I said I couldn't come home for the weekend and for when I had to drive home early. Even then, I wish I had come home more, especially in the first months of graduate school.

Thank you, everyone, from the bottom of my heart. I wouldn't be here today were it not for each of you.

The Effect of Temperature on the Transport Properties of High Performance Polymers

Kevin Anthony Stevens, Ph.D.

The University of Texas at Austin, 2016

Supervisor: Benny D. Freeman

The transport properties of high-performance polymers are typically studied near ambient conditions. However, many separations are performed at temperatures either above or below ambient conditions. The permeability and solubility of light gases in thermally rearranged (TR) polymers were measured as a function of temperature. Solubilities decreased with increasing temperature for all samples. At low TR conversion, the sorption process initially becomes less exothermic. However, enthalpies of sorption do not significantly change with TR conversion after thermal rearrangement. Permeabilities increase with increasing temperature for all but CO_2 at the highest TR conversion. As extent of thermal rearrangement increases, activation energies increase slightly before decreasing significantly at higher TR conversions. Activation energies of diffusion decreased with increasing TR conversion while enthalpies of sorption remained mostly constant. At the highest TR conversion, decreases in temperature move the polymer toward the upper right on the upper bound.

Polybenzimidazoles have been the focus of increasing amounts of study due to their good H_2/CO_2 separation properties and high thermal stability. Gas transport properties of a novel series of polybenzimidazoles based on a new tetraaminodiphenylsulfone (TADPS) monomer have been characterized at temperatures

from 35 to 190 °C. Permeability increases with increasing temperature for all gases. Separations with TADPS-based PBIs are strongly size selective, with CO_2/N_2, CO_2/CH_4, and N_2/CH_4 selectivities decreasing with increasing temperature. However, H_2/CO_2 selectivities increase with increasing temperature due to a lower activation energy of permeation for CO_2 than for H_2.

Table of Contents

List of Tables

List of Figures

Chapter 1: Introduction

1.1 GOALS OF THE DISSERTATION

Amine absorption is the dominant technology for separation of CO_2 from natural gas and other process streams [1]. However, conventional absorption becomes less advantageous for large process streams, such as flue gas from a coal-fired power plant [2]. Polymer membranes can also be used to remove CO_2 from natural gas and flue gas [1-3]. However, for economic and process reasons, it is not always convenient to operate a polymer-based separation near ambient conditions.

Transport properties of polymers are typically reported near ambient temperature (e.g., 25 to 35 °C). However, many membrane separations are performed at either higher or lower temperatures [1, 3-6]. For example, in natural gas separations, the expansion of CO_2 permeating through a membrane results in Joule-Thomson cooling [1]. Additionally, pre-combustion carbon capture systems in integrated gasification combined cycle (IGCC) power plants could, in principle, utilize hydrogen-selective membranes at temperatures of 150 °C or even higher near the exit at a water gas shift reactor [3]. Many transport property studies include only permeability measurements near ambient conditions, thereby limiting the availability of data necessary to understand, at a fundamental level, membrane performance at temperatures far from ambient conditions. Studies of gas transport beyond ambient conditions are beneficial in both screening new materials as well as validating and expanding fundamental understanding of temperature dependence of transport properties in high-performing polymers. This dissertation focuses on studying two families of polymers at different temperatures: TR polymers and polybenzimidazoles.

Thermally rearranged (TR) polymers, first reported by Park et al. in 2007, attracted interest for their potential in natural gas purification [7]. These TR polymers are

usually polybenzoxazoles (PBOs) derived from glassy, high free volume polyimide (PI) precursors and can have good selectivity and high permeability [7]. These polymers can exhibit good transport properties and resistance to plasticization [7]. Moreover, they are insoluble in organic solvents, which indicates a possibly crosslinked structure.

Polybenzimidazoles (PBIs) are a class of highly thermally stable aromatic polymers [8]. PBIs have been of interest due to their attractive H_2/CO_2 separation capabilities at high temperatures [5, 9-15]. The high thermal and chemical stability of PBIs [8] makes them attractive for H_2/CO_2 separations at high temperatures. For example, energy savings can be realized by performing carbon capture operations at the exit of a water-gas shift reactor, which would benefit from membrane operation at high temperature (e.g., 150 °C or more) [3]. Few membranes can withstand such aggressive environments.

The goals of this dissertation were to:

1. Determine the temperature dependence of gas permeation in TR polymers
2. Decouple the contributions of diffusion and sorption to gas permeation in TR polymers
3. Investigate the temperature-dependent properties of polybenzimidazoles at high temperatures

1.2 OUTLINE OF THE DISSERTATION

Chapter 2 covers theory and background to provide the framework and context of this dissertation. The temperature dependence of transport properties are discussed, and an overview of some prior studies on the temperature dependence of gas sorption and permeation through polymer membranes are covered. A summary of some previous work on TR polymers and PBIs is provided. The upper bound and its temperature dependence

are introduced, and the framework through which the dual mode model is used at multiple temperatures is discussed. Chapter 3 covers materials and experimental procedures used in these studies.

The body of work covered in this dissertation covers two classes of high performing polymers. The first group, TR polymers, is covered in Chapters 4 and 5. Chapter 4 discusses the temperature dependence of gas solubility in TR polymers. The solubilities of N_2, CH_4, and CO_2 were measured in HAB-6FDA polyimide and its TR polymer analogs. Solubility increased as TR conversion increased and decreased as temperature increased. Upon initial thermal rearrangement, enthalpies of sorption became less exothermic. At higher levels of conversion, TR conversion had little effect on enthalpies of sorption. Solubility selectivity decreased with increasing TR conversion and only changed minimally with temperature due to some pairs of gases having similar enthalpies of sorption at 10 atm.

Chapter 5 discusses the temperature dependence of diffusion and permeation in HAB-6FDA and its TR polymer analogs. Gas permeabilities of H_2, N_2, CH_4, and CO_2 were measured from -10 to 50 °C and pressures up to 32 atm. Permeabilities generally increased as temperature increased, but CO_2 permeability in the most highly converted TR polymer decreased as temperature increased. Significant plasticization was observed at low temperatures in the polyimide whereas no detectable plasticization was observed in the more highly converted TR polymers. Activation energies of permeation for all gases except CO_2 increased slightly upon initial thermal rearrangement. As TR conversion increases beyond the initial amount, activation energies of permeation decreased for all gases. In the case of CO_2, the activation energy of permeation decreased below zero. The temperature-dependence of gas permeation on the upper bound shifts from moving toward the upper left as temperature decreases to moving toward the upper

right as temperature decreases. Gas diffusivities, calculated from measured gas permeabilities and gas solubilities were also examined as a function of temperature. As TR conversion increases, initially increase slightly and then decrease significantly. The order of activation energies of diffusion also differed from the expected monotonic trend with gas size.

The transport characteristics of a new family of polybenzimidazoles based on tetraaminodiphenylsulfone (TADPS) are covered in Chapter 6. The temperature dependence of He, H_2, N_2, CH_4, and CO_2 in a series of TADPS-based PBIs (TADPS-TPA, TADPS-TPA, and TADPS-OBA) as well as *m*-PBI were studied. Permeabilities for all gases increased with increasing temperature. Activation energies of permeation increased as gas size increased with the exception of CO_2, which had the lowest activation energy of permeation for TADPS-based PBIs. CO_2/N_2, CO_2/CH_4, and N_2/CH_4 selectivities decreased as temperature increased, but H_2/CO_2 selectivities increased with increasing temperature due to a lower activation energy of permeation for CO_2 than for H_2. All TADPS-based PBIs moved towards the upper right on the H_2/CO_2 upper bound as temperature increased. Estimated diffusivities in TADPS-TPA increased significantly with temperature due to high activation energies of diffusion, consistent with the strongly size-sieving behavior of polybenzimidazoles.

Chapter 7 presents conclusions and recommendations.

1.3 REFERENCES

[1] R.W. Baker, K. Lokhandwala, Natural gas processing with membranes: an overview, Industrial & Engineering Chemistry Research, 47 (2008) 2109-2121.

[2] T.C. Merkel, H. Lin, X. Wei, R. Baker, Power plant post-combustion carbon dioxide capture: An opportunity for membranes, Journal of Membrane Science, 359 (2010) 126-139.

[3] T.C. Merkel, M. Zhou, R.W. Baker, Carbon dioxide capture with membranes at an IGCC power plant, Journal of Membrane Science, 389 (2012) 441-450.

[4] K. Ghosal, B.D. Freeman, Gas separation using polymer membranes: an overview, Polymers for Advanced Technologies, 5 (1994) 673-697.

[5] K.A. Berchtold, R.P. Singh, J.S. Young, K.W. Dudeck, Polybenzimidazole composite membranes for high temperature synthesis gas separations, Journal of Membrane Science, 415-416 (2012) 265-270.

[6] W.J. Koros, G.K. Fleming, Membrane-based gas separation, Journal of Membrane Science, 83 (1993) 1-80.

[7] H.B. Park, C.H. Jung, Y.M. Lee, A.J. Hill, S.J. Pas, S.T. Mudie, E. Van Wagner, B.D. Freeman, D.J. Cookson, Polymers with cavities tuned for fast selective transport of small molecules and ions, Science, 318 (2007) 254-258.

[8] T.-S. Chung, A critical review of polybenzimidazoles, Journal of Macromolecular Science, Part C, 37 (1997) 277-301.

[9] J. Sánchez-Laínez, B. Zornoza, S. Friebe, J. Caro, S. Cao, A. Sabetghadam, B. Seoane, J. Gascon, F. Kapteijn, C. Le Guillouzer, G. Clet, M. Daturi, C. Téllez, J. Coronas, Influence of ZIF-8 particle size in the performance of polybenzimidazole mixed matrix membranes for pre-combustion CO_2 capture and its validation through interlaboratory test, Journal of Membrane Science, 515 (2016) 45-53.

[10] X. Li, R.P. Singh, K.W. Dudeck, K.A. Berchtold, B.C. Benicewicz, Influence of polybenzimidazole main chain structure on H_2/CO_2 separation at elevated temperatures, Journal of Membrane Science, 461 (2014) 59-68.

[11] R.P. Singh, G.J. Dahe, K.W. Dudeck, C.F. Welch, K.A. Berchtold, High temperature polybenzimidazole hollow fiber membranes for hydrogen separation and carbon dioxide capture from synthesis gas, Energy Procedia, 63 (2014) 153-159.

[12] S.C. Kumbharkar, Y. Liu, K. Li, High performance polybenzimidazole based asymmetric hollow fibre membranes for H_2/CO_2 separation, Journal of Membrane Science, 375 (2011) 231-240.

[13] S.C. Kumbharkar, U.K. Kharul, Investigation of gas permeation properties of systematically modified polybenzimidazoles by N-substitution, Journal of Membrane Science, 357 (2010) 134-142.

[14] K.C. O'Brien, G. Krishnan, K.A. Berchtold, S. Blum, R. Callahan, W. Johnson, D.L. Roberts, D. Steele, D. Byard, J. Figueroa, Towards a pilot-scale membrane system for pre-combustion CO_2 separation, Energy Procedia, 1 (2009) 287-294.

[15] D.R. Pesiri, B. Jorgensen, R.C. Dye, Thermal optimization of polybenzimidazole meniscus membranes for the separation of hydrogen, methane, and carbon dioxide, Journal of Membrane Science, 218 (2003) 11-18.

Chapter 2: Theory and Background

2.1 THE SOLUTION-DIFFUSION MODEL

The solution-diffusion model describes transport of small molecules through non-porous polymer membranes [1]. According to this model, a gas molecule sorbs into the upstream side of a membrane, diffuses down a concentration gradient through transient gaps in a polymer matrix, and desorbs from the downstream side of a membrane [1]. The solution-diffusion model can be represented by Equation [2-1] [2]:

$$P = DS \qquad [2\text{-}1]$$

where P is the permeability coefficient, D is the diffusion coefficient, and S is the solubility coefficient. Permeability is defined as the thickness and driving force normalized flux [2]:

$$P = N\left(\frac{l}{\Delta p}\right) \qquad [2\text{-}2]$$

where N is the steady state flux, Δp is the pressure difference across the membrane, and l is film thickness. The gas solubility coefficient, S, is the concentration of gas sorbed into a polymer, C, at a specific pressure, p, and temperature (i.e., $S = C / p$).

The ideal selectivity of a membrane is defined as the ratio of pure gas permeabilities through the membrane. The selectivity of A with respect to B is also the product of the ratios of diffusivity selectivity and solubility selectivity [2]:

$$\alpha_{A/B} = \frac{P_A}{P_B} = \frac{D_A}{D_B}\frac{S_A}{S_B} \qquad [2\text{-}3]$$

where P, D, and S are the permeability, diffusivity, and solubility coefficients, and $\alpha_{A/B}$ is the ideal (i.e., pure gas) selectivity of A over B.

2.2 TEMPERATURE-DEPENDENCE OF TRANSPORT PROPERTIES

The effects of temperature on permeability, diffusivity, and solubility are typically described by the Arrhenius-van't Hoff equations [3]:

$$P = P_0 e^{\frac{-E_P}{RT}} \quad [2\text{-}4]$$

$$D = D_0 e^{\frac{-E_D}{RT}} \quad [2\text{-}5]$$

$$S = S_0 e^{\frac{-\Delta H_S}{RT}} \quad [2\text{-}6]$$

where E_P, E_D, and ΔH_S are the activation energy of permeation, activation energy of diffusion, and enthalpy of sorption, respectively, and P_0, D_0, and S_0 are exponential pre-factors. By combining Equations [2-1], [2-4], [2-5], and [2-6], E_P, E_D, and ΔH_S are related as follows [2]:

$$E_P = E_D + \Delta H_S \quad [2\text{-}7]$$

Van Amerongen observed a correlation (the "linear free energy" relationship) between the pre-exponential factor for diffusion and the activation energy of diffusion [4]:

$$\ln D_0 = a\left(E_D\right) - b \quad [2\text{-}8]$$

where *a* and *b* are adjustable parameters [4]. The value of a is constant, and the b values range from 7.6 to 10.6. Where a has a universal value, b is often fit to different classes of polymers, e.g., glasses or rubbers [2].

2.3 EFFECT ON GAS SIZE AND CONDENSABILITY ON DIFFUSIVITY AND SOLUBILITY

The activation energy of diffusion scales linearly with the square of penetrant diameter [2, 5, 6]:

$$E_D = c d_i^2 + f \quad [2\text{-}9]$$

where d_i is the effective gas diameter, and c and f are empirical parameters. The relationship between gas size and transport properties can be examined in the absence of

diffusivity data by using the activation energy of permeation (i.e., trends that are evident in E_D should be evident in E_P by [2-7] in the absence of large sorption effects). There are a variety of gas diameters that can be used for the analysis of gas diffusion in polymers [2, 7]. Robeson and Smith regressed diffusion diameters based on a database of experimental diffusivities and upper bound correlations [7] and found that these diffusion diameters, presented in Table 2.1, were more representative for correlation of transport properties of gases in polymers than prior zeolite-based diameters [7].

Table 2.1. Penetrant properties used for correlating gas diffusion and sorption.

Gas	Kinetic diameter, d_k (Å) [2]	Diffusion diameter d_D (Å) [7]	Critical temperature, T_c (K) [2]
He	2.60	2.55 ± 0.10	5.2
H_2	2.89	2.77 ± 0.08	33.2
O_2	3.46	2.23 ± 0.02	154.6
N_2	3.64	3.49 ± 0.06	126.2
CO_2	3.30	3.44 ± 0.06	304.2
CH_4	3.80	3.817	190.6

S usually increases exponentially with gas critical temperature (i.e., $\ln S = \ln S_0 + a_c T_c$) [2, 8]. The slope of this correlation, a_c, is almost always independent of polymer structure and morphology, and a_c is typically in the range of 0.015-0.019 K^{-1} [8] for a range of sorbents including liquids, rubbery polymers, and glassy polymers.

2.4 EFFECT ON FREE VOLUME ON PERMEABILITY AND DIFFUSIVITY

Permeability, diffusivity, and solubility are correlated with several polymer and penetrant properties such as polymer fractional free volume and penetrant condensability. Fractional free volume is defined as follows [3]:

$$FFV = \frac{V - V_0}{V} \qquad [2\text{-}10]$$

where V is the specific volume of the polymer at the temperature of interest, and V_0 is the specific occupied volume, which is generally estimated as 1.3 times the van der Waals volume of the polymer repeat unit (which, in turn, is estimated by a group contribution method) [5].

As the polymer structure is opened (i.e., FFV is increased), diffusion coefficients increase as follows [9]:

$$D = A_D e^{\left(-\frac{B}{FFV}\right)} \qquad [2\text{-}11]$$

where A_D and B are adjustable constants typically taken to be independent of temperature and diluent concentration.

FFV has been correlated with the activation energy of diffusion, where increasing FFV results in lower activation energies of diffusion and, correspondingly, lower activation energies of permeation [9, 10]. Furthermore, Lin proposed that [9]

$$E_D = \frac{-\frac{B}{FFV} + (\ln A_D + b)}{a/R - 1/RT} \qquad [2\text{-}12]$$

where B is linearly related to d_{LJ}^2 (the squared Lennard-Jones diameter of the penetrant) by

$$B = H + Ld_{LJ}^2 \qquad [2\text{-}13]$$

where H and L are adjustable constants [9].

2.5 THE DUAL MODE MODEL AS A FUNCTION OF TEMPERATURE

The dual mode model [3] is often used to describe gas sorption in glassy polymers. The gas concentration in the polymer is expressed as follows:

$$C = k_D p + C'_H \frac{bp}{1+bp} \qquad [2\text{-}14]$$

where C (cm^3 (STP) / cm^3 polymer) is the total gas concentration in the polymer, k_D (cm^3 (STP) / cm^3 polymer atm) is the Henry's law sorption coefficient, C'_H (cm^3 (STP) /

cm^3 polymer) is the Langmuir capacity parameter, b (atm^{-1}) is the Langmuir affinity constant, and p is the external penetrant pressure (atm) [11].

The temperature dependence of k_D and b are described using Arrhenius-van't Hoff relationships [3, 11]:

$$k_D = k_{D0} e^{\frac{-\Delta H_D}{RT}} \qquad [2\text{-}15]$$

$$b = b_0 e^{\frac{-\Delta H_b}{RT}} \qquad [2\text{-}16]$$

where ΔH_D and ΔH_b are the Henry's and Langmuir modes enthalpies of sorption, respectively. C'_H does not follow the same trend with temperature as k_D and b [11]. Excess free volume diminishes in the polymer matrix as temperature increases towards the glass transition temperature [2], so C'_H decreases as the glass transition temperature is approached and vanishes at the glass transition temperature [12, 13].

The three dual mode parameters are typically determined by non-linear regression of C vs. p at different temperatures (or S vs. p and T). In the limit of vanishing pressure, the dual mode equation for S becomes:

$$\lim_{p \to 0} S = S^{\inf} = k_D + C'_H b \qquad [2\text{-}17]$$

where $S^{\inf}$ is the infinite-dilution solubility coefficient.

2.6 ISOSTERIC ENTHALPY OF SORPTION

The concentration dependence of the enthalpy of sorption is given by [11]:

$$\left[\frac{\partial \ln p}{\partial (1/T)} \right]_C = \frac{\Delta H_I}{zR} \qquad [2\text{-}18]$$

where ΔH_I is the isosteric heat of sorption, p is the pressure associated with a given penetrant concentration C in the polymer, and z is the penetrant compressibility [11]. The isosteric heat of sorption represents the enthalpy of sorption at a fixed concentration

[11]. By calculating ΔH_I, the interactions between penetrants and polymer segments can be examined. Furthermore, this analysis can be performed independent of any specific model, such as the dual mode model.

2.7 THE UPPER BOUND AND ITS TEMPERATURE DEPENDENCE

Polymer-based separations appear to follow an inverse relationship between permeability and selectivity [14]. In 1991, Robeson described this relationship as a $\log \alpha_{A/B}$ versus $\log P_A$ line that represented the state of the art [14]. Figure 2.1 presents Robeson's original upper bound for CO_2/CH_4 separation along with the revised 2008 upper bound [14, 15].

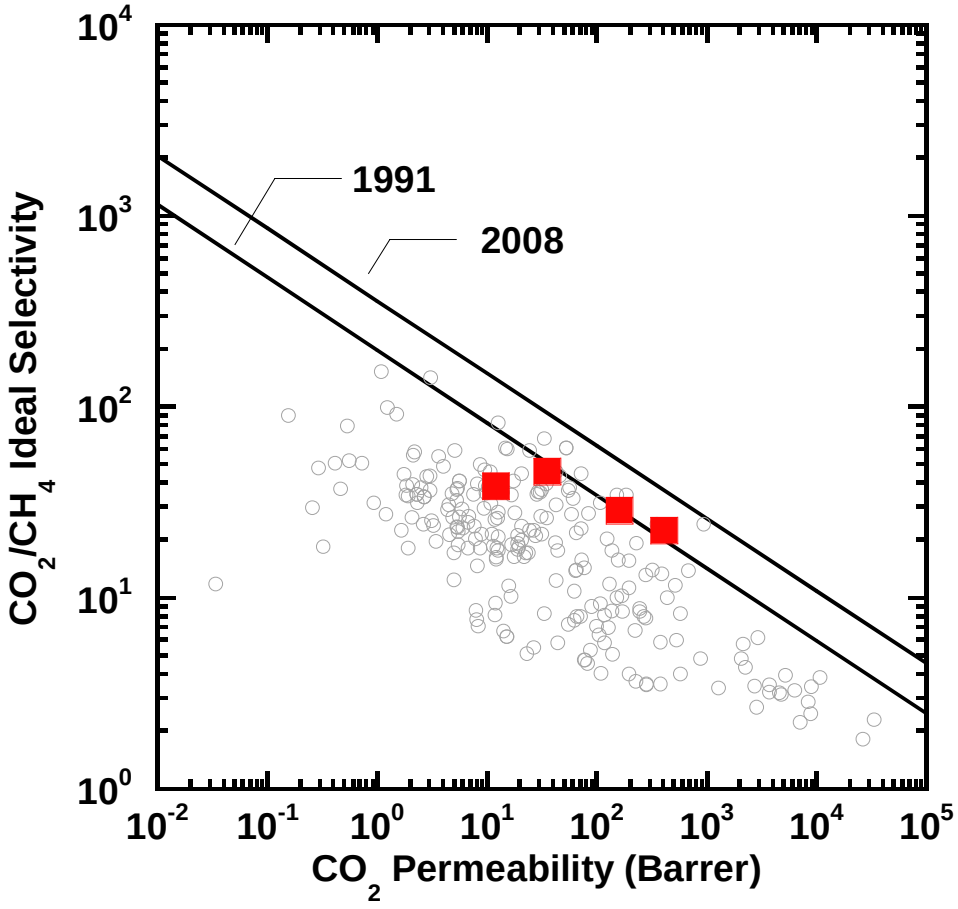

Figure 2.1. Data for HAB-6FDA polyimide and TRs (■) against the 1991 and 2008 Robeson upper bounds for CO_2/CH_4 [14, 15]. TR data from Sanders, et al. [16].

Freeman proposed a theoretical justification for the shape of the upper bound [17]. The inherent trade-off relationship of the upper bound stems from the size-sieving nature of rigid glassy polymers that populate the upper bound [17]. The upper bound follows can be described by:

$$\alpha_{A/B} = \frac{\beta_{A/B}}{P_A^{\lambda_{A/B}}} \qquad [2\text{-}19]$$

where $\lambda_{A/B}$ and $\beta_{A/B}$ are adjustable parameters, $\alpha_{A/B}$ is selectivity of A over B, and P_A is the permeability of species A. Freeman proposed that [17]

$$\lambda_{A/B} = (d_B / d_A)^2 - 1 \qquad [2\text{-}20]$$

where d_A and d_B are the kinetic diameters of species A and B, and [17]

$$\beta_{A/B} = \frac{S_A}{S_B} S_A^{\lambda_{A/B}} exp\left\{-\lambda_{A/B}\left[b - f\left(\frac{1-a}{RT}\right)\right]\right\} \qquad [2\text{-}21]$$

where S_i is the solubility of species *i*, b and a are constants from the linear free energy relation (cf., Equation [2-8]), and f is an adjustable constant (cf., Equation [2-9]) [17].

Rowe et al. expanded on this model to include temperature dependence [18]. The slope of the upper bound, defined by $\lambda_{A/B}$, is independent of temperature. The temperature dependence, then, lies in $\beta_{A/B}$. Rowe et al. proposed that [18]

$$\gamma = \frac{d \ln \beta_{A/B}}{d(1/T)} = -\frac{\Delta H_{S_A}}{R}(\lambda_{A/B} + 1) + \frac{\Delta H_{S_B}}{R} + \lambda_{A/B} f\left(\frac{1-a}{R}\right) \qquad [2\text{-}22]$$

The upper bound at a given temperature is then defined as

$$\alpha_{A/B} = \frac{\beta_{0,A/B} e^{\gamma/T}}{P_A^{\lambda_{A/B}}} \qquad [2\text{-}23]$$

where $\beta_{0,A/B}$ is a front factor, and γ is defined in Equation [2-22] [18]. Adjusting the CO_2/CH_4 upper bound to the temperatures used in the preliminary work in this study yields the upper bounds in Figure 2.2.

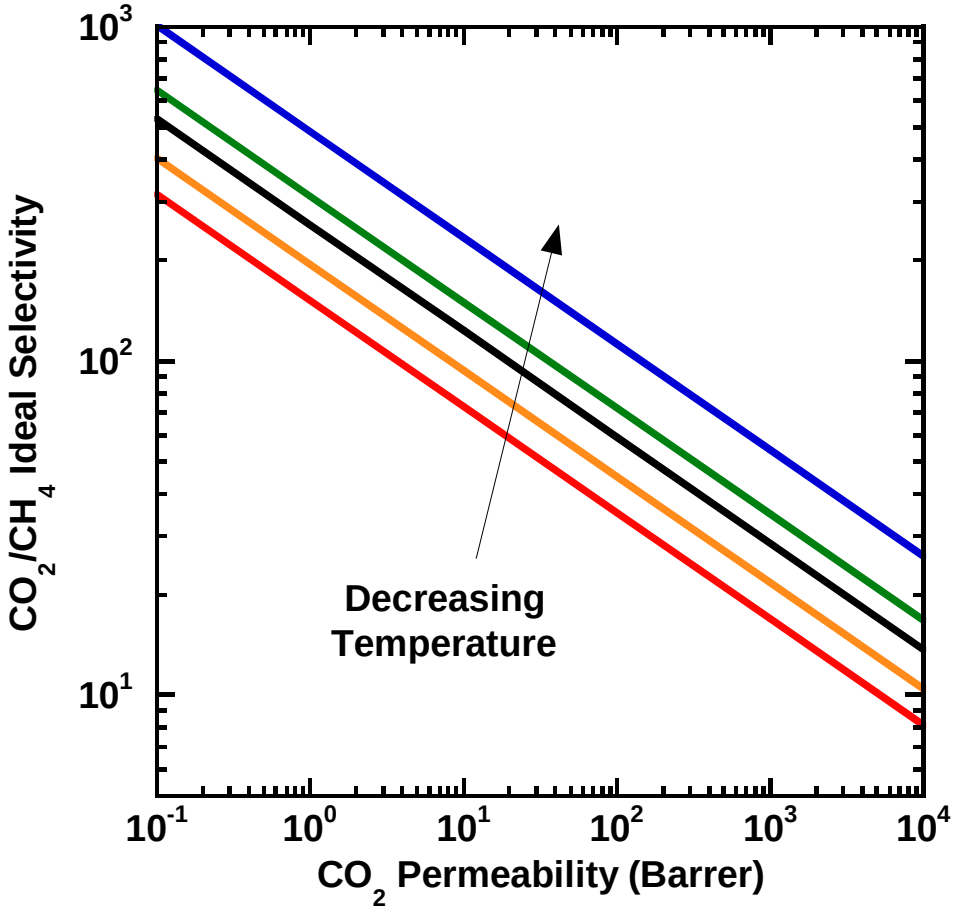

Figure 2.2. Influence of temperature on the Robeson upper bounds [18]. Temperatures shown decrease from 50 °C (red) to -10 °C (blue).

2.8 Effect of Temperature on Transport Properties

The temperature dependence of solubility has been previously examined in detail for a number of polymers. Koros and Paul reported CO_2 sorption in poly(ethylene terephthalate) (PET) from 25 to 115 °C [12]. The effects of temperature on solubility and dual mode parameters above and below the glass transition temperature of PET were elucidated [12]. As temperature increased, all dual mode parameters decreased. Beyond the glass transition temperature, the Langmuir contribution to solubility vanished

consistent with the lack of non-equilibrium free volume above the glass transition temperature [12]. Costello et al. studied transport properties of meta/para-isomers of 6FDA and hexafluoroisopropylidene diamines at ambient and higher temperatures [19]. The para-isomer was further below its glass transition temperature than the meta analog and had a higher fractional free volume, resulting in higher Langmuir sorption capacities than the para isomer. Solubility for He, N_2, O_2, CH_4, and CO_2 decreased with increasing temperature [19]. Merkel et al. studied the solubility and permeability of light gases, hydrocarbons, and fluorocarbons in a glassy random copolymer of polytetrafluoroethylene and poly(2,2-bis(trifluoromethyl)-4,5-difluoro-1,3-dioxole) (AF2400®) from 25 to 45 °C [20]. The transport properties of AF2400® were influenced strongly by its high free volume, which made enthalpies of sorption more exothermic than in lower free volume polymers and lowered activation energies of diffusion, resulting in low activation energies of permeation [20].

Zimmerman and Koros measured permeation, diffusion, and sorption in 6FDA-TAB and a series of 6FDA/PMDA-TAB copolymers from 35 to 80 °C [21]. Increases in free volume due to varying polymer structure were correlated with decreases in activation energies of diffusion and activation energies of permeation [21, 22]. The temperature dependence of gas permeability, solubility, and diffusivity in PIM-1 was reported by Li et al. [23]. The activation energies of permeation were near zero for light and condensable gases, indicating that low, but positive, activation energies of diffusion were mostly offset by negative enthalpies of sorption. Additionally, enthalpies and activation energies were pressure dependent and decreased in magnitude for the condensable gases [23]. Han et al. prepared a polybenzimidazole from a polypyrrolone precursor via thermal rearrangement [24]. This TR-PBI had high free volume (26.7%) and a CO_2 permeability above 1600 Barrer. The activation energies of permeation were negative for smaller and

more condensable penetrants, such as H_2 and CO_2, respectively, presumably as a result of the high free volume [24].

2.9 THERMALLY REARRANGED POLYMERS

Thermally rearranged (TR) polymers are aromatic polymers with interconnected heterocyclic rings derived from a post-processing thermal treatment (i.e., thermal rearrangement) of polyimides with ortho-functional groups [25]. Depending on the ortho-position group, TR polymers can take the form of polybenzimidazoles, polybenzothiazoles, and polybenzoxazoles [24-26]. Polybenzoxazoles are often insoluble in common organic solvents [27] and resistant to aggressive chemical environments [27].

The literature on temperature dependence of TR polymer transport properties is limited. Han et al. focused on polybenzimidazoles (PBIs) formed via a thermal rearrangement process [24]. The resulting TR-PBIs exhibited very high permeabilities of CO_2, CH_4, O_2, N_2, and H_2 with good selectivities near ambient conditions, but selectivities decreased with increasing temperature. Kim et al. examined the temperature dependence of transport of light gases in TR-β-polymers formed from poly(hydroxyamide) precursors and found that permeabilities and diffusivities increased with increasing temperature while solubility decreased [28]. Additionally, the lower permeabilities observed by Kim correlated with the lower free volume in TR-β-polymers than observed in polyimide-based PBOs [28]. Smith et al. studied the temperature-dependence of hydrogen sorption in several polymers, including TR polymers [29]. While the solubility of H_2 in TR polymers increased with TR conversion, enthalpies of sorption did not change significantly [29].

2.10 POLYBENZIMIDAZOLES

The most common PBI studied in the literature is *m*-PBI, otherwise known by its trade name, Celazole® [30-33]. *m*-PBI has high thermal stability, with a T_g of approximately 416 °C and a degradation temperature above 500 °C [30]. Though *m*-PBI has limited solubility in common organic solvents [31], hollow fibers of *m*-PBI have been made [32, 33]. Permeation experiments with *m*-PBI hollow fibers have been conducted at temperatures ranging from 250 to 350 °C and show permeances as high as 500 GPU (1 GPU = 10^{-6} cm^3 (STP) / (cm^2 s cmHg)) with H_2/CO_2 selectivities exceeding 15 [32]. Developing new PBI materials with attractive transport properties that are more soluble in common solvents could potentially simplify the hollow fiber spinning process and provide a rational structure/property basis to design even better materials for such separations.

Altering polymer structure impacts gas transport properties [2]. For example, the addition of large, bulky pendant groups, such as $-Si(CH_3)_3$, can increase permeability by several orders of magnitude [2]. Several studies have examined the effect of chemical structure on the transport properties of PBIs. *m*-PBI is typically synthesized from 3,3'-diaminobenzidine (DAB) and isophthalic acid (IPA) [34]. Kumbharkar et al. incorporated alternative diacids, including 5-*tert*-butyl isophthalic acid (BuI) and 4,4'-(hexafluoroisopropylidene)bis(benzoic acid) (HFA) [30]. The use of BuI and HFA resulted in 18- and 20-fold increases, respectively, in H_2 permeability of all gases at 35 °C relative to *m*-PBI [30]. Kumbharkar also studied the effect of N-substitution (i.e., substitution of the imidazole hydrogen) on PBI transport properties at 35 °C [35, 36]. N-substitution resulted in up to a 38-fold increase in H_2 permeability in a 4-*tert*-butylbenzyl-substituted PBI (the largest group tested) over *m*-PBI, and larger gases

exhibited more substantial permeability increases (i.e., a 128-fold increase for CH_4) than for other gases [36].

Li et al. studied the effect of varying diacid chemistry on high-temperature H_2/CO_2 separations for several fluorinated diacids as well as a phenylindane moiety [37]. Inclusion of the fluorinated groups and the phenylindane moiety yielded significantly increased permeabilities at high temperatures. Hydrogen permeabilities at 250 °C increased to 997 Barrer for a hexafluoroisopropylidene-containing structure as compared to 77 Barrer for *m*-PBI [37]. Activation energies of permeation also decreased as a result of changing the backbone structure, and the structures with the highest permeabilities had the lowest activation energies of permeation [37]. Finally, Han et al. studied the temperature dependence of a PBI made through a thermal rearrangement process (TR-PBI) [24]. The thermal rearrangement process resulted in very high permeabilities (e.g., H_2 permeability of 1779 Barrer with a H_2/CO_2 selectivity of 1.1 at 25 °C) and low activation energies of permeation (e.g., -1.48 and -4.93 kJ/mol for H_2 and CO_2, respectively) [24].

2.11 REFERENCES

[1] J.G. Wijmans, R.W. Baker, The solution-diffusion model: a review, Journal of Membrane Science, 107 (1995) 1-21.

[2] S. Matteucci, Y. Yampolskii, B.D. Freeman, I. Pinnau, Transport of gases and vapors in glassy and rubbery polymers, in: Y. Yampolskii, I. Pinnau, B. Freeman (Eds.) Materials science of membranes for gas and vapor separation, John Wiley & Sons, Ltd, Chichester, UK, 2006, pp. 1-47.

[3] K. Ghosal, B.D. Freeman, Gas separation using polymer membranes: an overview, Polymers for Advanced Technologies, 5 (1994) 673-697.

[4] G.J. van Amerongen, The Permeability of Different Rubbers to Gases and Its Relation to Diffusivity and Solubility, Journal of Applied Physics, 17 (1946) 972-972.

[5] D.W. van Krevelen, Properties of polymers, 3rd ed., Elsevier, Amsterdam, 1997.

[6] P. Meares, The Diffusion of Gases Through Polyvinyl Acetate, Journal of the American Chemical Society, 76 (1954) 3415-3422.

[7] L.M. Robeson, Z.P. Smith, B.D. Freeman, D.R. Paul, Contributions of diffusion and solubility selectivity to the upper bound analysis for glassy gas separation membranes, Journal of Membrane Science, 453 (2014) 71-83.

[8] R.S. Prabhakar, T.C. Merkel, B.D. Freeman, T. Imizu, A. Higuchi, Sorption and transport properties of propane and perfluoropropane in poly(dimethylsiloxane) and poly(1-trimethylsilyl-1-propyne), Macromolecules, 38 (2005) 1899-1910.

[9] H. Lin, B.D. Freeman, Gas permeation and diffusion in cross-linked poly(ethylene glycol diacrylate), Macromolecules, 39 (2006) 3568-3580.

[10] Y. Yampolskii, S. Shishatskii, A. Alentiev, K. Loza, Correlations with and prediction of activation energies of gas permeation and diffusion in glassy polymers, Journal of Membrane Science, 148 (1998) 59-69.

[11] W.J. Koros, D.R. Paul, G.S. Huvard, Energetics of gas sorption in glassy polymers, Polymer, 20 (1979) 956-960.

[12] W.J. Koros, D.R. Paul, CO_2 sorption in poly(ethylene terephthalate) above and below the glass transition, Journal of Polymer Science: Polymer Physics Edition, 16 (1978) 1947-1963.

[13] W.J. Koros, D.R. Paul, Observations concerning the temperature dependence of the langmuir sorption capacity of glassy polymers, Journal of Polymer Science: Polymer Physics Edition, 19 (1981) 1655-1656.

[14] L.M. Robeson, Correlation of separation factor versus permeability for polymeric membranes, Journal of Membrane Science, 62 (1991) 165-185.

[15] L.M. Robeson, The upper bound revisited, Journal of Membrane Science, 320 (2008) 390-400.

[16] D.F. Sanders, Z.P. Smith, C.P. Ribeiro, R. Guo, J.E. McGrath, D.R. Paul, B.D. Freeman, Gas permeability, diffusivity, and free volume of thermally rearranged polymers based on 3,3′-dihydroxy-4,4′-diamino-biphenyl (HAB) and 2,2′-bis-(3,4-dicarboxyphenyl) hexafluoropropane dianhydride (6FDA), Journal of Membrane Science, 409-410 (2012) 232-241.

[17] B.D. Freeman, Basis of permeability/selectivity tradeoff relations in polymeric gas separation membranes, Macromolecules, 32 (1999) 375-380.

[18] B.W. Rowe, L.M. Robeson, B.D. Freeman, D.R. Paul, Influence of temperature on the upper bound: Theoretical considerations and comparison with experimental results, Journal of Membrane Science, 360 (2010) 58-69.

[19] L.M. Costello, W.J. Koros, Thermally stable polyimide isomers for membrane-based gas separations at elevated temperatures, Journal of Polymer Science Part B: Polymer Physics, 33 (1995) 135-146.

[20] T.C. Merkel, V. Bondar, K. Nagai, B.D. Freeman, Y.P. Yampolskii, Gas sorption, diffusion, and permeation in poly(2,2-bis(trifluoromethyl)-4,5-difluoro-1,3-dioxole-co-tetrafluoroethylene), Macromolecules, 32 (1999) 8427-8440.

[21] C.M. Zimmerman, W.J. Koros, Polypyrrolones for membrane gas separations. II. Activation energies and heats of sorption, Journal of Polymer Science Part B: Polymer Physics, 37 (1999) 1251-1265.

[22] C.M. Zimmerman, W.J. Koros, Polypyrrolones for membrane gas separations. I. Structural comparison of gas transport and sorption properties, Journal of Polymer Science Part B: Polymer Physics, 37 (1999) 1235-1249.

[23] P. Li, T.S. Chung, D.R. Paul, Temperature dependence of gas sorption and permeation in PIM-1, Journal of Membrane Science, 450 (2014) 380-388.

[24] S.H. Han, J.E. Lee, K.-J. Lee, H.B. Park, Y.M. Lee, Highly gas permeable and microporous polybenzimidazole membrane by thermal rearrangement, Journal of Membrane Science, 357 (2010) 143-151.

[25] H.B. Park, C.H. Jung, Y.M. Lee, A.J. Hill, S.J. Pas, S.T. Mudie, E. Van Wagner, B.D. Freeman, D.J. Cookson, Polymers with cavities tuned for fast selective transport of small molecules and ions, Science, 318 (2007) 254-258.

[26] Z.P. Smith, K. Czenkusch, S. Wi, K.L. Gleason, G. Hernández, C.M. Doherty, K. Konstas, T.J. Bastow, C. Álvarez, A.J. Hill, A.E. Lozano, D.R. Paul, B.D. Freeman, Investigation of the chemical and morphological structure of thermally rearranged polymers, Polymer, (2014) 1-9.

[27] D.F. Sanders, Z.P. Smith, R. Guo, L.M. Robeson, J.E. McGrath, D.R. Paul, B.D. Freeman, Energy-efficient polymeric gas separation membranes for a sustainable future: A review, Polymer, 54 (2013) 4729-4761.

[28] S. Kim, J.G. Seong, Y.S. Do, Y.M. Lee, Gas sorption and transport in thermally rearranged polybenzoxazole membranes derived from polyhydroxylamides, Journal of Membrane Science, 474 (2015) 122-131.

[29] Z.P. Smith, R.R. Tiwari, T.M. Murphy, D.F. Sanders, K.L. Gleason, D.R. Paul, B.D. Freeman, Hydrogen sorption in polymers for membrane applications, Polymer, 54 (2013) 3026-3037.

[30] S.C. Kumbharkar, P.B. Karadkar, U.K. Kharul, Enhancement of gas permeation properties of polybenzimidazoles by systematic structure architecture, Journal of Membrane Science, 286 (2006) 161-169.

[31] W.S. Lyoo, J.H. Choi, S.S. Han, W.S. Yoon, M.S. Park, B.C. Ji, J. Cho, Preparation of organo-soluble poly[(2,2′-m-phenylene)-5,5′-bibenzimidazole] with high yield

by homogeneous nitration reaction, Journal of Applied Polymer Science, 78 (2000) 438-445.

[32] R.P. Singh, G.J. Dahe, K.W. Dudeck, C.F. Welch, K.A. Berchtold, High temperature polybenzimidazole hollow fiber membranes for hydrogen separation and carbon dioxide capture from synthesis gas, Energy Procedia, 63 (2014) 153-159.

[33] S.C. Kumbharkar, Y. Liu, K. Li, High performance polybenzimidazole based asymmetric hollow fibre membranes for H_2/CO_2 separation, Journal of Membrane Science, 375 (2011) 231-240.

[34] T.-S. Chung, A critical review of polybenzimidazoles, Journal of Macromolecular Science, Part C, 37 (1997) 277-301.

[35] S.C. Kumbharkar, U.K. Kharul, N-substitution of polybenzimidazoles: Synthesis and evaluation of physical properties, European Polymer Journal, 45 (2009) 3363-3371.

[36] S.C. Kumbharkar, U.K. Kharul, Investigation of gas permeation properties of systematically modified polybenzimidazoles by N-substitution, Journal of Membrane Science, 357 (2010) 134-142.

[37] X. Li, R.P. Singh, K.W. Dudeck, K.A. Berchtold, B.C. Benicewicz, Influence of polybenzimidazole main chain structure on H_2/CO_2 separation at elevated temperatures, Journal of Membrane Science, 461 (2014) 59-68.

Chapter 3: Materials and Experimental Methods

3.1 PREPARATION OF TR POLYMERS

3.1.1 Polyimide synthesis

The diamine monomer, 3,3'-dihydroxy-4,4'-diamino-biphenyl (HAB, Wakayama Seika Kyogo Co., Wakayama, Japan), was covered with aluminum foil to shield it from light and heated under vacuum to 60 °C overnight before use. The dianhydride monomer, 2,2'-bis-(3,4-dicarboxyphenyl) hexafluoropropane dianhydride (6FDA, Alfa Aesar, Ward Hill, MA, USA), was heated to 200 °C for 6 hours under -10 inHg of vacuum before being cooled to 120 °C under full vacuum overnight. Acetic anhydride (AA, 99.5%, Sigma Aldrich, St. Louis, MO, USA), pyridine (≥ 99.9%, Sigma Aldrich, St. Louis, MO, USA), and anhydrous 1-methyl-2-pyrrolidinone (NMP, Sigma Aldrich, St. Louis, MO, USA) were used as received. Nitrogen, methane, and carbon dioxide (UHP grade) were obtained from Airgas (Radnor, PA, USA).

The precursor polyimide used in this study was synthesized via chemical imidization as described previously [1]. For a typical synthesis, HAB (19.9 mmol) was added to a three-necked flask equipped with a mechanical stirrer and allowed to dissolve under nitrogen in anhydrous NMP. Next, 6FDA (20.0 mmol) was added along with more NMP to make a 0.15 g solids per cm^3 NMP solution. The flask was then placed in an ice bath, and the monomers were allowed to react for 24 hours. The resulting poly(amic acid) was imidized by adding 8 mol of acetic anhydride and 8 mol of pyridine per mole of HAB followed by further dilution with anhydrous NMP to make a 0.08 g (6FDA, HAB, AA, pyridine) per cm^3 NMP solution. The solution was stirred under N_2 for a further 24 hours. Finally, the reaction flask was equipped with a condenser, and the solution was heated to 60 °C for one hour to drive the reaction to completion.

The final HAB-6FDA polymer was further diluted with NMP to obtain a 5% (w/v) solution before precipitating the solution in a blender containing methanol (VWR, Radnor, PA, USA). Precipitated fibers were filtered and washed with methanol in a Büchner funnel before being placed in a stirred methanol bath for two consecutive 24-hour extraction steps. Fresh methanol was used for each extraction step. The light brown polymer fibers were dried under vacuum for 24 hours at 80 °C, 24 hours at 120 °C, and 48 hours at 200 °C. The ^{1}H NMR spectrum was consistent with the expected polyimide structure (cf., Figure 3.1).

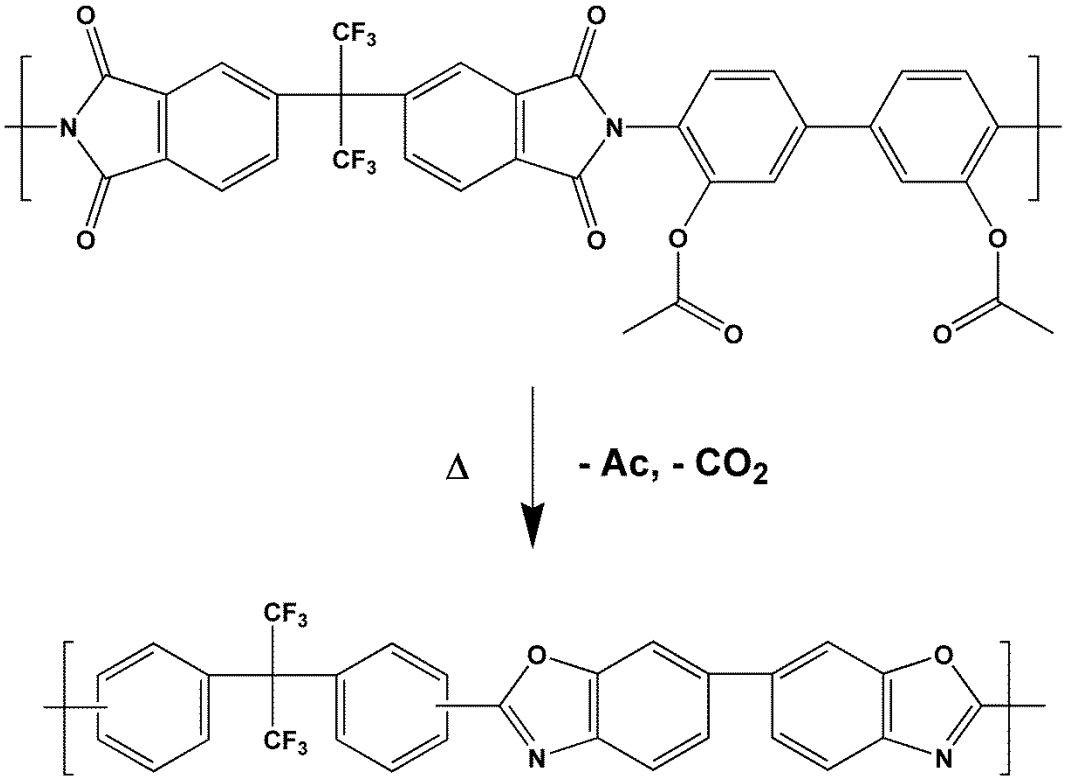

Figure 3.1. HAB-6FDA polyimide and TR polymer structure, where -Ac represents an acetate moiety.

3.1.2 Polyimide film casting

Approximately 1 g of HAB-6FDA was dissolved in *N*,*N*-dimethylacetamide (DMAc, Sigma Aldrich) with stirring to make a 2% (w/w) solution. The solution was filtered through a 5.0 µm Millex-LS PTFE filter (EMD Millipore; Billerica, MA, USA) into a glass ring silicone caulked to a clean glass plate. The solution and plate were placed on a level surface in a vacuum oven. The oven was partially evacuated to -25 inHg, after which the oven was purged three times with dry air pulled into the oven through a Drierite column (W. A. Hammond DRIERITE Co., Xenia, OH, USA). The solution was then allowed to evaporate slowly at 80 °C and -10 inHg for 24 hours. The films were then peeled off the glass plate and placed between two glass plates with spacers and dried at 200 °C overnight under full vacuum, resulting in ~35 µm thick solvent-free films, as verified by thermogravimetric analysis. Thickness was measured as an average of several points using a Mitutoyo Digimatic Micrometer (MDC-1" PJ, #293-340, Mitutoyo America Corporation, Aurora, IL).

3.1.3 Thermal rearrangement

Polyimide films were thermally rearranged to their corresponding polybenzoxazole (PBO) structures (cf., Figure 3.1) in a Carbolite Split-Tube Furnace (Carbolite, Watertown, WI, USA). Solvent-free films were weighed and sandwiched between ceramic plates with spacers to allow for film contraction during rearrangement. The temperature was raised to 300 °C at 5 °C/min under nitrogen purge (900 cm^3/min). After a dwell period of 1 hr, the temperature was raised again to the target thermal rearrangement temperature for a prescribed time before the furnace was allowed to cool down at a maximum rate of 10 °C/min. The thermal rearrangement conditions are summarized in Table 3.1. The three thermal rearrangement protocols considered in this study were selected for consistency with our previous studies [1-5] and are denoted by

their thermal rearrangement conditions. Each protocol is named TRX-Y where "X" is the final dwell temperature in °C and "Y" is the final dwell time. Percent conversion from polyimide to PBO was calculated by mass loss:

$$\%\ Conversion = \frac{Actual\ mass\ loss}{Theoretical\ mass\ loss} \times 100\% \qquad \text{Eq. [3-1]}$$

where the actual mass loss is the measured difference in mass before and after thermal rearrangement, and the theoretical mass loss is calculated from the polymer repeat unit molecular weights assuming that all *ortho*-position functional groups undergoing TR do so by rearranging to the polybenzoxazole structure [2]. For samples prepared via this protocol, the extent of conversion varied by ± 5% from sample to sample.

Table 3.1. Thermal rearrangement conditions and extent of conversion.

Sample Name	Conversion time (min)	Dwell Temperature (°C)	Approximate % Conversion
HAB-6FDA	--	--	--
TR350-1hr	60	350	40
TR400-1hr	60	400	62
TR450-30m	30	450	72

3.2 PREPARATION OF POLYBENZIMIDAZOLES

3.2.1 Film casting

Films of *m*-PBI were cast using the following method. A dope solution (26% solids by weight in *N,N*-dimethylacetamide) of *m*-PBI was purchased from PBI Performance Products, Inc. (Charlotte, NC) and contained 1.5 wt% lithium chloride as a phase stabilizer. The solution was diluted to 2 wt% polymer with DMAc, filtered through an 0.45 μm PTFE filter into a clean scintillation vial, sonicated for 30 minutes, and cast

onto a clean glass plate inside a glass ring. The nascent film was held under full vacuum at room temperature overnight. The temperature was increased to 60 °C for 4 hours and then 100 °C for one hour. The film was delaminated from the glass plate using deionized (DI) water and boiled in water for four hours to remove any residual DMAc. Lithium chloride in the film was extracted by soaking the boiled film in DI water for 24 hours, changing the water multiple times. Lithium chloride removal was verified by ion chromatography. The final film was dried at 140 °C under full vacuum overnight. Complete solvent removal was verified by thermogravimetric analysis.

The methods of synthesis and film formation of TADPS-based PBIs were described by Borjigin et al. [6], and films were provided by Virginia Tech for the purposes of this study. Films of TADPS-based PBIs were cast from polymer powder similar to above with the exception of the 24-hour extraction described above.

3.3 Experimental Methods

3.3.1 Temperature-dependent solubility

The solubility of N_2 in each sample was measured over a range of temperatures (0 °C to 50 °C) gravimetrically, using a Rubotherm Magnetic Suspension Balance (Rubotherm Präzisionsmeßtechnik GmbH; Bochum, Germany). N_2 sorption measurements were performed following the procedure outlined in Ref. [3]. Additionally, a liquid argon trap was used in the gas feed line to remove any condensable impurities. The effect of buoyancy on the resultant gas sorption isotherms was accounted for using a procedure described previously [3].

The solubilities of CH_4 and CO_2 in each sample were determined at temperatures from -10 to 50 °C using a dual-volume pressure decay apparatus [7]. Approximately 0.5-0.75 g of polymer was cut into small pieces and stacked in the sample cell. The cell

was held under vacuum overnight to degas the polymer film, and the system was then brought to the desired measurement temperature. The charge cell, which is separated from the sample cell by a valve, was filled with penetrant gas and allowed to reach thermal equilibrium. Next, the valve was opened briefly to allow gas to flow from the charge cell into the sample cell. The pressure in the sample cell decayed as gas sorbed into the polymer. After equilibrium was reached, more gas was introduced into the charge cell, and the experiment was repeated in a stepwise manner to a maximum pressure of approximately 27 atm. The resultant equilibrium pressures, the volumes of the sample chamber, and the volume of the polymer sample (estimated from its mass and density) were used to perform a mole balance at each pressure step using the Soave-Redlich-Kwong (SRK) equation of state [8] to generate the sorption isotherms [7]. After the sorption isotherm measurement, the sample was again held under vacuum in preparation for the next experiment. To avoid effects of CO_2 conditioning [9], fresh samples were used after each CO_2 isotherm.

3.3.2 Temperature-dependent permeability

CH_4, H_2, N_2, and CO_2 permeabilities were measured using a constant volume, variable pressure method [7]. The upstream pressure was measured with a Honeywell STJE 1500 psig (104 bara) pressure transducer (Honeywell Sensotec, Columbus, OH, USA), and the downstream pressure was measured with an MKS Baratron 626B capacitance manometer (MKS Instruments, Andover, MS, USA) with a range of 0 to 10 torr (1.33 kPa). The area available for gas transport was controlled by masking the sample with an impermeable brass disk and sealing with epoxy. Each sample was mounted in a Millipore 47 mm diameter filter holder (Millipore, Billerica, MA, USA) for testing. Vacuum was pulled before and between permeation experiments to degas the

polymer sample, using a vacuum pump equipped with a liquid nitrogen cold trap, and the downstream pressure was maintained at less than 10 torr for the duration of the experiment. The gases (UHP grade, Airgas, Radnor, PA, USA) were tested in the order listed above at pressures ranging from 3 atmospheres to approximately 32 atmospheres. The temperature was controlled by a water bath at 10, 20, 35, and 50 °C. For permeation testing at -10 °C, a methanol/water bath was used. To minimize the effects of CO_2 conditioning [9], permeation samples were exchanged for fresh films after exposure to CO_2 at any temperature.

3.3.3 High-temperature permeability

The permeabilities of H_2, He, N_2, CH_4, and CO_2 in four PBIs were measured over a range of temperatures by a constant-volume, variable-pressure method [7]. Downstream pressure was measured by an MKS Baratron 631C (MKS Instruments, Andover, MA) with a range of 0-10 torr, and the upstream pressure was recorded with a Honeywell STJE (Honeywell Sensotec, Columbus, OH) with a 150 psig (11.4 bara) range. Films of uniform thickness were mounted to brass support disks using Master Bond EP46HT-2 epoxy (Master Bond Inc., Hackensack, NJ) with a separate glass fiber filter backing to protect the polymer film. Samples were loaded in a modified CF flange (i.e., knife-edge and copper gasket seal) over a sintered stainless steel disk for mechanical support. The sample holder was attached to the permeation system, housed in a Thermo Fisher Scientific Heratherm OMH60 oven (Waltham, MA). The sample was degassed under vacuum (with a liquid nitrogen trap) at 190 °C overnight. For fragile samples, the film was allowed to degas at 35 °C for 24 hours followed by an overnight degas at 190 °C. The downstream pressure rise was measured at upstream pressures of 3 to 10 atm. Care was taken to prevent ambient atmosphere from entering the system after degassing do

limit exposure of the samples to water, since PBIs are more hygroscopic [6] than typical gas separation polymers such as Matrimid® and polysulfone [10]. He, H_2, CH_4, N_2, and CO_2 permeabilities were measured in the order listed at 190, 150, 125 (N_2 and CH_4 only), 100, 50 (He, H_2, and CO_2 only), and 35 °C (He, H_2, and CO_2 only). Pressure was limited to 10 atm to minimize any CO_2 conditioning. The largest gases, N_2 and CH_4, were not tested at temperatures below 100 °C due to low permeabilities, which were near the detection limit of the apparatus, as well as long times to reach steady state.

3.4 REFERENCES

[1] Z.P. Smith, D.F. Sanders, C.P. Ribeiro, R. Guo, B.D. Freeman, D.R. Paul, J.E. McGrath, S. Swinnea, Gas sorption and characterization of thermally rearranged polyimides based on 3,3′-dihydroxy-4,4′-diamino-biphenyl (HAB) and 2,2′-bis-(3,4-dicarboxyphenyl) hexafluoropropane dianhydride (6FDA), Journal of Membrane Science, 415-416 (2012) 558-567.

[2] D.F. Sanders, Z.P. Smith, C.P. Ribeiro, R. Guo, J.E. McGrath, D.R. Paul, B.D. Freeman, Gas permeability, diffusivity, and free volume of thermally rearranged polymers based on 3,3′-dihydroxy-4,4′-diamino-biphenyl (HAB) and 2,2′-bis-(3,4-dicarboxyphenyl) hexafluoropropane dianhydride (6FDA), Journal of Membrane Science, 409-410 (2012) 232-241.

[3] Z.P. Smith, R.R. Tiwari, T.M. Murphy, D.F. Sanders, K.L. Gleason, D.R. Paul, B.D. Freeman, Hydrogen sorption in polymers for membrane applications, Polymer, 54 (2013) 3026-3037.

[4] D.F. Sanders, R. Guo, Z.P. Smith, Q. Liu, K.A. Stevens, J.E. McGrath, D.R. Paul, B.D. Freeman, Influence of polyimide precursor synthesis route and ortho-position functional group on thermally rearranged (TR) polymer properties: Conversion and free volume, Polymer, 55 (2014) 1636-1647.

[5] D.F. Sanders, R. Guo, Z.P. Smith, K.A. Stevens, Q. Liu, J.E. McGrath, D.R. Paul, B.D. Freeman, Influence of polyimide precursor synthesis route and ortho-position functional group on thermally rearranged (TR) polymer properties: Pure gas permeability and selectivity, Journal of Membrane Science, 463 (2014) 73-81.

[6] H. Borjigin, K.A. Stevens, R. Liu, J.D. Moon, A.T. Shaver, S. Swinnea, B.D. Freeman, J.S. Riffle, J.E. McGrath, Synthesis and characterization of

polybenzimidazoles derived from tetraaminodiphenylsulfone for high temperature gas separation membranes, Polymer, 71 (2015) 135-142.

[7] H. Czichos, T. Saito, L. Smith, Springer handbook of materials measurement methods, Springer Verlag, 2006.

[8] J.M. Smith, H.C. Van Ness, M.M. Abbott, Introduction to chemical engineering thermodynamics, McGraw-Hill, Boston, 2005.

[9] A.G. Wonders, D.R. Paul, Effect of CO_2 exposure history on sorption and transport in polycarbonate, Journal of Membrane Science, 5 (1979) 63-75.

[10] B.W. Rowe, B.D. Freeman, D.R. Paul, Effect of Sorbed Water and Temperature on the Optical Properties and Density of Thin Glassy Polymer Films on a Silicon Substrate, Macromolecules, 40 (2007) 2806-2813.

Chapter 4: Influence of temperature on gas solubility in thermally rearranged (TR) polymers

4.1 SUMMARY

Thermally rearranged (TR) polymers have been the subject of many fundamental studies, but the effect of TR conversion on temperature-dependent transport properties is largely unexplored. Sorption isotherms for N_2, CH_4, and CO_2 in HAB-6FDA polyimide and its TR analogs were measured at temperatures ranging from -10 °C to 50 °C and pressures up to 27 atm. Solubilities increase with decreasing temperature for each gas and sample tested. At low TR conversions, the sorption process initially becomes less exothermic. However, enthalpies of sorption do not significantly change with TR conversion after the initial rearrangement. Enthalpies of sorption in TR polymers are qualitatively similar to those of other high free volume materials. Solubility selectivity for CO_2/CH_4 at 10 atm did not change with temperature due to similar enthalpies of sorption for CO_2 and CH_4. Sorption data were fit to the dual mode model at different temperatures, and model parameters were correlated with polymer and penetrant properties.

4.2 RESULTS AND DISCUSSION

4.2.1 Gas sorption isotherm measurements

Gas solubility was measured for N_2, CH_4, and CO_2 in HAB-6FDA and three of its TR analogs. To provide a broader context to these results, additional H_2 data from a previous study were included in the analysis [1]. The uncertainties presented here were calculated by the propagation of errors method [2].

Sorption isotherms for CH_4, N_2, and CO_2 in the polyimide precursor and TR polymers are shown in Figures 4.1, 4.2, and 4.3, respectively. Solubility increases with

decreasing temperature for all samples in this study. For example, increasing the temperature from 35 to 50 °C resulted in the concentration of CH_4 at 10 atm in the HAB-6FDA polyimide decreasing from 10.6 to 8.7 cm^3(STP)/cm^3 polymer (17% decrease). Decreasing the temperature from 35 to 20 °C resulted in an increase of 27% from 10.6 to 13.4 cm^3(STP)/cm^3 polymer. At 27 atm (the highest pressure measured for CH_4), concentrations ranged from 15.6 (at 50 °C) to 32.5 (at -10 °C) cm^3(STP)/cm^3 polymer. As TR conversion proceeds, solubilities increase for all gases tested, as previously reported [3].

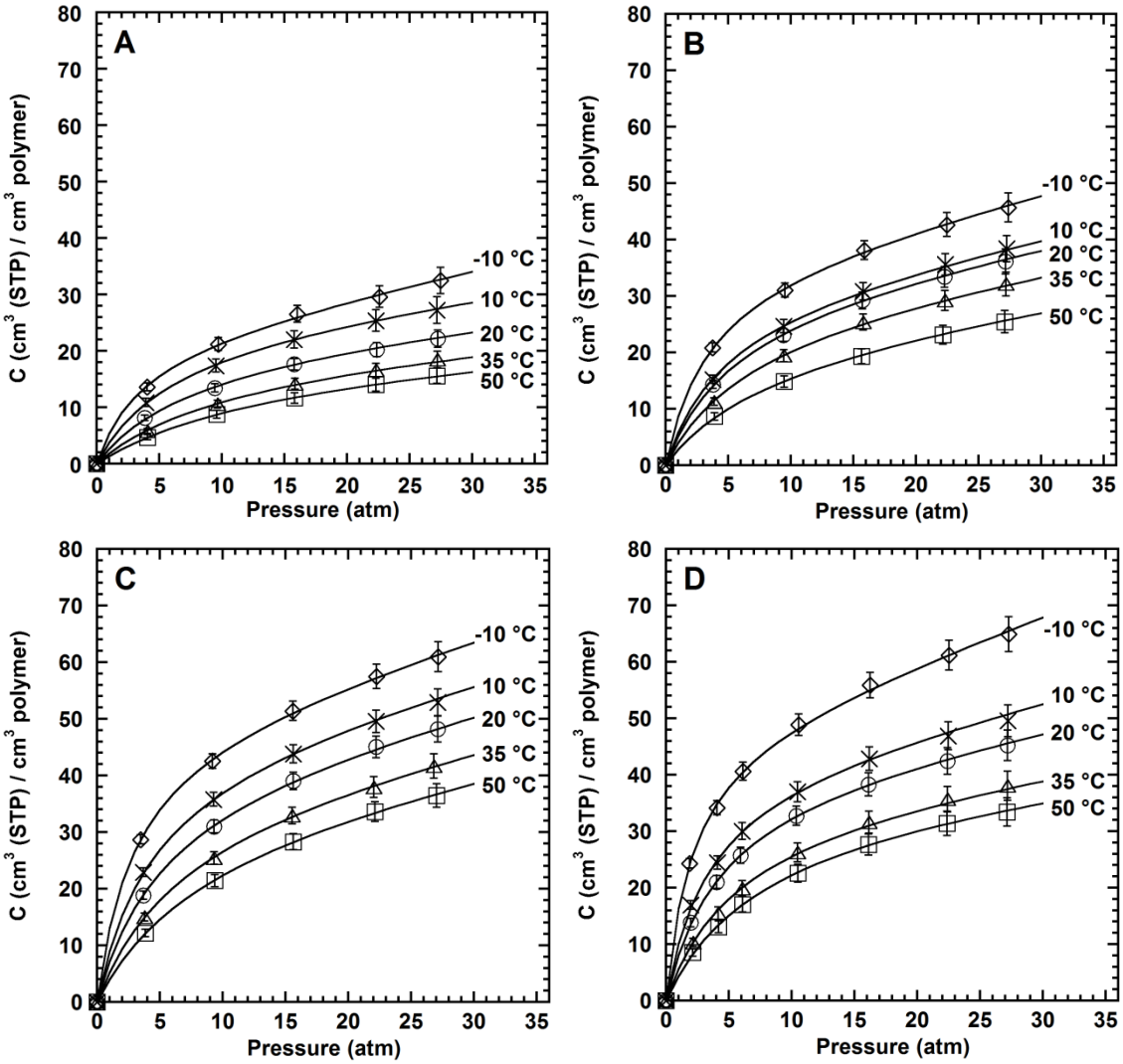

Figure 4.1. Concentration as a function of pressure of CH_4 at 50 °C (open squares), 35 °C (open triangles), 20 °C (open circles), 10 °C (crosses) and -10 °C (open diamonds) in: A) HAB-6FDA-CI polyimide, B) TR350-1hr, C) TR400-1hr, and D) TR450-30m. The continuous lines are dual mode model fits.

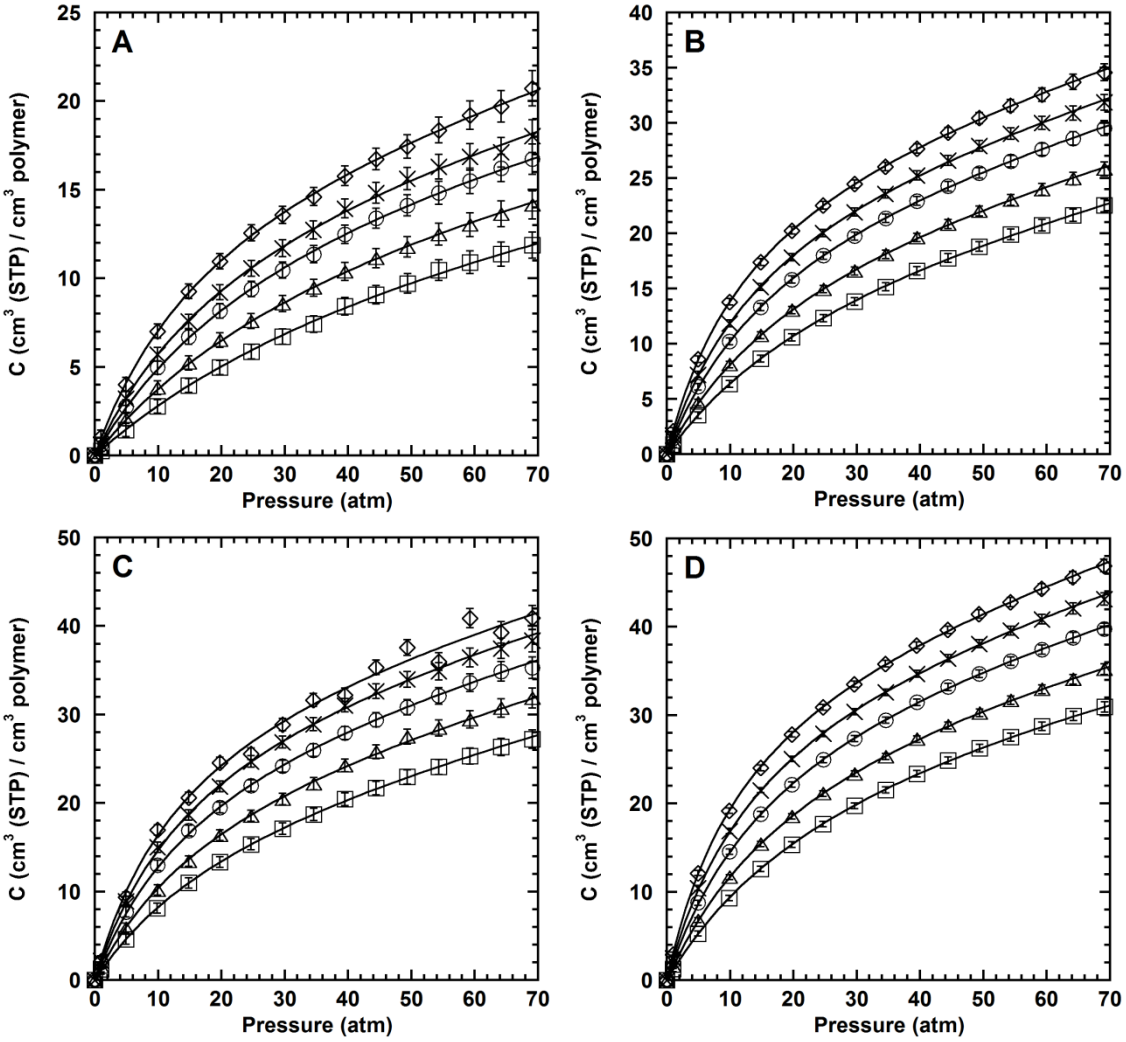

Figure 4.2. Concentration as a function of pressure of N_2 at 50 °C (open squares), 35 °C (open triangles), 20 °C (open circles), 10 °C (crosses) and 0 °C (open diamonds) in: A) HAB-6FDA-CI polyimide, B) TR350-1hr, C) TR400-1hr, and D) TR450-30m. The continuous lines are dual mode model fits.

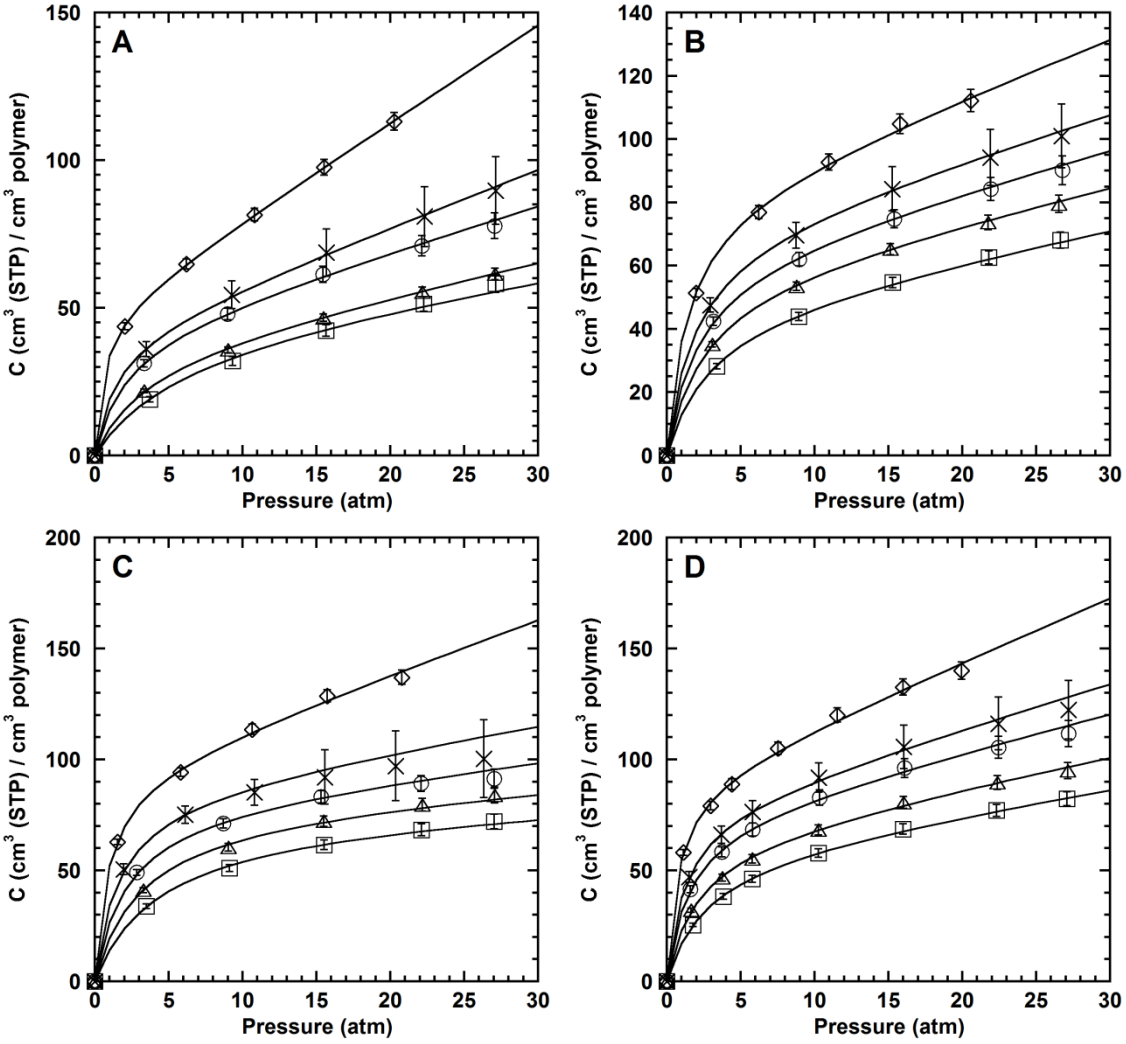

Figure 4.3. Concentration as a function of pressure of CO_2 at 50 °C (open squares), 35 °C (open triangles), 20 °C (open circles), 10 °C (crosses) and -10 °C (open diamonds) in: A) HAB-6FDA-CI polyimide, B) TR350-1hr, C) TR400-1hr, and D) TR450-30m. The continuous lines are dual mode model fits.

Gas solubilities at 10 atm are presented in Table 4.1 for HAB-6FDA and its TR analogs alongside Matrimid®, 6FDA-TAB, PTMSP, and Teflon AF2400® [1, 4-7] for comparison. As TR conversion increases, solubility increases for all gases with some decrease in solubility selectivity. As expected, solubility increases monotonically with increasing penetrant critical temperature (e.g., in the polyimide, solubility at 10 atm and

35 °C increased from 0.037 cm^3 (STP) / (cm^3 polymer atm) for N_2 to 1.0 for CH_4 and 3.8 for CO_2). Gas solubilities in HAB-6FDA polyimide are close to those in Matrimid® [6] with similar (if slightly higher) solubilities and correspondingly lower solubility selectivities (cf., Table 4.2). In general, solubility selectivities decrease as TR conversion increases.

Table 4.1. Solubilities of H_2, N_2, CH_4, and CO_2 in HAB-6FDA, its TR polymer analogs, Matrimid®, 6FDA-TAB, PTMSP, and AF2400®.

	S @ 35 °C, 10 atm (cm^3(STP) /(cm^3 polymer atm))				Ref.
	H_2	N_2	CH_4	CO_2	
T_c (K)	33.2	126.2	190.6	304.2	[8]
HAB-6FDA	0.110 ± 0.007	0.37 ± 0.04	1.0 ± 0.1	3.8 ± 0.1	H_2 from [1]; Remainder from this work
TR350-1hr	0.16 ± 0.01	0.79 ± 0.07	1.9 ± 0.2	5.5 ± 0.2	
TR400-1hr	0.25 ± 0.01	0.99 ± 0.08	2.6 ± 0.2	6.1 ± 0.3	
TR450-30m	0.27 ± 0.01	1.1 ± 0.1	2.5 ± 0.2	6.8 ± 0.3	
Matrimid®	0.12	0.30[a]	0.78[a]	3.4[a]	[1, 6]
6FDA-TAB	--	1.1[a]	2.3[a]	6.7[a]	[7]
PTMSP	0.42[a]	0.99[a]	2.8[a]	4.8[a]	[5]
AF2400®	0.21	0.60	0.98	2.6	[1, 4]

[a] Calculated from dual mode parameters.
NOTE: Uncertainties calculated by propagation of errors [2].

Table 4.2. Solubility selectivities in HAB-6FDA, its TR polymer analogs, Matrimid®, 6FDA-TAB, PTMSP, and AF2400® at 10 atm.

	Solubility Selectivities					Ref.
	CO_2/N_2	CO_2/CH_4	H_2/N_2	H_2/CO_2	H_2/CH_4	
HAB-6FDA	10± 1	3.6± 0.4	0.29 ± 0.03	0.029 ± 0.002	0.11 ± 0.01	H_2 from [1]; Remainder from this work
TR350-1hr	6.8± 0.5	2.9± 0.3	0.2 ± 0.02	0.03 ± 0.003	0.08 ± 0.01	
TR400-1hr	6.0± 0.8	2.4± 0.2	0.25 ± 0.03	0.041 ± 0.003	0.099 ± 0.009	
TR450-30m	5.8± 0.3	2.7± 0.3	0.23 ± 0.02	0.04 ± 0.003	0.11 ± 0.01	
Matrimid®	11	4.4	0.40	0.035	0.15	[1, 6]
6FDA-TAB	6.1	2.9	--	--	--	[7]
PTMSP	4.8	1.9	0.42	0.088	0.15	[5]
AF2400®	4.3	2.7	0.35	0.081	0.21	[1, 4]

NOTE: Uncertainties calculated by propagation of errors [2].

4.2.2 Effect of temperature on gas solubility

The temperature dependence of gas solubility coefficients in each of the samples is presented in Figure 4.4. S increased with increasing TR conversion, coinciding with an increase in FFV with thermal conversion (as discussed further below). At 35 °C, increases in solubility with TR conversion are similar to those reported by Smith et al. [3], with solubility increasing roughly 2-3 times the original value. This increase in solubility is ascribed, in part, to an increase in non-equilibrium free volume in the TR polymer structure [3]. For all species, solubility increases as temperature decreases and follows Arrhenius-like behavior. For each sample, H_2 solubility was approximately 70%

higher at -10 °C than at 50 °C. N_2, CH_4, and CO_2 solubilities were approximately 100% higher over the same range of temperatures.

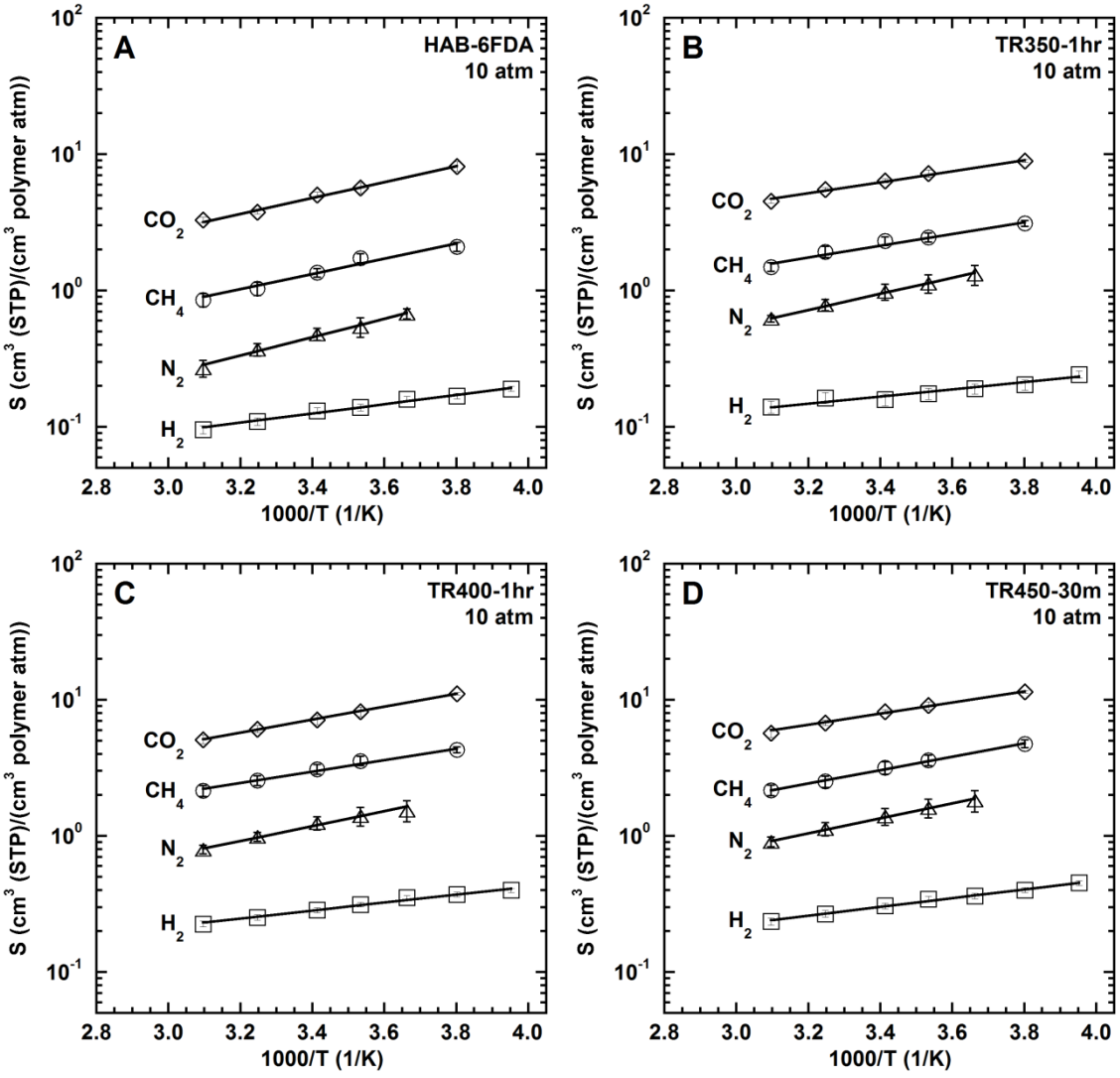

Figure 4.4. Solubilities at 10 atm for CO_2, CH_4, N_2, and H_2 at multiple temperatures for A) HAB-6FDA Polyimide, B) TR350-1hr, C) TR400-1hr, and D) TR450-30m. H_2 data are from Smith et al. [1].

In Figure 4.5, the CO_2 sorption coefficient is presented at multiple temperatures for a number of rubbery and glassy polymers, including HAB-6FDA polyimide and its

TR450-30m analogue. For PDMS, since it is a rubbery polymer, there is no contribution to S from Langmuir mode sorption, so gas solubility is lower than in the glassy polymers in Figure 4.5 [9]. HAB-6FDA and its TR polymer analogs have temperature-dependent sorption behavior similar to that of other high free volume, hexafluoroisopropylidene (6F)-containing polymers such as 6FDA-TAB [10].

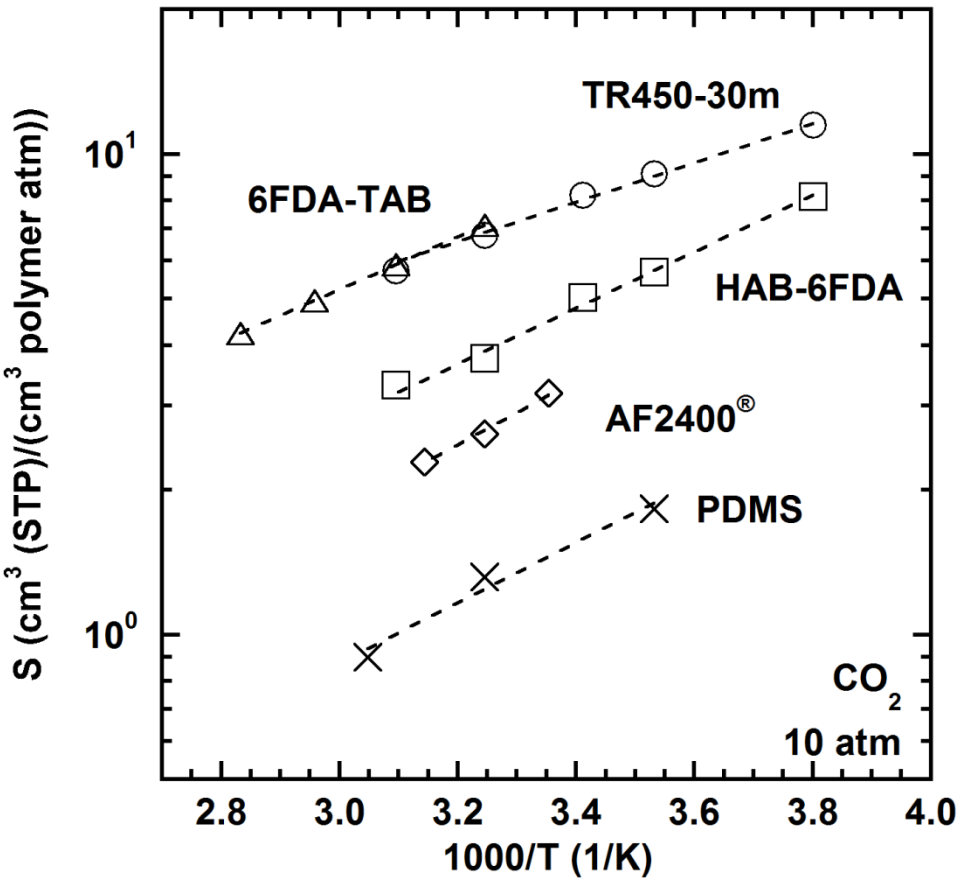

Figure 4.5. Solubility of CO_2 at 10 atm in HAB-6FDA polyimide (open squares) and TR450-30m (open circles), [10], AF2400® (open diamonds) [4], and PDMS (crosses) [11].

The slopes of the lines in Figure 4.4 may be used to calculate the enthalpies of sorption at 10 atm (cf., Equation [2-6]). The slopes of $\ln S$ versus $1/T$ change relatively

little with TR conversion, with CO_2 exhibiting the most significant variation. Values of ΔH_S for each gas and polymer at 10 atm are presented in Table 4.3. For many polymers, enthalpies of sorption become more exothermic with increasing penetrant T_c (i.e., $CO_2 < CH_4 < N_2 < H_2$) [8]. However, HAB-6FDA and its TR polymers exhibit an unusual order of enthalpies of sorption ($N_2 < CH_4 \approx CO_2 < H_2$). This trend has been observed previously in high FFV materials such as 6FDA-TAB [10]. Two factors are often invoked to rationalize this behavior. First, in the dual mode model, while b can have a strong temperature dependence, the temperature dependence of $b/(1+bp)$ is weaker and reduces the magnitude of the Langmuir contribution to the enthalpy of sorption. Additionally, C'_H typically is less temperature-dependent than b. Zimmerman and Koros found that, in polymers with large, relatively temperature-independent values of C'_H, the order of enthalpies of sorption can be affected by these factors [10].

Table 4.3. Enthalpies of sorption of HAB-6FDA, its TR analogs, 6FDA-TAB, 6FDA-6FpDA, and PIM-1 at 10 atm.

	% Conversion	ΔH_S (kJ/mol)				Ref.
		H_2	N_2	CH_4	CO_2	
T_c (K)		33.2	126.2	190.6	304.2	[8]
HAB-6FDA	0	-6.5 ± 0.6	-13 ± 2	-11 ± 1	-11 ± 1	H_2 from [1]; Remainder from this work
TR350-1hr	37	-5.0 ± 0.9	-11 ± 2	-8.2 ± 0.9	-7.7 ± 0.5	
TR400-1hr	58	-5.6 ± 0.5	-10 ± 2	-8 ± 1	-9.1 ± 0.6	
TR450-30m	67	-6.1 ± 0.6	-11 ± 2	-9 ± 1	-8 ± 1	
6FDA-TAB	--	--	-11.7	-11.7	-10.5	[10]
6FDA-6FpDA[a]	--	--	-13	-14.6	-15	[12]
PIM-1	--	--	-8.6	-11.2	-10.4	[13]

[a] Data at 5 atm.

As TR conversion increases, free volume increases [3, 14, 15]. As a result of higher free volume, S increases for all gases with increasing TR conversion due predominantly to a large Langmuir site contribution to solubility. Figure 4.6 presents the effect of TR conversion on CH_4 solubility at several temperatures. Solubility increases by a factor of 2-3. Similar increases in S as a function of TR conversion were observed for other gases, with CO_2 displaying the smallest increase in solubility, consistent with prior observations that smaller increase in CO_2 sorption, as compared to increases in sorption for gases such as N_2 and CH_4, is a result of the loss of acetate and carbonyl functional groups during thermal rearrangement [3].

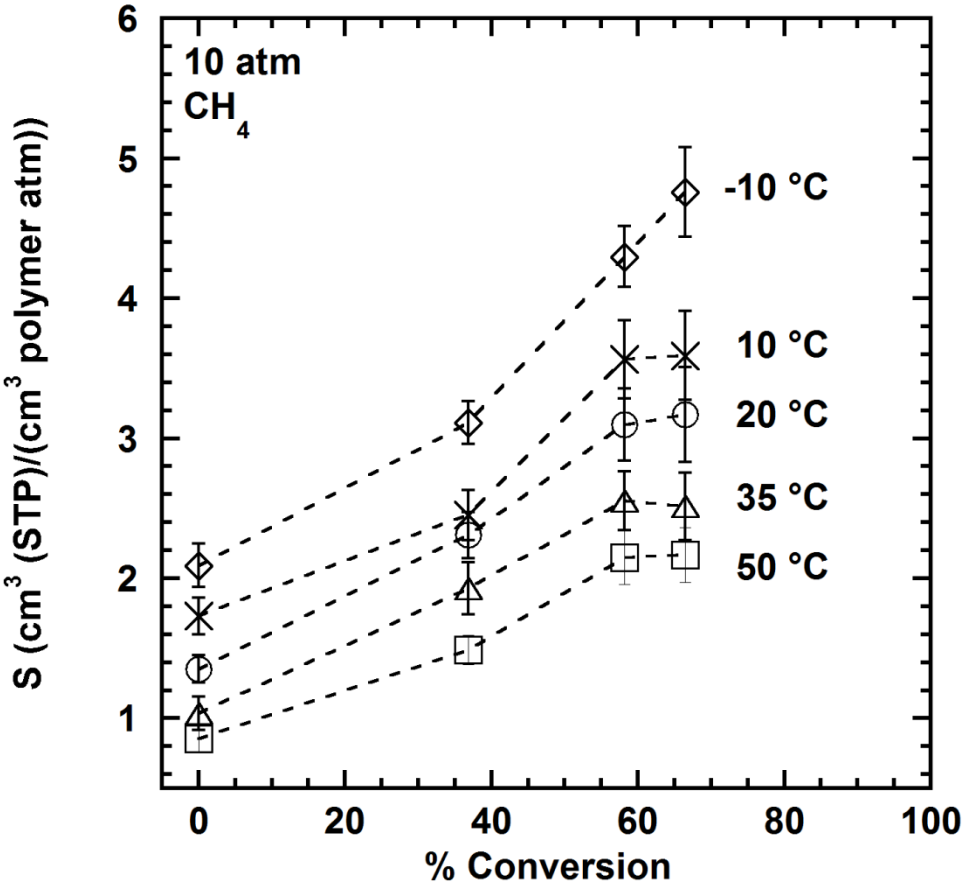

Figure 4.6. Solubility of CH_4 at various temperatures as a function of TR conversion.

While solubility increases with TR conversion, only modest changes in ΔH_S are observed (cf., Table 4.3). As TR conversion (and FFV) increase, the ratio of Langmuir to Henry's law sorption increases (as will be demonstrated below). Langmuir sorption lacks the energetic penalty of creating gaps between polymer chains to accommodate penetrant molecules that is commonly associated with Henry's Law sorption sites [16], so ΔH_S should become more exothermic as TR conversion increases. However, any trends in ΔH_S between the TR samples are largely within the uncertainty of the measurements. The most significant change in ΔH_S with TR conversion occurs between HAB-6FDA and TR350-1hr. ΔH_S decreases in magnitude for all gases for TR350-1hr. At this level of conversion, it is not quantitatively clear what fraction of mass loss comes from solid-state deprotection of the o-position acetate group in the form of acetic acid and what fraction comes from conversion of polyimide to PBO. However, Sanders et al. have predicted that most if not all of the acetate o-position moiety has been removed and replaced with hydroxyl functionality under these conditions [14]. The presence of hydroxyl functionality on unconverted polymer chain segments can lead to hydrogen bonding and a corresponding increase in the energy penalty associated with Henry's law sorption.

While solubilities change as a function of temperature, solubility selectivities remain relatively constant with temperature. Solubility selectivity can be expressed as a function of temperature according to a van't Hoff relationship:

$$\alpha_{S_A/S_B} = \frac{S_A}{S_B} = \frac{S_{0,A}}{S_{0,B}} e^{\frac{-1}{RT}\left(\Delta H_{S,A} - \Delta H_{S,B}\right)} \qquad [4\text{-}1]$$

where the variables are as defined in Equation [2-6]. If there is no significant difference in ΔH_S for a gas pair (for example, CO_2 and CH_4 for the TR450-30m sample have enthalpies of sorption of -8 ± 1 and -9 ± 1, respectively), $\Delta H_{S,A} - \Delta H_{S,B}$ is 0, and the exponential term of Equation [4-1] is 1. Solubility selectivities for all four samples

considered are plotted against inverse temperature in Figure 4.7. For all four samples at 10 atm, ΔH_S is nearly equivalent for CO_2 and CH_4, resulting in no substantial changes with CO_2/CH_4 selectivity as temperature is varied.

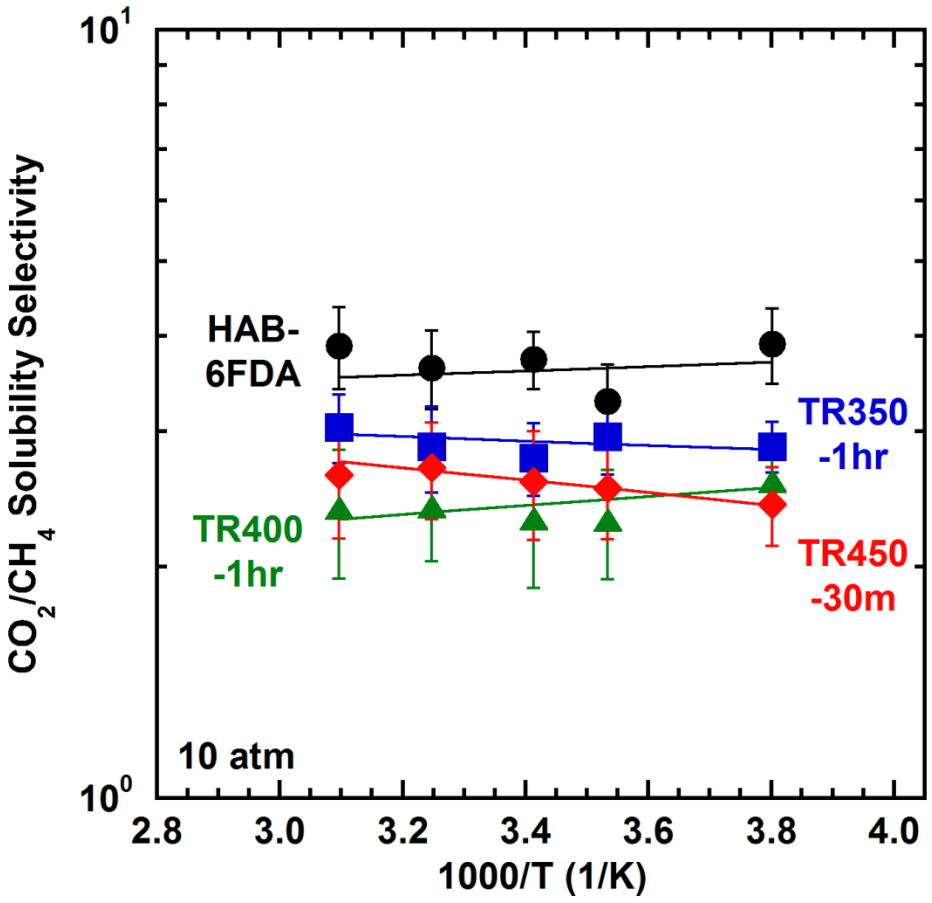

Figure 4.7. CO_2/CH_4 solubility selectivity as a function of inverse temperature for HAB-6FDA (black circles), TR350-1hr (blue squares), TR400-1hr (green triangles), and TR450-1hr (red diamonds). All data in this figure are at an upstream pressure of 10 atm.

The enthalpy of sorption can also be determined as a function of penetrant concentration [4, 16]. Figure 4.8A presents ΔH_I, the isosteric heat of sorption, as a function of penetrant concentration for several penetrants in the TR450-30m sample. The

dual mode model was used to interpolate concentration versus pressure isotherms and to calculate ΔH_I according to the method described by Koros et al. [16]. For N_2, the Langmuir sites were not yet saturated at the highest concentrations achieved, resulting in no significant change in ΔH_I. For CO_2 (the most condensable penetrant considered), the upturn in ΔH_I above 60 cm^3 (STP) / cm^3 polymer is ascribed to filling the Langmuir sites, leading to increasing sorption into Henry's law regions where the endothermic barrier to gas sorption becomes significant. This effect is not observed for the other penetrants. Koros et al. predict a minimum in ΔH_I [16] though this minimum is not always observed and likely occurs outside the range of concentrations (i.e., pressures) considered. Similar plots for other samples are reported in Figure 4.9 and exhibit similar trends as those presented in Figure 4.8A. ΔH_I represents redistribution of penetrant molecules between Henry's law and Langmuir populations as pressure and temperature are varied to maintain a constant temperature and is not always directly comparable to ΔH_S at a constant pressure.

Except for H_2, where solubility was nearly independent of pressure, enthalpies of sorption become less exothermic as gas pressure increased. As gases dissolve into the polymer matrix, there is initially only a minor contribution from Henry's law sorption to overall sorption. At higher concentrations, the endothermic penalty in creating Henry's law sorption sites results in an endothermic shift in ΔH_S. An example of this behavior is presented in Figure 4.8B.

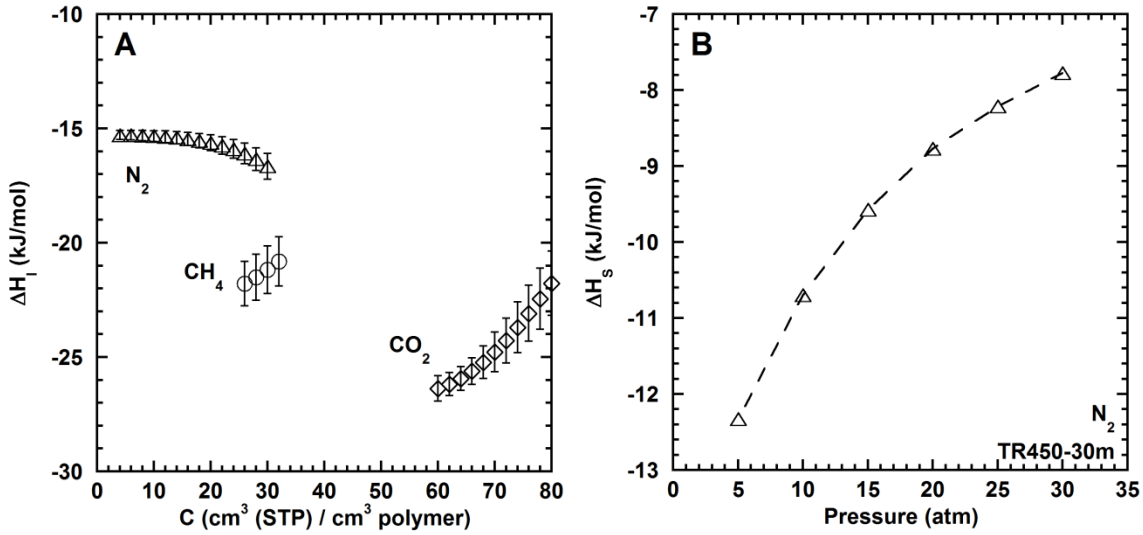

Figure 4.8. A) Isosteric heat of sorption (ΔH_1) for N_2, CH_4, and CO_2 in TR450-30m. Uncertainties were estimated [2] to be approximately 5-10%. B) Enthalpy of sorption for N_2 in TR450-30m as a function of pressure. The dashed line is a guide for the eye.

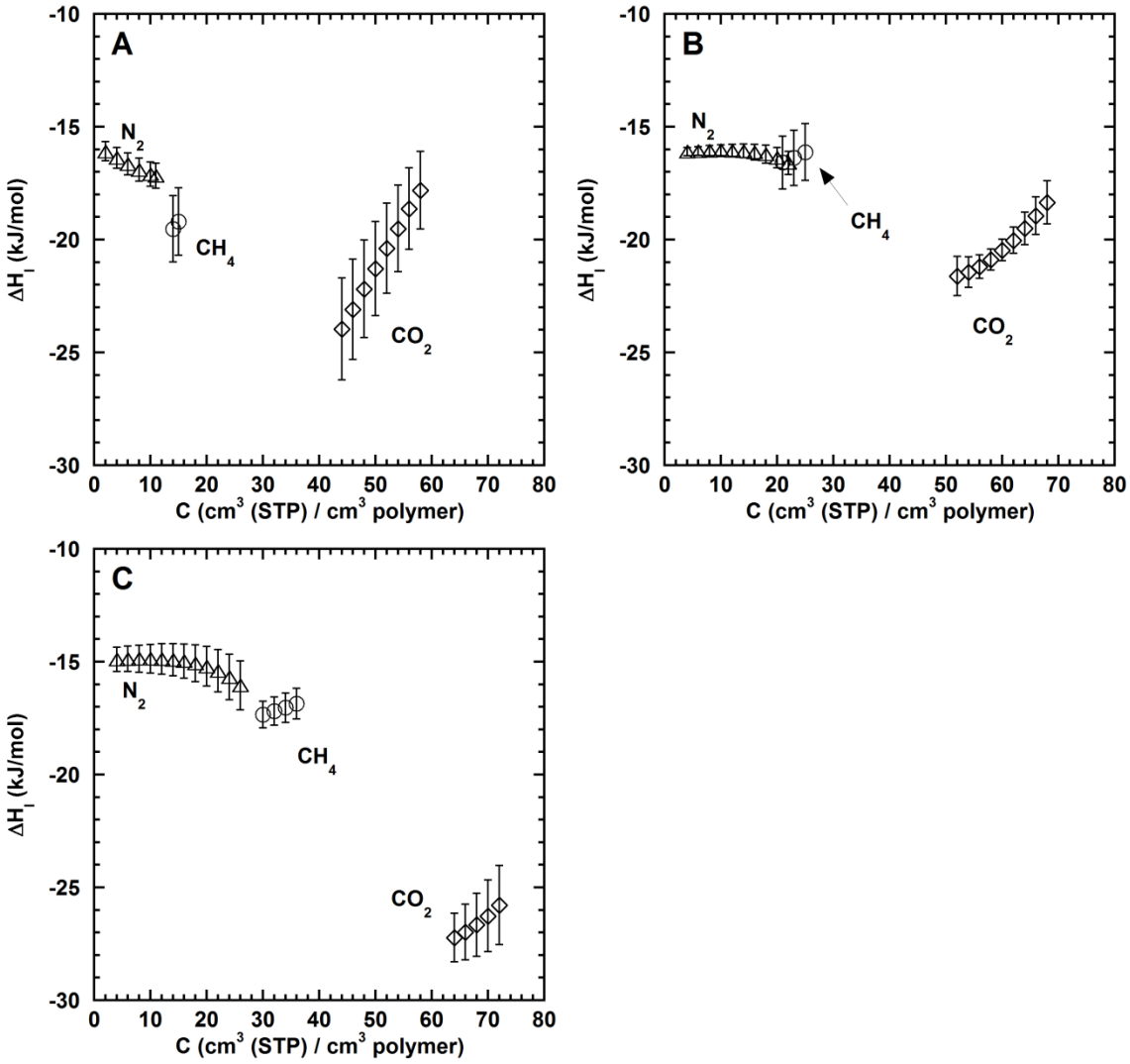

Figure 4.9. Isosteric heat of sorption (ΔH_I) for N_2, CH_4, and CO_2 in: A) HAB-6FDA, B) TR350-1hr, and C) TR400-1hr.

4.2.3 Method of dual mode modeling as a function of temperature

The dual mode model was used to analyze the sorption data presented in this study. Each sorption isotherm (C versus p for one gas and one temperature) can be considered separately and represented by a set of dual mode parameters (i.e., k_D, b, and

C'_H). The best-fit parameters were determined by a nonlinear least-squares optimization. χ^2 was calculated using Equation [4-2] [2]:

$$\chi^2 = \sum_{i=1}^{N} \frac{1}{\sigma_i^2}\left[\left(S_i - S_{i,model}\right)^2\right] = \sum_{i=1}^{N} \frac{1}{\sigma_i^2}\left[\left(S_i - \left(k_D + C'_H \frac{b}{1+bp_i}\right)\right)^2\right] \qquad [4\text{-}2]$$

where σ_i is the experimental uncertainty in the solubility measurement, p_i is the pressure at each step, and N is the number of data points.

The dual mode model is sensitive to variations in measurements, pressure range, and parameter estimation methodology [17-20], so any set of dual mode parameters must be considered in conjunction with these factors. Furthermore, more complex data sets (such as those including several gases, temperatures, samples, and ranges of pressure) can complicate the fitting procedure and result in different best-fit parameter values [20, 21]. Several methods of fitting were attempted. The first fit was an unconstrained fit of each isotherm for each gas at each temperature in each sample.

Some trends with temperature are expected: k_D and b should follow Arrhenius-van't Hoff relations, and C'_H values should diminish as temperatures increase but do not follow a van't Hoff relation [16]. The second method fit all isotherms measured for each gas and sample, constraining k_D and b using Eqs. [2-15] and [2-16], and allowing C'_H to vary with temperature. The third method of fitting was similar to the second, but $\ln k_D$ and $\ln b$ at 35 °C were constrained to be linear with penetrant critical temperature with a slope of 0.017 K^{-1} [22, 23].

Method 1 was used as a first approximation, and some expected trends ($\ln k_D$ and $\ln b$ being linear with $1/T$) were observed, albeit with some variation. Method 2 enforced these trends, but did not enforce any correlation of k_D and b between the different gases considered. Method 2 also had slopes of $\ln k_D$ versus T_c for some, but not all, samples that were below the expected value (i.e., 0.017 K^{-1}). Method 3 enforced the

relationship between $\ln k_D$ and $\ln b$ at 35 °C and T_c and provided a self-consistent modeling results. Therefore, Method 3 was selected for further analysis.

To obtain initial parameter estimates, a graphical fitting method [24] was first used to estimate values of k_D, C'_H, and b for each isotherm. The slopes and intercepts of $\ln k_D$ and $\ln b$ with $1/T$ (enthalpies and exponential prefactors in Eqs. [2-15] and [2-16]) from the graphical fit were estimated and used as starting values for the constrained fit of Method 3. The ultimate fitting considered each temperature and gas simultaneously in a given sample (see Table 4.4 for a list of equations used) and found the minimum in χ^2 by varying the intercepts for $\ln k_D$ and $\ln b$ (i.e., N_1 and N_2) versus T_c, ΔH_D, ΔH_b, and five separate values of C'_H for each gas, one for each temperature considered. The values of ΔH_D and ΔH_b, the heats of sorption in the Henry's law and Langmuir modes, respectively, were constrained to be negative. Additionally, M, the slope of $\ln k_D$ and $\ln b$ versus T_c, was constrained to 0.017 K^{-1}. This value was selected to be in the range of literature values of k_D 0.017 to 0.019 K^{-1} reported for other Henry's law sorption coefficients such as those in liquids and rubbery polymers [22, 23]. Tables 4.5 through 4.7 present the final dual mode parameters.

Table 4.4. Equations used in dual mode fitting of each sample.

Equation	Notes
$\ln k_{D,r} = N_1 + MT_c$ $\ln b_r = N_2 + MT_c$	$M = 0.017\ K^{-1}$, [22, 23] N_1 and N_2 are adjustable parameters.
$k_D = k_{D,r} e^{\frac{-\Delta H_D}{R}\left(\frac{1}{T}-\frac{1}{T_r}\right)}$ $b = b_r e^{\frac{-\Delta H_b}{R}\left(\frac{1}{T}-\frac{1}{T_r}\right)}$ C'_H $(unconstrained)$	$T_r = 308.15\ K$ Individual values for each temperature and gas.
$S_{i,model} = k_D + C'_H \frac{b}{1+bp}$	Calculated for each gas, temperature, and pressure.
$\chi^2 = \sum_{gas}\sum_{T}\sum_{i}\frac{1}{\sigma_i^2}\left[\left(S_i - S_{i,model}\right)^2\right]$	

Table 4.5. Dual mode parameters for N_2 at various temperatures.

Sample	T (°C)	k_D cm^3(STP) / (cm^3 polymer atm))	b (1/atm)	C'_H (cm^3(STP) / cm^3 polymer)
HAB-6FDA	0	0.08 + 0.04 - 0.04	0.05 + 0.02 - 0.01	19 + 5 - 4
	10	0.08 + 0.02 - 0.03	0.040 + 0.008 - 0.007	17 + 3 - 3
	20	0.07 + 0.01 - 0.02	0.034 + 0.004 - 0.004	17 + 2 - 2
	35	0.069 + 0.004 - 0.004	0.027 + 0.003 - 0.003	15 + 1 - 1
	50	0.06 + 0.02 - 0.01	0.022 + 0.005 - 0.004	12 + 2 - 2
TR350-1hr	0	0.16 + 0.02 - 0.02	0.075 + 0.006 - 0.006	29 + 2 - 2
	10	0.12 + 0.01 - 0.01	0.057 + 0.003 - 0.003	29 + 1 - 1
	20	0.096 + 0.005 - 0.006	0.045 + 0.002 - 0.002	29.9 + 0.9 - 0.8
	35	0.069 + 0.004 - 0.004	0.032 + 0.001 - 0.001	30.3 + 0.8 - 0.8
	50	0.052 + 0.004 - 0.004	0.023 + 0.002 - 0.001	30 + 1 - 1
TR400-1hr	0	0.19 + 0.03 - 0.04	0.074 + 0.009 - 0.008	34 + 3 - 3
	10	0.13 + 0.02 - 0.02	0.057 + 0.005 - 0.005	37 + 2 - 2
	20	0.096 + 0.008 - 0.009	0.045 + 0.003 - 0.002	38 + 1 - 1
	35	0.061 + 0.005 - 0.005	0.033 + 0.002 - 0.002	39 + 1 - 1
	50	0.04 + 0.005 - 0.004	0.024 + 0.002 - 0.002	38 + 2 - 2
TR450-30m	0	0.21 + 0.02 - 0.02	0.080 + 0.005 - 0.004	39 + 2 - 1
	10	0.16 + 0.01 - 0.01	0.063 + 0.002 - 0.002	40 + 1 - 1
	20	0.123 + 0.005 - 0.005	0.050 + 0.001 - 0.001	40.0 + 0.8 - 0.7
	35	0.086 + 0.004 - 0.004	0.037 + 0.001 - 0.001	40.3 + 0.7 - 0.7
	50	0.062 + 0.004 - 0.004	0.028 + 0.001 - 0.001	40 + 1 - 1

Table 4.6. Dual mode parameters for CH_4 at various temperatures.

Sample	T (°C)	k_D cm^3(STP) / (cm^3 polymer atm))	b (1/atm)	C'_H (cm^3(STP) / cm^3 polymer)
HAB-6FDA	-10	0.5 + 0.2 - 0.3	0.3 + 0.3 - 0.2	21 + 10 - 5
	10	0.33 + 0.06 - 0.12	0.17 + 0.06 - 0.05	23 + 6 - 3
	20	0.27 + 0.03 - 0.06	0.12 + 0.02 - 0.02	20 + 3 - 2
	35	0.21 + 0.01 - 0.01	0.081 + 0.010 - 0.009	19 + 2 - 2
	50	0.16 + 0.05 - 0.02	0.06 + 0.01 - 0.01	20 + 4 - 4
TR350-1hr	-10	0.5 + 0.2 - 0.3	0.31 + 0.11 - 0.09	35 + 8 - 6
	10	0.34 + 0.06 - 0.1	0.17 + 0.03 - 0.03	35 + 4 - 3
	20	0.28 + 0.03 - 0.05	0.14 + 0.01 - 0.01	37 + 3 - 2
	35	0.21 + 0.01 - 0.01	0.095 + 0.004 - 0.004	37 + 1 - 1
	50	0.16 + 0.03 - 0.02	0.070 + 0.007 - 0.006	33 + 3 - 3
TR400-1hr	-10	0.7 + 0.2 - 0.2	0.35 + 0.08 - 0.07	48 + 6 - 5
	10	0.35 + 0.05 - 0.07	0.19 + 0.02 - 0.02	52 + 4 - 3
	20	0.27 + 0.03 - 0.03	0.14 + 0.01 - 0.01	51 + 2 - 2
	35	0.18 + 0.01 - 0.01	0.098 + 0.005 - 0.005	51 + 2 - 2
	50	0.13 + 0.02 - 0.01	0.069 + 0.006 - 0.006	52 + 3 - 3
TR450-30m	-10	0.9 + 0.2 - 0.2	0.6 + 0.1 - 0.1	45 + 5 - 4
	10	0.48 + 0.05 - 0.06	0.26 + 0.03 - 0.02	44 + 3 - 2
	20	0.37 + 0.02 - 0.03	0.18 + 0.01 - 0.01	45 + 2 - 2
	35	0.26 + 0.01 - 0.01	0.110 + 0.003 - 0.003	44 + 1 - 1
	50	0.19 + 0.02 - 0.01	0.070 + 0.005 - 0.004	49 + 3 - 3

Table 4.7. Dual mode parameters for CO_2 at various temperatures.

Sample	T (°C)	k_D cm^3(STP) / (cm^3 polymer atm))	b (1/atm)	C'_H (cm^3(STP) / cm^3 polymer)
HAB-6FDA	-10	3.2 + 0.5 - 0.4	1.7 + 3.3 - 0.7	49 + 8 - 8
	10	2.2 + 0.1 - 0.1	1.0 + 0.7 - 0.2	37 + 4 - 4
	20	1.81 + 0.09 - 0.09	0.8 + 0.3 - 0.1	35 + 2 - 3
	35	1.42 + 0.08 - 0.09	0.56 + 0.07 - 0.06	27 + 2 - 2
	50	1.1 + 0.1 - 0.1	0.4 + 0.1 - 0.1	27 + 4 - 3
TR350-1hr	-10	1.7 + 0.4 - 0.3	0.69 + 0.18 - 0.09	83 + 5 - 8
	10	1.6 + 0.2 - 0.1	0.68 + 0.09 - 0.05	65 + 4 - 4
	20	1.5 + 0.1 - 0.1	0.67 + 0.05 - 0.04	56 + 2 - 2
	35	1.43 + 0.07 - 0.07	0.66 + 0.03 - 0.03	47 + 1 - 1
	50	1.36 + 0.09 - 0.10	0.65 + 0.04 - 0.05	36 + 2 - 2
TR400-1hr	-10	2.1 + 0.3 - 0.4	1.0 + 0.2 - 0.1	99 + 7 - 6
	10	1.6 + 0.1 - 0.2	0.82 + 0.08 - 0.07	76 + 4 - 4
	20	1.5 + 0.1 - 0.1	0.76 + 0.05 - 0.04	65 + 2 - 2
	35	1.26 + 0.09 - 0.1	0.67 + 0.04 - 0.03	55 + 2 - 2
	50	1.1 + 0.1 - 0.1	0.61 + 0.05 - 0.05	47 + 2 - 2
TR450-30m	-10	2.8 + 0.3 - 0.3	1.4 + 0.3 - 0.2	90 + 5 - 5
	10	2.2 + 0.1 - 0.1	1.03 + 0.1 - 0.08	72 + 3 - 3
	20	2.04 + 0.09 - 0.1	0.91 + 0.05 - 0.04	66 + 2 - 2
	35	1.78 + 0.08 - 0.08	0.76 + 0.02 - 0.02	54 + 1 - 1
	50	1.6 + 0.1 - 0.1	0.64 + 0.04 - 0.04	45 + 2 - 2

4.2.4 Method of calculating dual mode parameter uncertainties

In simple, non-coupled systems, the uncertainty of any given parameter can be probed by varying that parameter around its optimal value with all other parameters fixed to determine the point at which the change in χ^2 ($\Delta\chi^2 = \chi^2 - \chi^2_{\min}$) is equal to unity [2]. By varying two parameters independently, a 2-dimensional cross-section can be drawn where $\Delta\chi^2 = 1$. In well behaved, non-coupled systems, this contour is elliptical, and the limits of this 2-dimensional shape in each parameter axis represent the uncertainty in that parameter [2]. However, this treatment underestimates the true uncertainty when the parameters are coupled, such as those in the dual-mode model, which have $\Delta\chi^2 = 1$ boundaries that are non-elliptical [2].

The uncertainty in each dual mode parameter was determined during the fitting process to estimate parameter values. First, a coarse estimation of the uncertainty in each parameter was made by varying each parameter (with all other parameters fixed) around $\chi^2_{\min}$, fitting a parabola to $\Delta\chi^2$ with respect to the varied parameter values, and estimating the point at which $\Delta\chi^2 = 1$. Then, a Monte Carlo method (described previously [19, 25]) was utilized to provide a more accurate estimate of the uncertainties in each fitted parameter.

The Monte Carlo method for determining uncertainties begins with selection of a random parameter, perturbing and fixing its value, and allowing all other parameters to vary to a new value to minimize χ^2. If the value of $\Delta\chi^2$ is below 0.95, another parameter is randomly selected and perturbed, and all non-fixed parameters are optimized. The same parameter can be randomly selected multiple times. This selection-perturbation-optimization process repeats until $\Delta\chi^2$ is between 0.95 and 1. (If a $\Delta\chi^2$ > 1 is found, that step is rejected and another parameter is chosen.) The final set of parameters are compared to the best-fit ($\chi^2_{\min}$), and the distance from best-fit for each

parameter is recorded as the uncertainty for that step. This process can be summarized as a random walk through parameter space starting at the minimum (best fit) χ^2 with re-optimization of all non-perturbed parameters at each step. The largest perturbations (largest uncertainties) in each parameter are compared, and the final uncertainty is recorded by taking the maximum positive and negative deviations from best-fit.

The above method probes the regions of parameter-space where $\Delta\chi^2 = 1$. By taking cross-sections of this region of space and fixing all other parameters, the $\Delta\chi^2 = 1$ surface can be visualized in two dimensions. The confidence interval boundary (uncertainty boundary) for dual-mode parameters can result in so-called "banana" shaped curves [18, 19].

The above process becomes accurate after a large number of iterations. A Monte Carlo simulation of 5000 iterations was found to be sufficient to accurately estimate the uncertainties presented in Tables 4.5 through 4.7 alongside the dual mode parameters. The iteration count was found by increasing the iteration number until no further change in uncertainties was observed. While the uncertainties for these parameters can be quite large, calculations of quantities based on dual-mode parameters (such as S^{inf}, etc.) are more accurate, as noted previously [19]. Utilizing the parameter uncertainties in Tables 4.5-4.7 directly to predict the uncertainties of calculated quantities is misleading due to the coupled nature. Calculated value uncertainties can be estimated alongside parameter uncertainties by a method identical to the estimation of parameter uncertainties [19, 25]. More specifically, the end of each random walk may include perturbations of parameters such that the change in one is offset. For example, a two-fold increase in b could combine with a two-fold decrease in C_H' while k_D is constant, resulting in a value of S^{inf} that has not changed. This behavior can result in lower uncertainties than predicted based

on the final parameters. Uncertainties by the Monte Carlo method are often asymmetric and are displayed as such.

4.2.5 Dependence of temperature on infinite dilution solubility

The sorption characteristics of HAB-6FDA and its corresponding TR polymer analogs were further analyzed with the dual mode model. The coupled nature of the model parameters makes unique values difficult to obtain, so one must be cautious in interpreting the parameter values [18]. Furthermore, different regression methods can yield different parameter values [17-20]. Predictions and calculations with the dual mode parameters (such as C versus p isotherms and, to a lesser extent, infinite dilution solubilities) are relatively more certain, because perturbations of dual mode parameters moving in opposite directions can result in the same predicted values (e.g., an increase in C_H' can offset a decrease in b, but values of, for example, S^{inf} in Equation [2-17] can remain largely unchanged). However, further calculations based on predicted values can result in propagation of any variations, so the output of dual mode modeling must be considered with caution.

Infinite dilution solubility coefficients were estimated using Equation [2-17], and the values exhibit a clear trend with critical temperature for all gases, as shown in Figure 4.10. Infinite dilution solubilities at 35 °C are presented in Table 4.8. The slopes of the logarithm of S^{inf} against T_c are between 0.018-0.019 K^{-1} for all samples, which is within the range typically observed for both glassy and rubbery polymers [8, 22]. Similar to solubilities at 10 atm, solubilities at infinite dilution increase by a factor of 2-4 with increasing TR conversion.

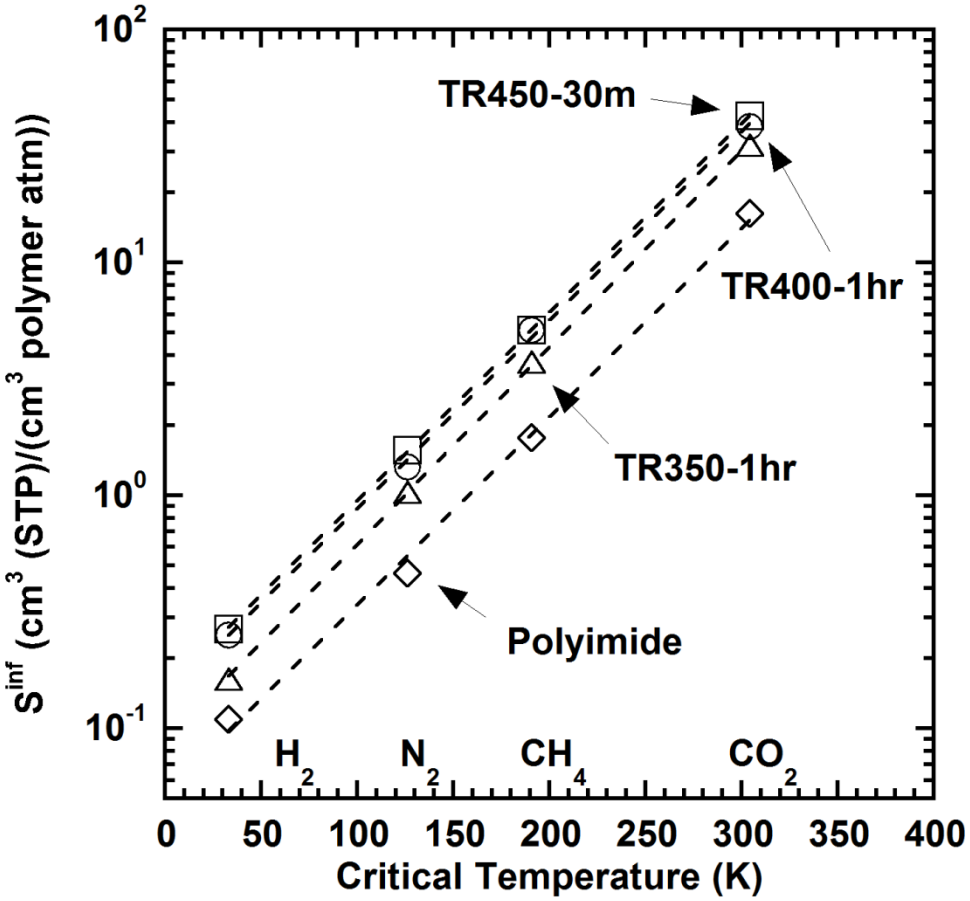

Figure 4.10. Infinite dilution solubilities of HAB-6FDA polyimide (diamonds), TR350-1hr (triangles), TR400-1hr (circles), and TR450-30m (squares) versus penetrant critical temperature.

Table 4.8. Infinite dilution solubilities of H_2, N_2, CH_4, and CO_2 in HAB-6FDA, its TR polymer analogs, Matrimid®, 6FDA-TAB, PTMSP, and AF2400.

	S^{inf} at 35 °C (cm^3(STP) /(cm^3 polymer atm))				Ref.
	H_2	N_2	CH_4	CO_2	
T_c (K)	33.2	126.2	190.6	304.2	[8]
HAB-6FDA	0.110 ± 0.007	$0.47^{+0.02}_{-0.02}$	$1.8^{+0.1}_{-0.1}$	16^{+1}_{-1}	H_2 from [1]; Remainder from this work
TR350-1hr	0.16 ± 0.01	$1.04^{+0.02}_{-0.02}$	$3.7^{+0.1}_{-0.1}$	32^{+1}_{-1}	
TR400-1hr	0.25 ± 0.01	$1.33^{+0.04}_{-0.03}$	$5.1^{+0.2}_{-0.2}$	39^{+1}_{-1}	
TR450-30m	0.27 ± 0.01	$1.56^{+0.02}_{-0.02}$	$5.1^{+0.1}_{-0.1}$	$42.6^{+0.8}_{-1.0}$	
Matrimid®	0.118	0.46	1.64	10.8	[1, 6]
6FDA-TAB	--	1.55	5.64	44.2	[7]
PTMSP	0.44	1.12	3.60	6.25	[5]
AF2400®	0.21[a]	0.68	1.25	3.42	[4]

[a] Data at 25 °C. [b] Calculated from dual mode parameters. NOTE: Uncertainties calculated by Monte Carlo simulation [19, 25].

Infinite dilution solubility selectivities were calculated and are included in Table 4.9. Infinite dilution solubility selectivities are higher than the corresponding solubility selectivities at 10 atm. As at 10 atm, infinite dilution solubility selectivities decrease with TR conversion but are significantly higher than those of high free volume materials such as PTMSP and AF2400® [4, 5]. Robeson and Smith found a slight dependence of solubility selectivity on fractional free volume through analysis of a large data set of solubility data for polymers [26]. The higher solubility selectivities than other high free volume materials seen here could be ascribed to a form of structured free volume

elements (such as, for example, hour glass shaped pores [15]) that are more well defined than in other polymers.

Table 4.9. Infinite dilution selectivities in HAB-6FDA, its TR polymer analogs, Matrimid®, 6FDA-TAB, PTMSP, and AF2400.

	Infinite Dilution Solubility Selectivities at 35 °C					Ref.
	CO_2/N_2	CO_2/CH_4	H_2/N_2	H_2/CO_2	H_2/CH_4	
HAB-6FDA	34 ± 3	8.9 ± 0.7	0.23 ± 0.02	0.0069 ± 0.0006	0.061 ± 0.005	H_2 from [1]; Remainder from this work
TR350-1hr	31 ± 1	8.6 ± 0.4	0.15 ± 0.01	0.0050 ± 0.0003	0.043 ± 0.003	
TR400-1hr	29 ± 1	7.6 ± 0.4	0.188 ± 0.009	0.0060 ± 0.0003	0.049 ± 0.003	
TR450-30m	27.3 ± 0.7	8.4 ± 0.2	0.173 ± 0.007	0.0063 ± 0.0003	0.053 ± 0.002	
Matrimid®	23	6.6	0.26	0.011	0.07	[1, 6]
6FDA-TAB	29	7.8	--	--	--	[7]
PTMSP	5.6	1.7	0.39	0.070	0.12	[5]
AF2400®	5.0	2.7	0.31	0.06	0.17	[4]

NOTE: Uncertainties calculated by propagation of errors [2].

4.3 REFERENCES

[1] Z.P. Smith, R.R. Tiwari, T.M. Murphy, D.F. Sanders, K.L. Gleason, D.R. Paul, B.D. Freeman, Hydrogen sorption in polymers for membrane applications, Polymer, 54 (2013) 3026-3037.

[2] P.R. Bevington, D.K. Robinson, Data reduction and error analysis for the physical sciences, McGraw Hill, Boston, 2003.

[3] Z.P. Smith, D.F. Sanders, C.P. Ribeiro, R. Guo, B.D. Freeman, D.R. Paul, J.E. McGrath, S. Swinnea, Gas sorption and characterization of thermally rearranged polyimides based on 3,3′-dihydroxy-4,4′-diamino-biphenyl (HAB) and 2,2′-bis-(3,4-dicarboxyphenyl) hexafluoropropane dianhydride (6FDA), Journal of Membrane Science, 415-416 (2012) 558-567.

[4] T.C. Merkel, V. Bondar, K. Nagai, B.D. Freeman, Y.P. Yampolskii, Gas sorption, diffusion, and permeation in poly(2,2-bis(trifluoromethyl)-4,5-difluoro-1,3-dioxole-co-tetrafluoroethylene), Macromolecules, 32 (1999) 8427-8440.

[5] T.C. Merkel, V. Bondar, K. Nagai, B.D. Freeman, Sorption and transport of hydrocarbon and perfluorocarbon gases in poly(1-trimethylsilyl-1-propyne), Journal of Polymer Science Part B: Polymer Physics, 38 (2000) 273-296.

[6] T.T. Moore, W.J. Koros, Gas sorption in polymers, molecular sieves, and mixed matrix membranes, Journal of Applied Polymer Science, 104 (2007) 4053-4059.

[7] C.M. Zimmerman, W.J. Koros, Polypyrrolones for membrane gas separations. I. Structural comparison of gas transport and sorption properties, Journal of Polymer Science Part B: Polymer Physics, 37 (1999) 1235-1249.

[8] S. Matteucci, Y. Yampolskii, B.D. Freeman, I. Pinnau, Transport of gases and vapors in glassy and rubbery polymers, in: Y. Yampolskii, I. Pinnau, B. Freeman (Eds.) Materials science of membranes for gas and vapor separation, John Wiley & Sons, Ltd, Chichester, UK, 2006, pp. 1-47.

[9] T.C. Merkel, V.I. Bondar, K. Nagai, B.D. Freeman, I. Pinnau, Gas sorption, diffusion, and permeation in poly(dimethylsiloxane), Journal of Polymer Science Part B: Polymer Physics, 38 (2000) 415-434.

[10] C.M. Zimmerman, W.J. Koros, Polypyrrolones for membrane gas separations. II. Activation energies and heats of sorption, Journal of Polymer Science Part B: Polymer Physics, 37 (1999) 1251-1265.

[11] V.M. Shah, B.J. Hardy, S.A. Stern, Solubility of carbon dioxide, methane, and propane in silicone polymers: Effect of polymer side chains, Journal of Polymer Science Part B: Polymer Physics, 24 (1986) 2033-2047.

[12] L.M. Costello, W.J. Koros, Thermally stable polyimide isomers for membrane-based gas separations at elevated temperatures, Journal of Polymer Science Part B: Polymer Physics, 33 (1995) 135-146.

[13] P. Li, T.S. Chung, D.R. Paul, Temperature dependence of gas sorption and permeation in PIM-1, Journal of Membrane Science, 450 (2014) 380-388.

[14] D.F. Sanders, R. Guo, Z.P. Smith, Q. Liu, K.A. Stevens, J.E. McGrath, D.R. Paul, B.D. Freeman, Influence of polyimide precursor synthesis route and ortho-position functional group on thermally rearranged (TR) polymer properties: Conversion and free volume, Polymer, 55 (2014) 1636-1647.

[15] H.B. Park, C.H. Jung, Y.M. Lee, A.J. Hill, S.J. Pas, S.T. Mudie, E. Van Wagner, B.D. Freeman, D.J. Cookson, Polymers with cavities tuned for fast selective transport of small molecules and ions, Science, 318 (2007) 254-258.

[16] W.J. Koros, D.R. Paul, G.S. Huvard, Energetics of gas sorption in glassy polymers, Polymer, 20 (1979) 956-960.

[17] E.S. Sanders, High-pressure sorption of pure and mixed gases in glassy polymers (Ph.D. Dissertation), North Carolina State University, Raleigh, 1983.

[18] W.J. Koros, A.H. Chan, D.R. Paul, Sorption and transport of various gases in polycarbonate, Journal of Membrane Science, 2 (1977) 165-190.

[19] K.L. Gleason, Z.P. Smith, Q. Liu, D.R. Paul, B.D. Freeman, Pure- and mixed-gas permeation of CO_2 and CH_4 in thermally rearranged polymers based on 3,3'-dihydroxy-4,4'-diamino-biphenyl (HAB) and 2,2'-bis-(3,4-dicarboxyphenyl) hexafluoropropane dianhydride (6FDA), Journal of Membrane Science, 475 (2015) 204-214.

[20] V.I. Bondar, Y. Kamiya, Y.P. Yampol'skii, On pressure dependence of the parameters of the dual-mode sorption model, Journal of Polymer Science Part B: Polymer Physics, 34 (1996) 369-378.

[21] A. Morisato, B.D. Freeman, I. Pinnau, C.G. Casillas, Pure hydrocarbon sorption properties of poly(1-trimethylsilyl-1-propyne) (PTMSP), poly(1-phenyl-1-propyne) (PPP), and PTMSP/PPP blends, Journal of Polymer Science Part B: Polymer Physics, 34 (1996) 1925-1934.

[22] R.S. Prabhakar, B.D. Freeman, I. Roman, Gas and vapor sorption and permeation in poly(2,2,4-trifluoro-5-trifluoromethoxy-1,3-dioxole-co-tetrafluoroethylene), Macromolecules, 37 (2004) 7688-7697.

[23] G.E. Serad, B.D. Freeman, M.E. Stewart, A.J. Hill, Gas and vapor sorption and diffusion in poly(ethylene terephthalate), Polymer, 42 (2001) 6929-6943.

[24] W.J. Koros, D.R. Paul, A.A. Rocha, Carbon dioxide sorption and transport in polycarbonate, Journal of Polymer Science: Polymer Physics Edition, 14 (1976) 687-702.

[25] S. Mazumdar, Monte Carlo methods for confidence bands in nonlinear regression (M.S. Thesis), University of North Florida, Jacksonville, 1995.

[26] L.M. Robeson, Z.P. Smith, B.D. Freeman, D.R. Paul, Contributions of diffusion and solubility selectivity to the upper bound analysis for glassy gas separation membranes, Journal of Membrane Science, 453 (2014) 71-83.

Chapter 5: Influence of temperature on gas permeability and diffusivity in thermally rearranged polymers

5.1 SUMMARY

Gas permeation properties of thermally rearranged (TR) polymers have been broadly studied, but the effect of temperature on gas permeation has not been fully explored. Permeabilities of H_2, N_2, CH_4, and CO_2 in HAB-6FDA and its TR polymer analogs were measured as a function of pressure (up to 32 atm) and temperature between -10 and 50 °C. Permeabilities increased with increasing temperature, with the exception of CO_2 in the most highly converted TR polymer, and diffusivities increased with increasing temperature for all samples. CO_2 plasticization was observed at low temperatures for the polyimide and lower converted samples but was not observed in highly converted TR samples, indicating increased plasticization resistance in more highly converted TR samples. Activation energies of permeation increased slightly at low levels of TR conversion then decreased substantially at higher TR conversions. Activation energies of diffusion decreased with increasing TR conversion while enthalpies of sorption remained mostly constant, consistent with the substantial increase in FFV due to thermal rearrangement. At the highest TR conversion, decreases in temperature move the polymer toward the upper right on the upper bound (i.e., simultaneously increasing both permeability and selectivity), consistent with reports from other high free volume, high permeability polymers.

5.2 RESULTS AND DISCUSSION

5.2.1 Effect of temperature on permeability and selectivity

Permeabilities of CH_4, H_2, N_2, and CO_2 were measured in HAB-6FDA and its three TR analogs at pressures up to 32 atm. Figures 5.1 through 5.4 present permeability

versus pressure curves for HAB-6FDA and its three TR analogs. All gases (except H_2) generally exhibit decreasing permeability with increasing pressure, consistent with dual-mode behavior, although CO_2 did exhibit plasticization (and the attendant increase in permeability with pressure) at lower temperatures in some samples as discussed below. The dual-mode effect (i.e., the decrease in permeability as pressure increases) is more significant for more condensable penetrants such as CO_2. For the remainder of this discussion, all permeabilities and diffusivities are reported at 10 atm except as indicated otherwise. All uncertainties were calculated by the propagation of errors method [1]. CO_2 permeability at -10 °C is not reported at pressures above 25 atm due to the approach to the saturation pressure of CO_2 at this temperature.

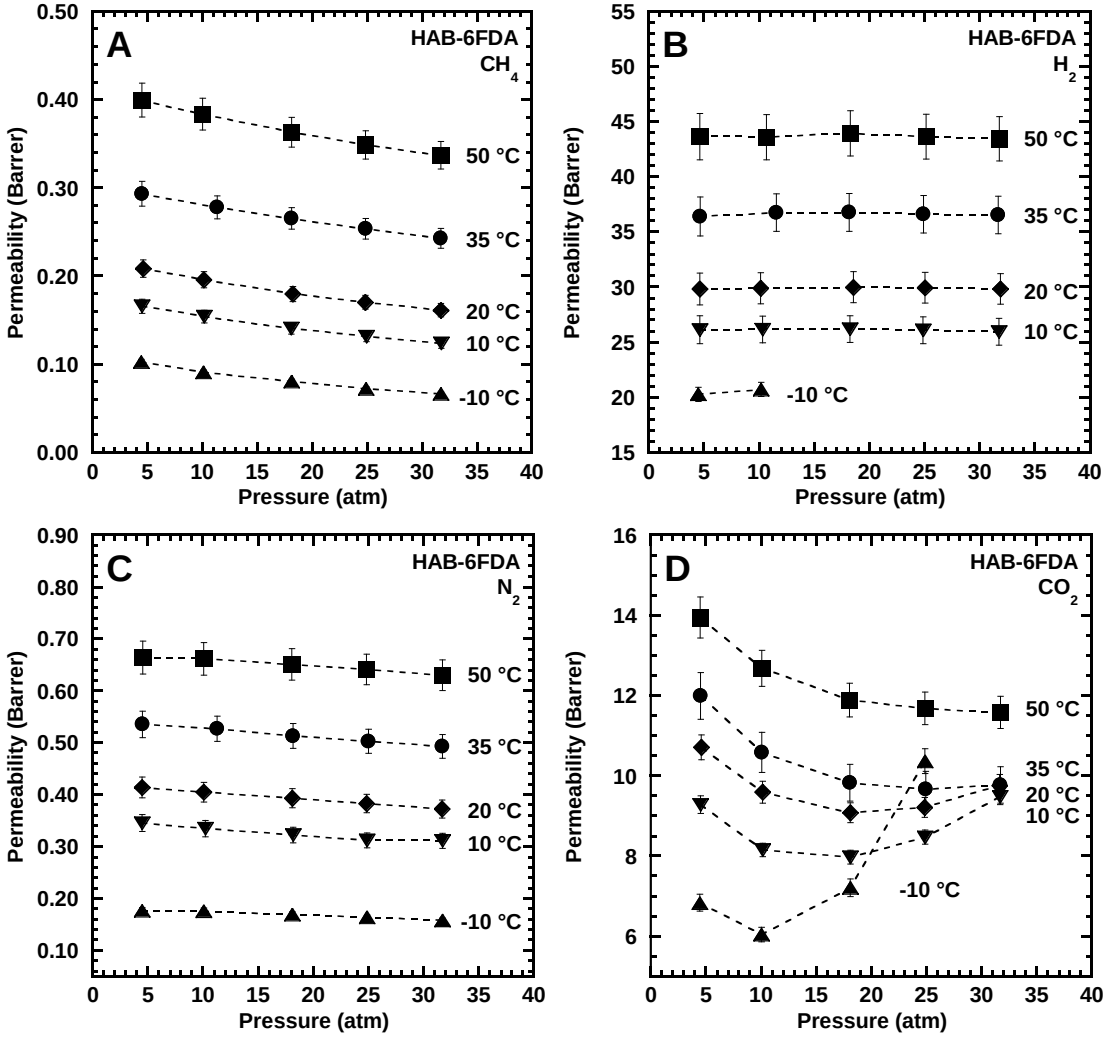

Figure 5.1. Influence of upstream pressure and temperature on permeability of: A) CH_4, B) H_2, C) N_2, and D) CO_2 in HAB-6FDA. Dashed lines are guides for the eye.

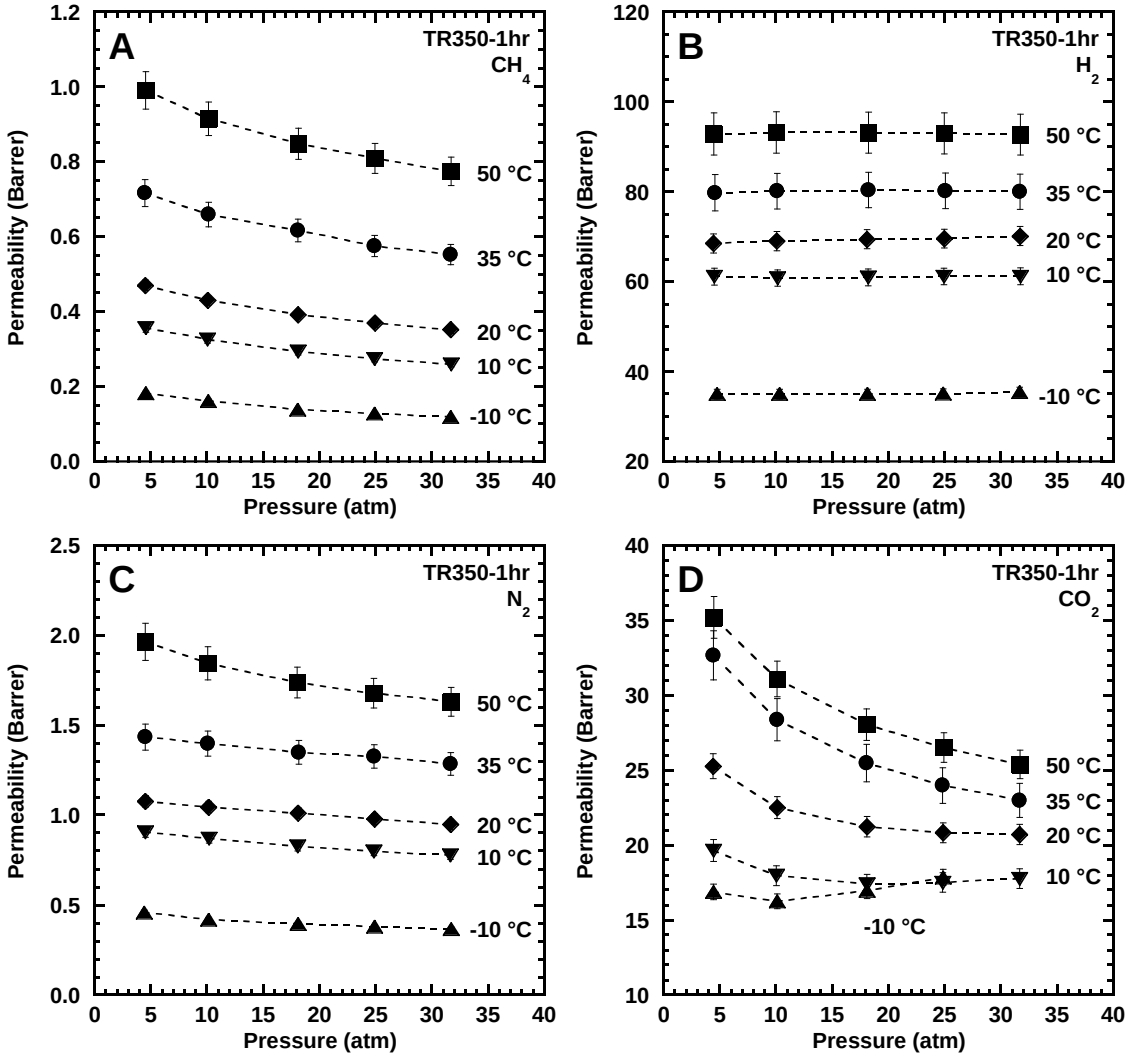

Figure 5.2. Influence of upstream pressure and temperature on permeability of: A) CH_4, B) H_2, C) N_2, and D) CO_2 in TR350-1hr. Dashed lines are guides for the eye.

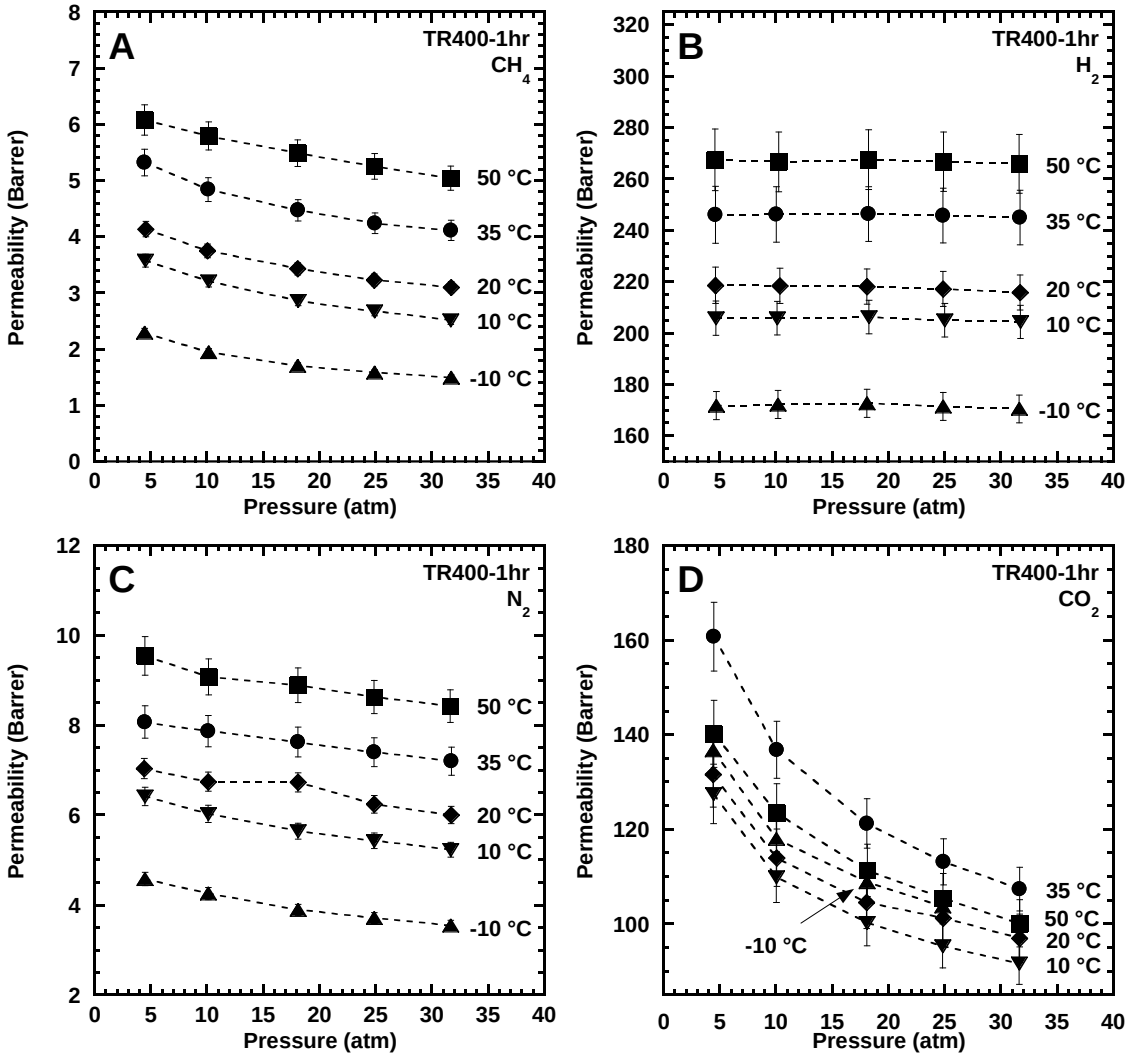

Figure 5.3. Influence of upstream pressure and temperature on permeability of: A) CH_4, B) H_2, C) N_2, and D) CO_2 in TR400-1hr. Dashed lines are guides for the eye.

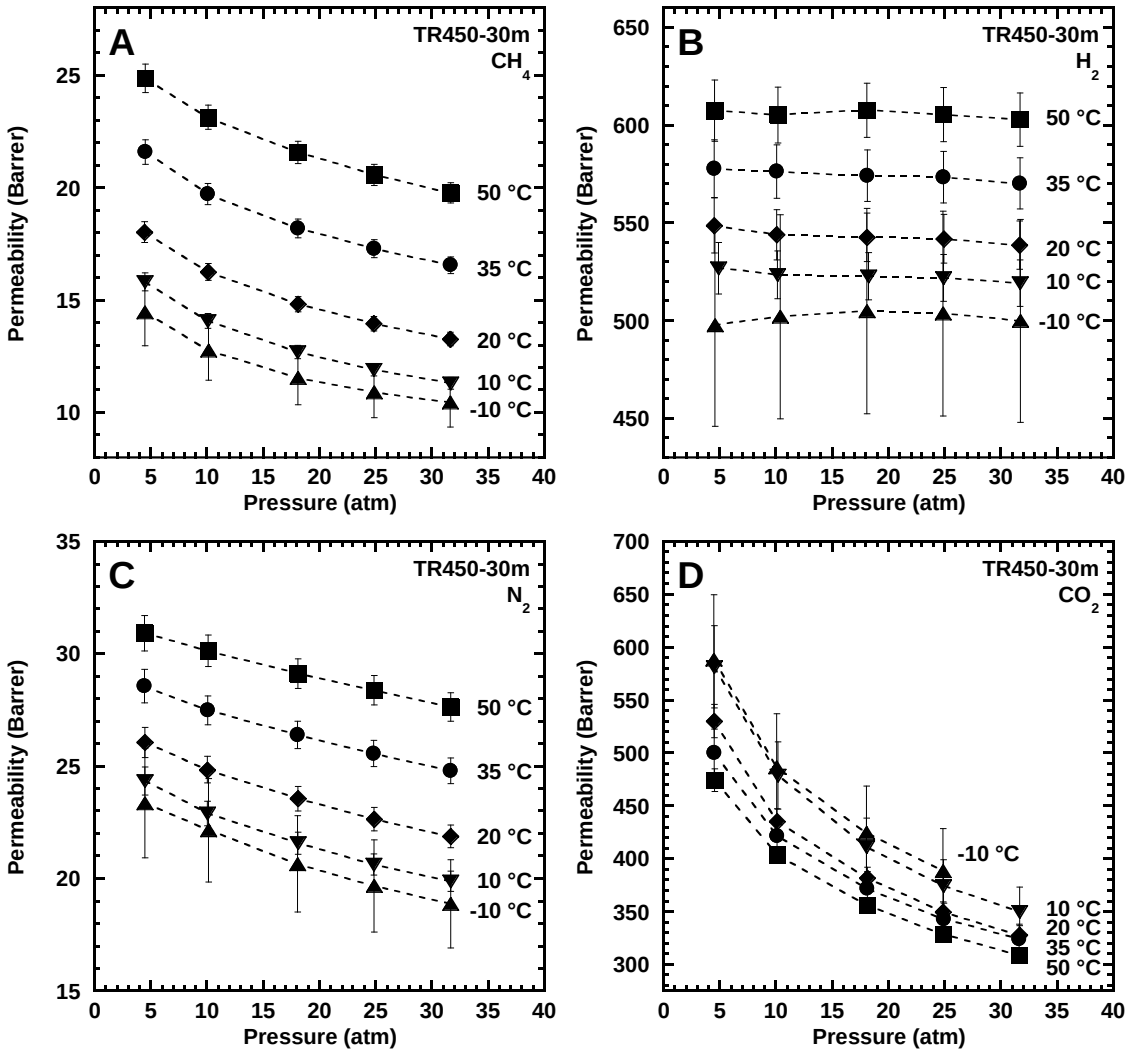

Figure 5.4. Influence of upstream pressure and temperature on permeability of: A) CH_4, B) H_2, C) N_2, and D) CO_2 in TR450-30m. Dashed lines are guides for the eye.

Condensable penetrants, such as CO_2, can plasticize polymers at elevated pressure [2-4]. In the HAB-6FDA polyimide precursor, CO_2 permeability initially decreases with increasing pressure as expected, but, at high enough pressures and temperatures of 20 °C and below, permeability begins to increase (cf., Figure 5.1D). At lower temperatures, this effect is more significant. At 10 °C, CO_2 permeability begins to increase at approximately

15 atm. At -10 °C, the minimum in CO_2 permeability is at approximately 10 atm, and CO_2 permeability at 25 atm (the highest pressure considered at -10 °C) is 94% higher than the permeability at its minimum value. Plasticization (i.e., an increase in CO_2 permeability with pressure) is only observed at 10 and -10 °C in TR350-1hr and is not observed in TR400-1hr and TR450-30m (cf., Figures 5.1 through 5.4).

As temperature decreases, permeability decreases for all gases in all samples, with the notable exception of CO_2 permeability in TR450-30m, which increases as temperature decreases. Activation energies of permeation can be calculated at a given pressure using Equation [2-4]. Permeabilities at 10 atm as a function of inverse temperature are presented in Figure 5.5. The solid lines represent fits of the data to the Arrhenius equation (Equation [2-4]). As temperature increases, permeability increases in every case except CO_2 in the most highly converted sample (i.e., TR450-30m). As discussed in more detail below, activation energies tend to be more positive for larger penetrants than for smaller penetrants, such as CH_4 and N_2 as compared to H_2. Gas permeability in HAB-6FDA (cf., Figure 5.5A), always increases with increasing temperature.

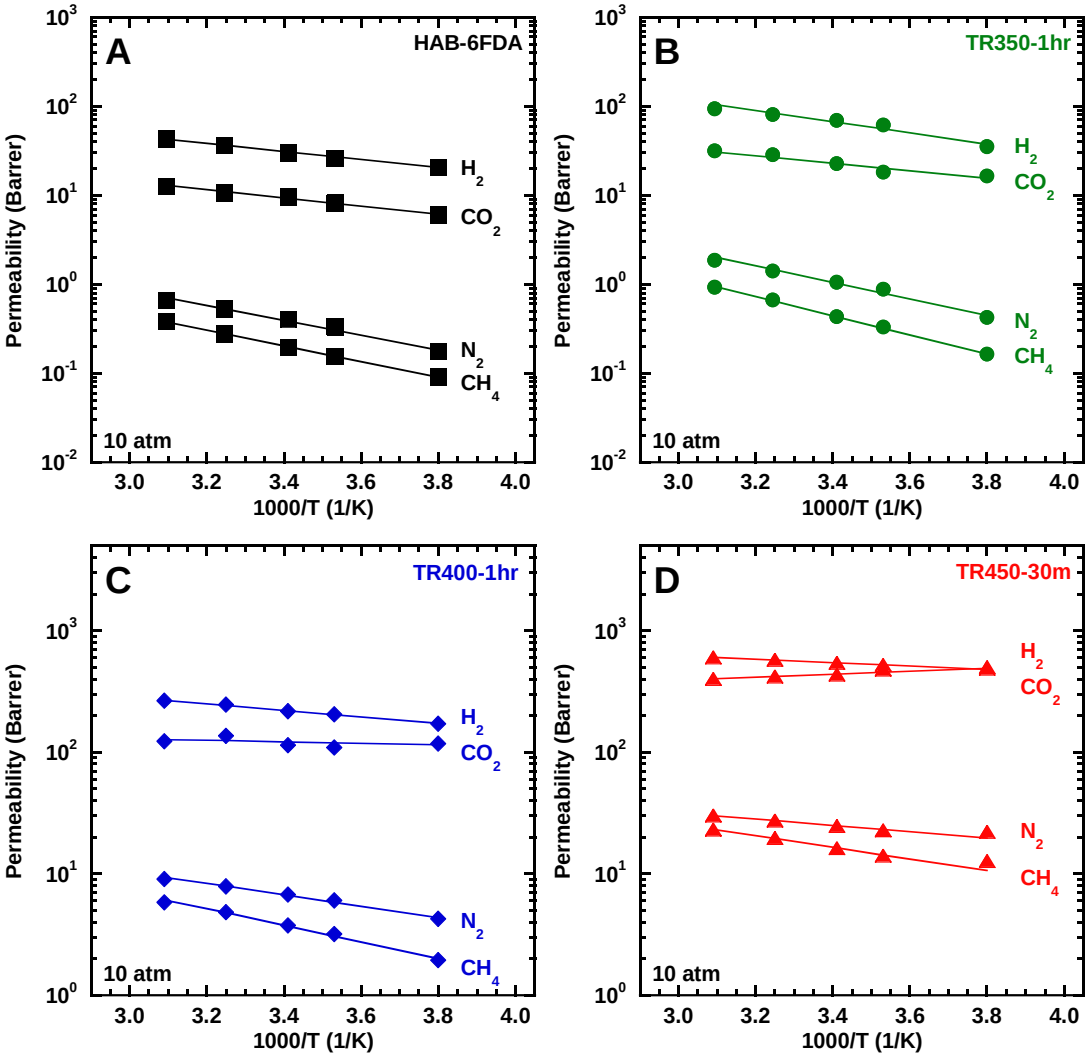

Figure 5.5. The effect of temperature on permeability in: A) HAB-6FDA, B) TR350-1hr, C) TR400-1hr, and D) in TR450-30m. The solid lines were calculated from Arrhenius fits. All data reported in this figure are at a feed pressure of 10 atm.

As permeability increases, selectivity generally decreases. For example, Figure 5.6 presents CO_2/CH_4 pure gas selectivities as a function of inverse temperature for each sample. As seen previously [5], there is a slight increase in CO_2/CH_4 selectivity at 35 °C upon thermal conversion, from 38 for HAB-6FDA to 43 for TR350-1hr. At higher TR

conversions, CO_2/CH_4 selectivity decreases to 28 for TR400-1hr and 21 for TR450-30m. As temperature decreases, selectivity increases significantly. Interestingly, selectivity increases more with decreasing temperature for more highly converted samples than it does for HAB-6FDA, indicating that a larger difference between the activation energies of permeation for CO_2 and CH_4 is observed in the TR polymers than in HAB-6FDA.

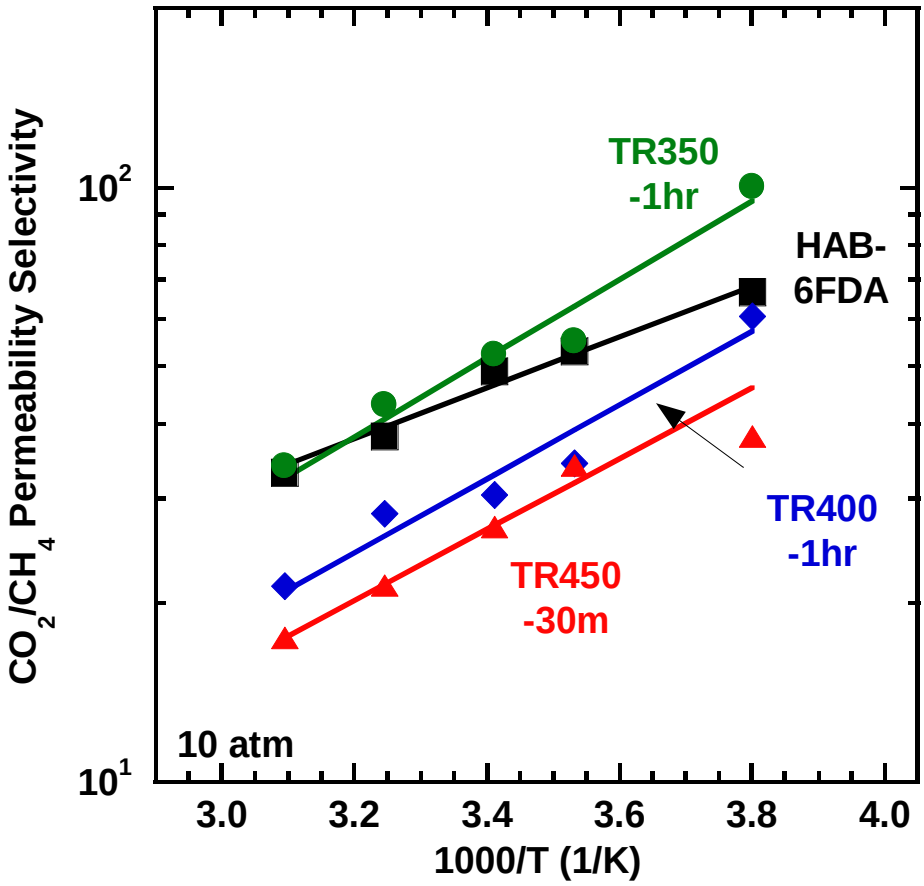

Figure 5.6. The effect of temperature on CO_2/CH_4 selectivity in HAB-6FDA (black squares), TR350-1hr (green circles), TR400-1hr (blue diamonds), and TR450-30m (red triangles). The solid lines were calculated from Arrhenius fits. All data reported in this figure are at a feed pressure of 10 atm.

CO_2/N_2 selectivity also decreases with both increasing extent of thermal rearrangement and increasing temperature as presented in Figure 5.7. Unlike CO_2/CH_4, CO_2/N_2 selectivity does not initially increase upon thermal rearrangement, suggesting that the increase in CO_2/CH_4 selectivity could be due to, perhaps, a favorable free volume distribution [5, 6]. H_2/CO_2 selectivity decreases with increasing extent of thermal rearrangement and increases slightly with temperature for thermally rearranged samples (cf., Figure 5.8).

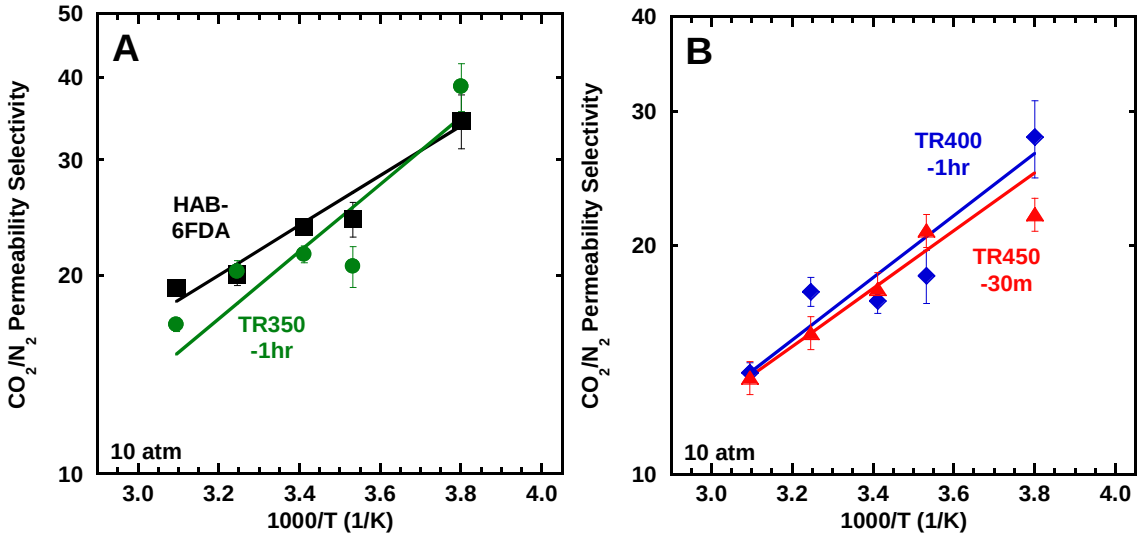

Figure 5.7. Effect of temperature on CO_2/N_2 permeability selectivity at 10 atm in A) HAB-6FDA (black squares) and TR350-1hr (green circles) and B) TR400-1hr (blue diamonds) and TR450-30m (red triangles). The solid lines were calculated from Arrhenius fits. Uncertainties from propagation of errors [1], and uncertainties not shown were smaller than the symbols.

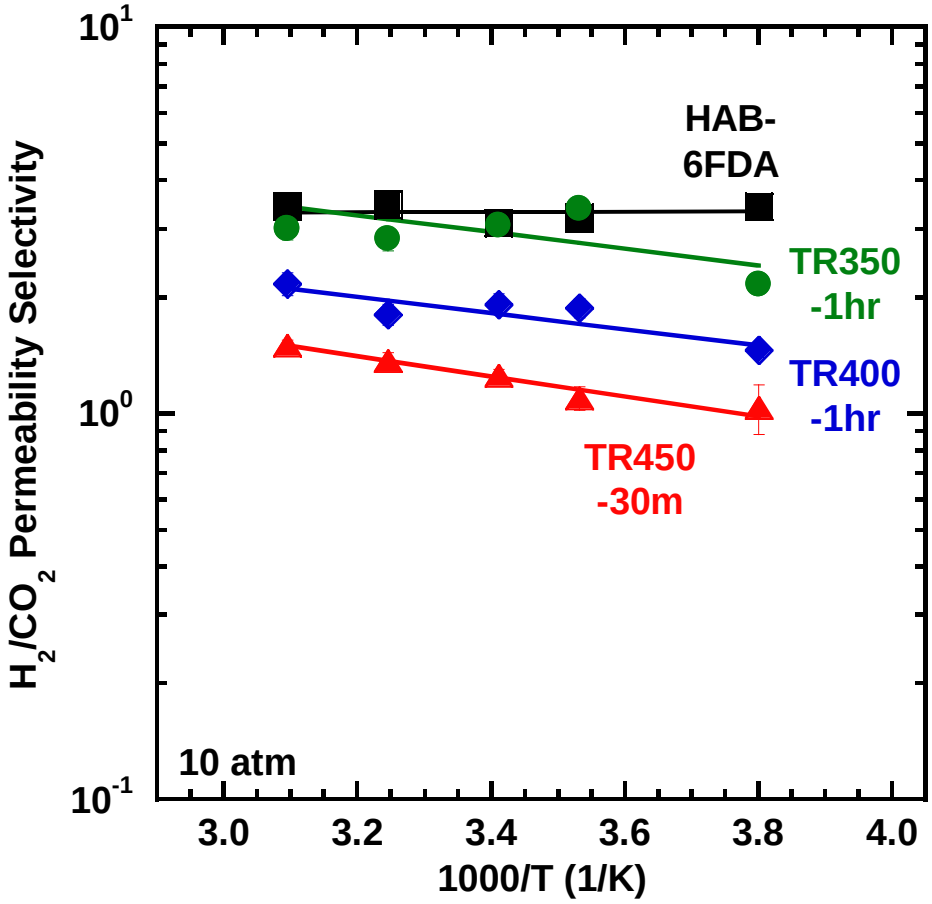

Figure 5.8. Effect of temperature on H_2/CO_2 permeability selectivity at 10 atm in HAB-6FDA (black squares), TR350-1hr (green circles), TR400-1hr (blue diamonds), and TR450-30m (red triangles). The solid lines were calculated from Arrhenius fits. Uncertainties from propagation of errors [1], and uncertainties not shown were smaller than the symbols.

Figure 5.9 presents activation energies of permeation calculated using Equation [2-4]. Relative to the polyimide precursor (i.e., HAB-6FDA), there is a slight increase in the activation energy of permeation for H_2, N_2, and CH_4 at approximately 40% TR conversion (i.e., TR350-1hr). This increase is ascribed to potential cross-linking reactions between polymer chains [7] as well as potential hydrogen bonding due to the development of hydroxyl functionality in the TR350-1hr sample [5, 8]. Further TR

conversion results in a decrease in E_P. E_P for CO_2 becomes negative at the highest level of TR conversion (i.e., TR450-30m). At high levels of TR conversion, the effects of hydrogen bonding vanish due to conversion to a polybenzoxazole structure, and free volume effects (i.e., an increase in free volume, which increases permeability and decreases activation energies [9]) outweigh the contribution to activation energies from crosslinking.

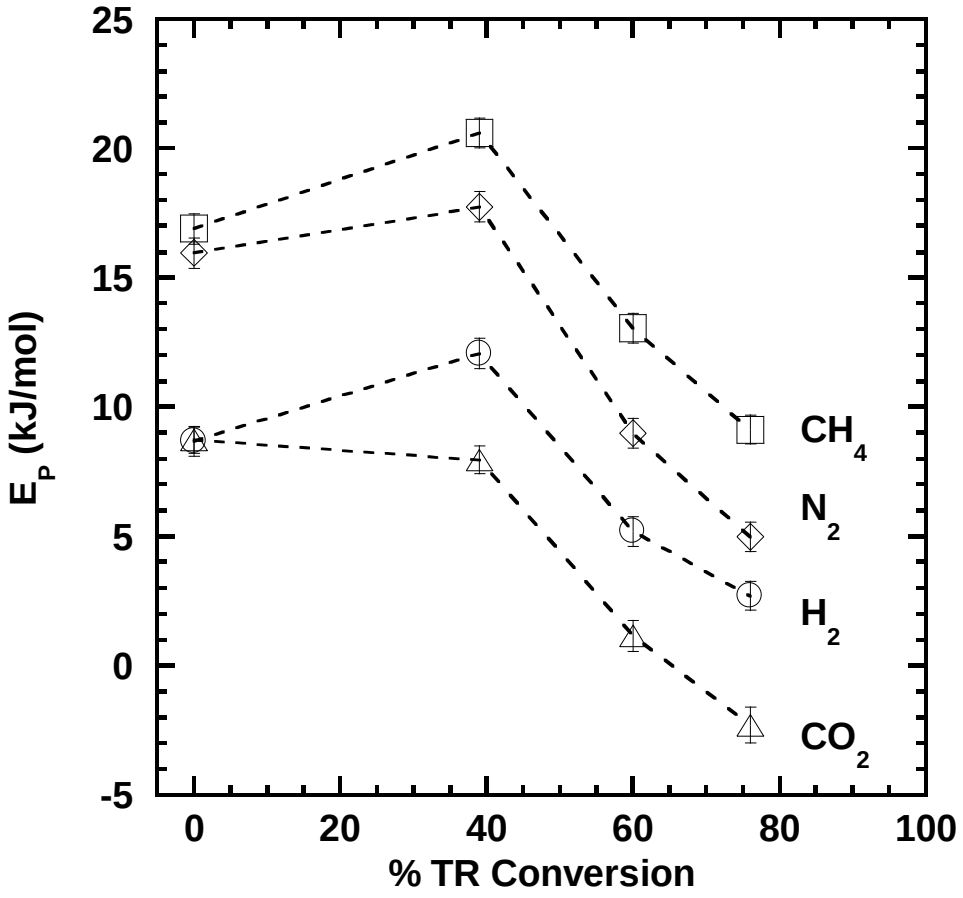

Figure 5.9. The effect of TR conversion on activation energy of permeation at 10 atm. Dashed lines are guides for the eye, and uncertainties were calculated by propagation of errors [1].

The activation energies of permeation for HAB-6FDA and its TR analogues are tabulated in Table 5.1 together with data from the literature. Among the TR samples in Table 5.1 as well as the reference materials, as FFV increases, E_P tends to decrease, and the highest free volume polymer considered, PTMSP, exhibited the lowest activation energies of permeation. The order of E_P values in HAB-6FDA was: $CH_4 \approx N_2 > H_2 \approx CO_2$. In the TR450-30m sample as well as the reference materials in Table 5.1, the order

was: $CH_4 > N_2 > H_2 > CO_2$. For HAB-6FDA, the more negative enthalpy of sorption for CO_2 [10] as compared to that of H_2 [11] is offset by the higher activation energy of diffusion for CO_2 (as described below), resulting in similar activation energies of permeation for H_2 and CO_2. A similar effect is observed for CH_4 and N_2, though the values are slightly different. The relative balance between E_D and ΔH_S changes with extent of thermal rearrangement, so similar values of E_P between different gases are only seen in HAB-6FDA.

Table 5.1. Activation energies of permeation for HAB-6FDA and its TR analogs at 10 atm and other relevant materials.

	FFV (%)	E_P (kJ/mol) at 10 atm			
		CH_4	N_2	CO_2	H_2
Gas Diffusion Diameter [12] (Å)		3.817	3.49	3.44	2.77
HAB-6FDA	15[a]	16.9 ± 0.6	16 ± 0.6	8.7 ± 0.5	8.7 ± 0.6
TR350-1hr	15.1[a]	20.6 ± 0.6	17.7 ± 0.6	8 ± 0.5	12.1 ± 0.6
TR400-1hr	16.3[a]	13 ± 0.6	9 ± 0.6	1.1 ± 0.6	5.2 ± 0.6
TR450-30m	19.6[a]	9.1 ± 0.6	5 ± 0.6	-2.3 ± 0.7	2.7 ± 0.6
Matrimid®[b]	15.7	26	21	9.8	--
6FDA-TAB[c]	17.4[d]	17.2	10.9	2.6	--
PIM-1[e]	25	17.5	11.9	-1.2	1.7
PTMSP[f]	32[g]	-6.3	-5.1	-9.7	-2.7

[a]: [5], [b]: [13], 1 bar, [c]: [14], [d]: [15], [e]: [16], [f]: [17], 1 atm, [g]: [18]

The Robeson upper bounds can be used to characterize the relative performance of different materials [19, 20]. In Figure 5.10A, the CO_2/CH_4 transport performance of HAB-6FDA and its three TR polymer analogs are compared. Permeability increases substantially as thermal conversion increases, but selectivity generally decreases. Decreasing temperature (cf., Figure 5.10A) increases selectivity. This effect is most substantial for TR350-1hr, which has the largest difference in activation energies between CH_4 and CO_2. As TR conversion is increased, E_P for CO_2 decreases and eventually becomes negative, so the trend with decreasing temperature shifts from toward the upper left to toward the upper right on the upper bound plot. Similar behavior occurs for CO_2/N_2 as shown in Figure 5.11.

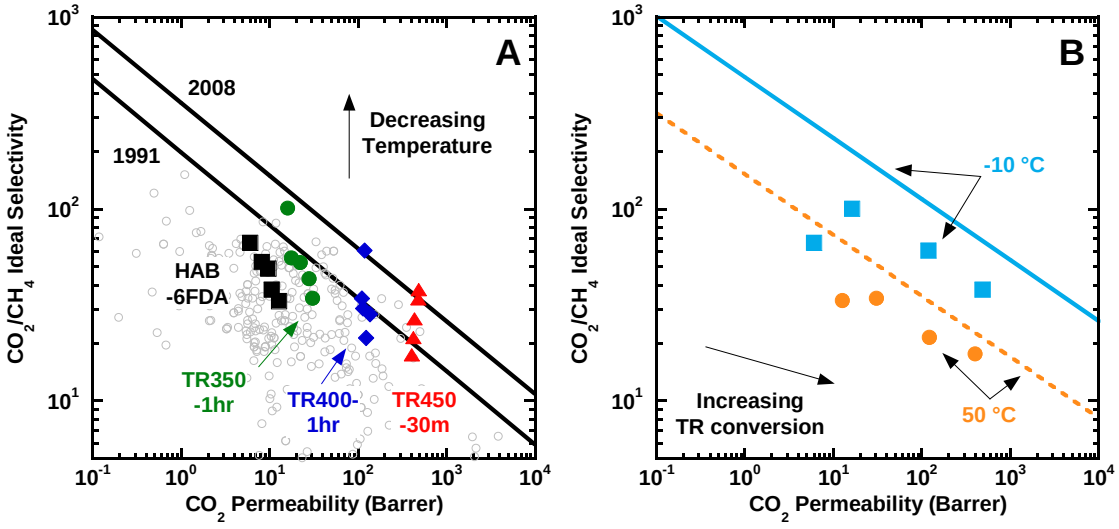

Figure 5.10. CO_2/CH_4 permeability selectivity versus CO_2 permeability of HAB-6FDA and its TR analogs at 10 atm: A) from -10 to 50 °C with the 1991 and 2008 upper bounds [19, 20] and B) at -10 °C (light blue line and squares) and 50 °C (dashed orange line and circles) with temperature-adjusted upper bounds [21].

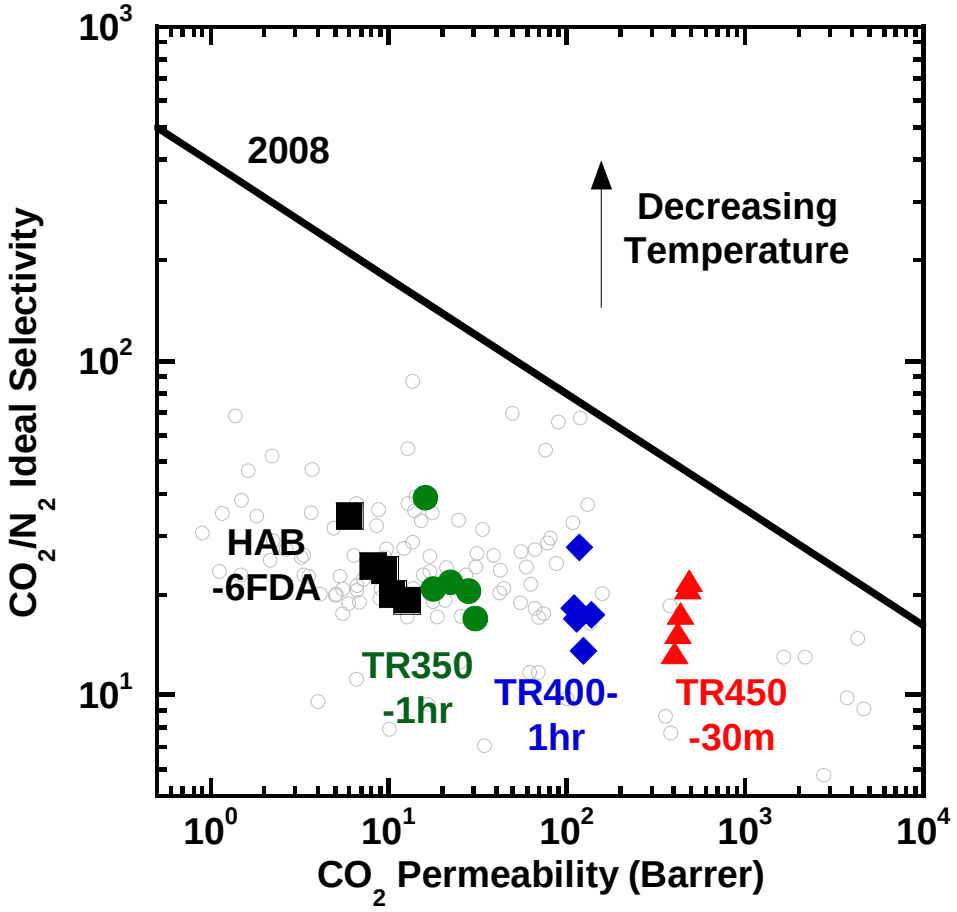

Figure 5.11. CO_2/N_2 permeability selectivity versus CO_2 permeability of HAB-6FDA and its TR analogs at 10 atm from -10 to 50 °C with the 2008 upper bound [20].

Rowe et al. [21] proposed a model of the temperature dependence of the upper bound, and Figure 5.10B presents temperature-corrected upper bounds for -10 and 50 °C based on this model. As temperature decreases, selectivity increases at a given CO_2 permeability, as represented by an upward shift in the CO_2/CH_4 upper bound. At both temperatures shown, an initial increase in selectivity is observed in TR350-1hr, and this effect is most substantial at the lowest temperatures. As temperature decreases, the distance of the samples from the upper bound increases.

Free volume increases with TR conversion, and E_P decreases, even to negative values of E_P for CO_2. Polymers with high FFVs tend to populate the right hand region of the upper bound. As such, polymers further to the right on the upper bound plot, such as high FFV materials like PTMSP, should move to the right (e.g., increase in CO_2 permeability) as temperature decreases. Figure 5.12 presents the temperature-dependence of CO_2 permeability and CO_2/CH_4 permeability selectivity in HAB-6FDA, TR450-30m, and a selection of other 6F-containing and high FFV materials along with the 2008 upper bound for comparison [20]. The activation energies of permeation were used to adjust the temperature range of each sample to match the -10 to 50 °C temperature range of this study. Each of the samples has an arrow connecting the two extremes, and the arrow points in the direction of decreasing temperature. Decreasing temperature increases selectivity and can either increase or decrease permeability (i.e., the line from 50 to -10 °C moves either to the upper left or upper right). Different polymers exhibit different extents of change in selectivity with temperature.

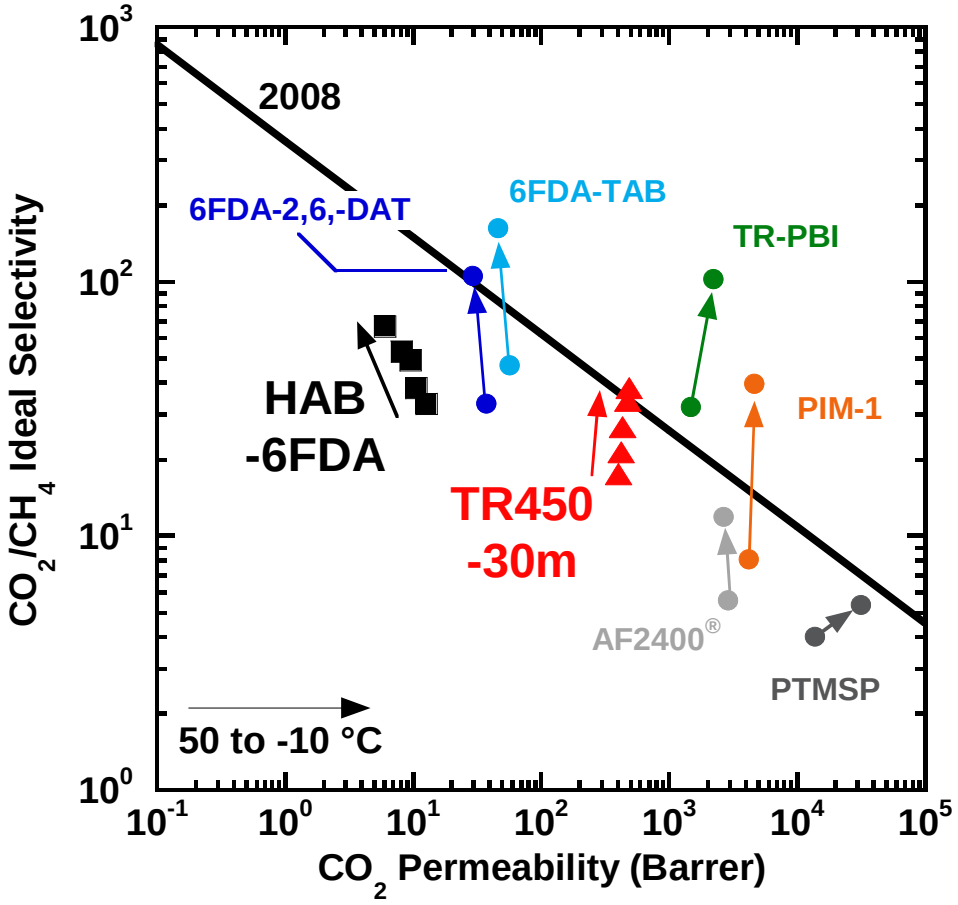

Figure 5.12. Temperature-dependence of HAB-6FDA and TR450-30m with other high-performing polymers against the 2008 upper bound [20]. Permeabilities and selectivities adjusted to -10 and 50 °C based on activation energies and exponential prefactors. Arrows indicate direction of decreasing temperature. Data from [14, 16, 17, 22-24].

The direction of movement (i.e., toward the upper left or upper right with decreasing temperature) for each polymer in Figure 5.12 is a function of E_p for CO_2. The most left-leaning (e.g., moving to the upper left with decreasing temperature) slope, HAB-6FDA, has the highest activation energy for permeation for CO_2 (i.e., 8.7 kJ/mol), while the most right-leaning line is PTMSP, with an activation energy of -9.7 kJ/mol. The vertical movement of each line is determined by the difference between E_p for CH_4 and

CO_2. The largest difference occurs for PIM-1, with a difference of 18.7 kJ/mol, while the least change in selectivity over the temperature range is observed in the case of PTMSP, with a difference of only 3.4 kJ/mol. Other polymers varied between these two extremes. In general, as FFV increases, E_P for CO_2 decreases, but trends in the difference between E_P for CH_4 and CO_2 among the various polymers are less clear.

5.2.2 The effect of temperature on diffusivity

Diffusion coefficients at 10 atm are presented in Figure 5.13. They were calculated from the permeability data and previously reported sorption data [10, 11]. Nitrogen diffusivities are only calculated and presented at temperatures for which the permeability and sorption data were available at the same temperature. Additionally, a difference in the extent of TR conversion for TR450-30m between this study (e.g., 75.4% ± 5%) and the prior sorption study (e.g., 67% ± 5%) [10] should be noted. However, solubility and enthalpies of sorption do not change significantly with TR conversion at high extents of conversion [10], so the approximation here in calculating diffusivities for TR450-30m despite some difference in extent of TR conversion should be reasonable.

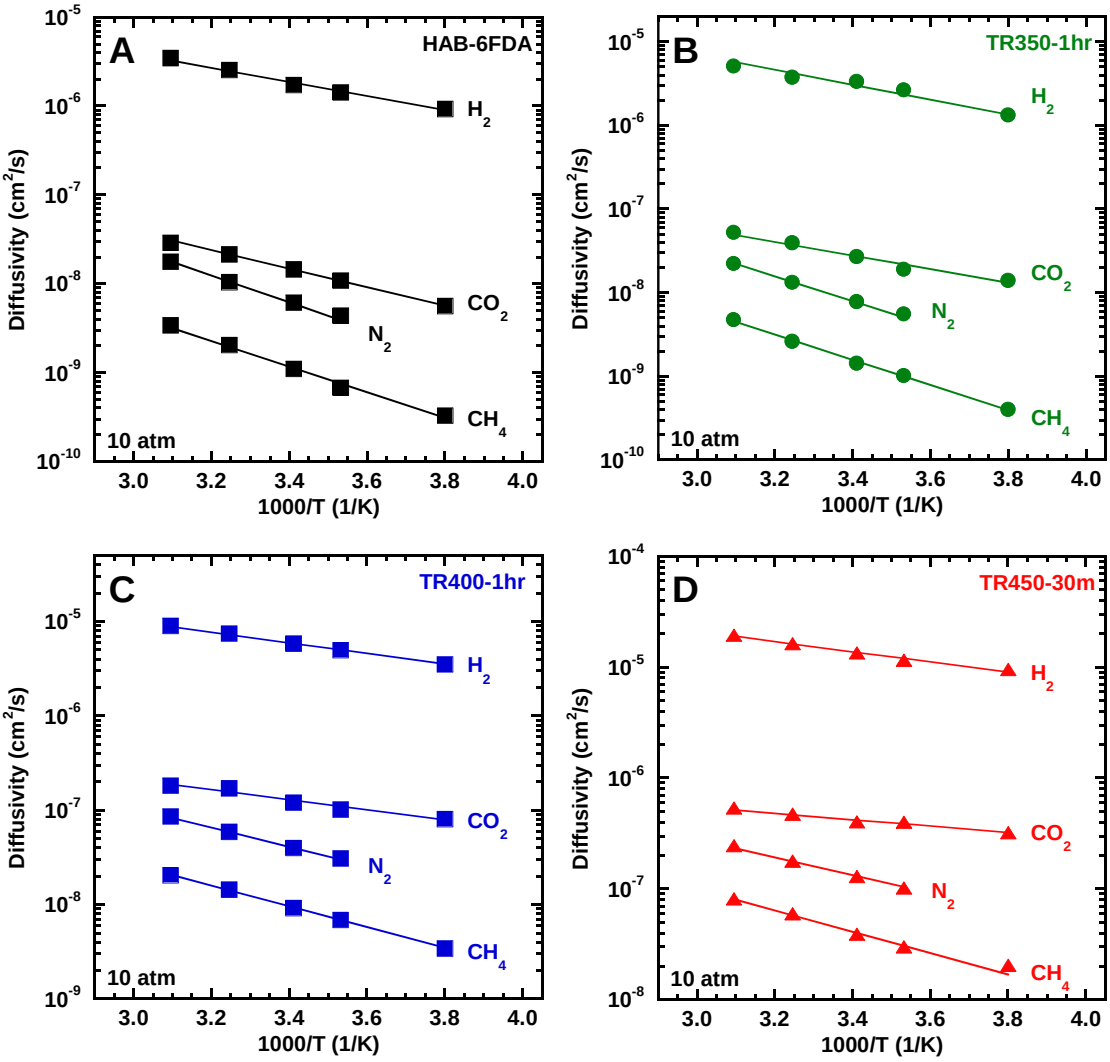

Figure 5.13. The effect of temperature on diffusivity of H_2, CO_2, N_2, and CH_4 in: A) HAB-6FDA, B) TR350-1hr, C) TR400-1hr, and D) TR450-30m. The solid lines were calculated from Arrhenius fits. All data reported in this figure are at a feed pressure of 10 atm.

As TR conversion increases, diffusivities increase significantly, as noted previously [5]. H_2 and CH_4 diffusivity coefficients increase by factors of approximately 6.4 and 29, respectively, as TR conversion increases from 0 to approximately 76% (i.e., TR450-30m). Figure 5.14 presents CO_2/CH_4 diffusivity selectivity as a function of

temperature for each of the samples. For example, at 35 °C (i.e., 1000/T = 3.25 K^{-1}), there is initially a slight increase in CO_2/CH_4 diffusivity selectivity for TR350-1hr (15.0) as compared to HAB-6FDA (10.5) followed by a decrease in selectivity with increasing thermal rearrangement (e.g., 11.8 for TR400-1hr and 7.9 for TR450-30m). The increase in diffusivity selectivity upon initial thermal rearrangement to TR350-1hr can be ascribed to several phenomena. First, the acetate moiety in HAB-6FDA is believed to be replaced replaced by hydroxyl functionality in the first step of thermal rearrangement [5, 8]. The introduction of hydroxyl groups can allow hydrogen bonding between polymer chains, which would reduce chain mobility and tend to increase diffusivity selectivity. Second, TR polymers are likely cross-linked, which would also tend to increase diffusivity selectivity [5, 7, 8]. This behavior is similar to that observed in permeability, which indicates that these materials are best described by their size-sieving characteristics. At higher extents of thermal rearrangement (e.g., TR400-1hr and TR450-30m), diffusivity selectivity decreases due to the opening of the polymer structure (i.e., increased FFV), which tends to increase the diffusivities of larger, slower gases more than those of smaller gases.

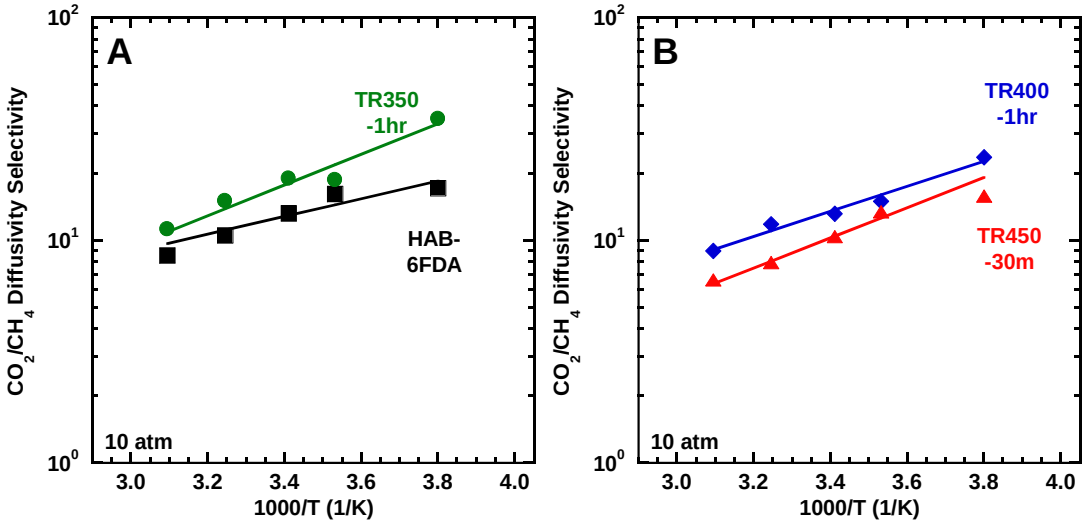

Figure 5.14. The effect of temperature on CO_2/CH_4 diffusivity selectivity in: A) HAB-6FDA (black squares) and TR350-1hr (green circles), and B) TR400-1hr (blue diamonds) and TR450-30m (red triangles). The solid lines were calculated from Arrhenius fits. All data reported in this figure are at a feed pressure at 10 atm.

All diffusivities increased with increasing temperature, though the larger penetrants (CH_4 and N_2) exhibited stronger temperature dependencies (i.e., steeper slopes in Figure 5.13). As shown in Figure 5.14, diffusivity selectivities increase as temperature decreases. The increase in diffusivity selectivity with decreasing temperature reflects differences in activation energies of diffusion of the two gases considered. Larger differences in activation energies of diffusion result in more significant increases in diffusivity selectivity with changing temperature (e.g., more difference between the values of E_D for two gases in Figure 5.15). CO_2/N_2 diffusivity selectivity behaves similarly to that of CO_2/CH_4 (cf., Figure 5.16). H_2/CO_2 diffusivity selectivity for each sample is presented in Figure 5.17. H_2/CO_2 diffusivity selectivity increases with decreasing temperature for HAB-6FDA but either remains essentially constant (TR350-1hr and TR400-1hr) or decreases slightly with decreasing temperature (TR450-30m).

This interesting effect is due to the similar activation energies of diffusion for H_2 and CO_2 at 10 atm as explained further below.

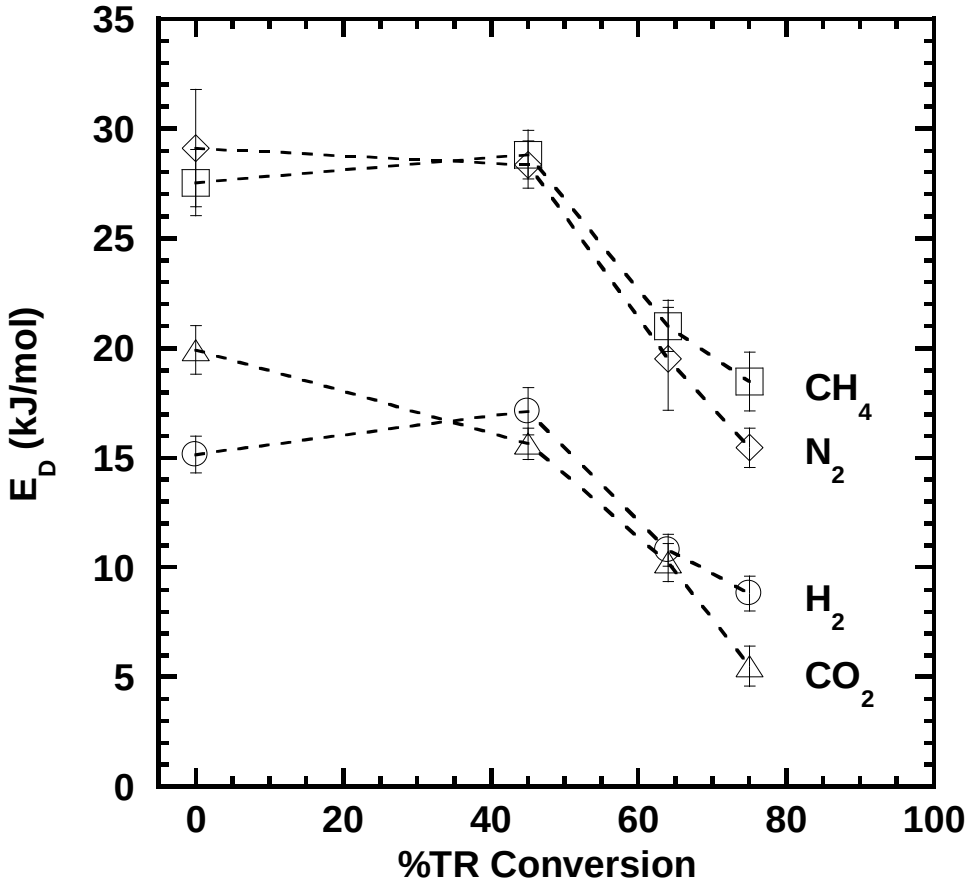

Figure 5.15. The effect of TR conversion on activation energy of diffusion. Dashed lines are guides for the eye, and uncertainties were calculated by propagation of errors [1].

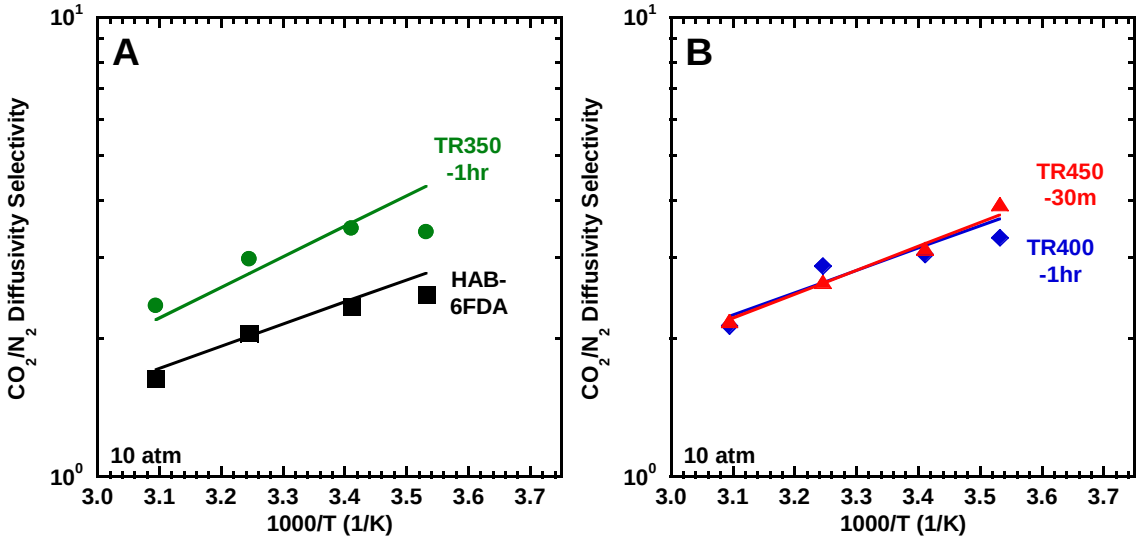

Figure 5.16. Effect of temperature on CO_2/N_2 diffusivity selectivity at 10 atm in A) HAB-6FDA (black squares) and TR350-1hr (green circles) and B) TR400-1hr (blue diamonds) and TR450-30m (red triangles). The solid lines were calculated from Arrhenius fits.

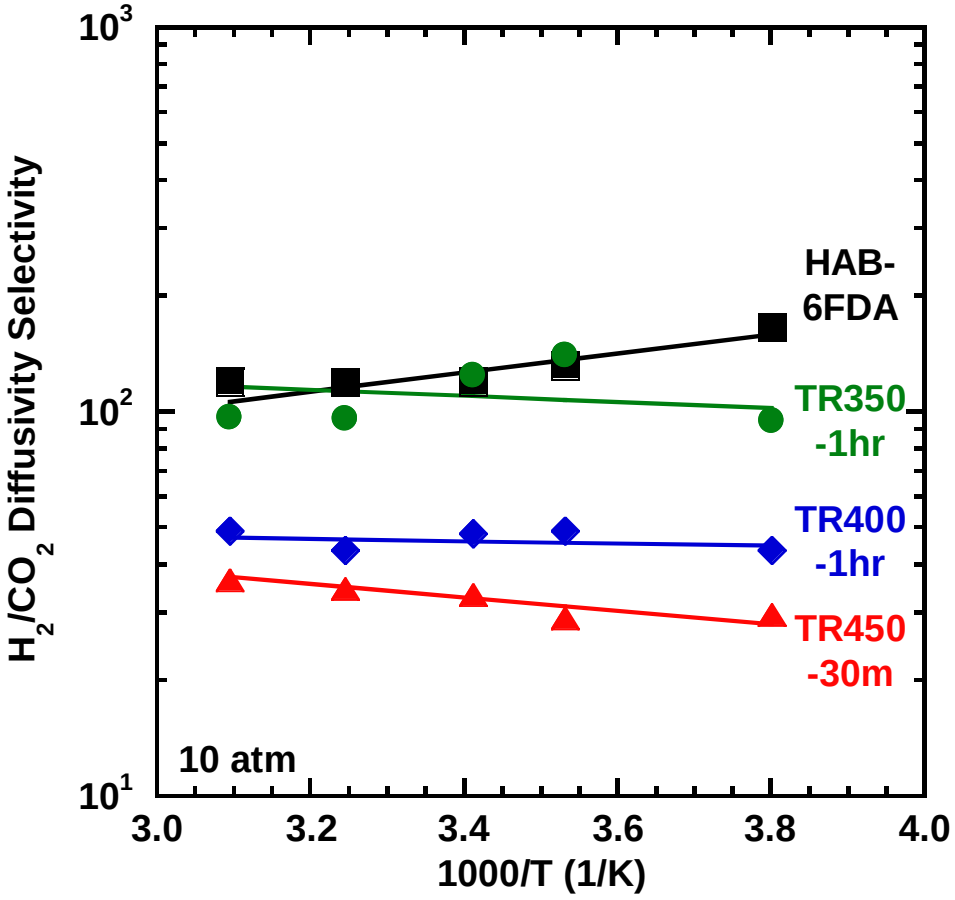

Figure 5.17. Effect of temperature on H_2/CO_2 diffusivity selectivity at 10 atm in HAB-6FDA (black squares), TR350-1hr (green circles), TR400-1hr (blue diamonds), and TR450-30m (red triangles). Solid lines were calculated from Arrhenius fits.

Values of E_D were calculated using the above E_P and previously reported ΔH_S values [10, 11] using Equation [2-7] and are presented in Figure 5.15. Activation energies of diffusion are also presented in Table 5.2. ΔH_S values change relatively little with TR conversion [10, 11], so the changes in E_P with TR conversion stem primarily from change in E_D. The TR conversion for each E_D value in Figure 5.15 is shown at the same TR conversion of the E_P value from which it was calculated. Values of E_D typically

increase with gas size (e.g., diffusion diameter [12]). For example, the typical order of E_D values is $CH_4 > N_2 > CO_2 > H_2$.

Table 5.2. Activation energies of diffusion at 10 atm for HAB-6FDA and its TR polymer analogues.

	FFV (%)	E_D (kJ/mol) at 10 atm			
		CH_4	H_2	N_2	CO_2
HAB-6FDA	15	28 ± 2	15.1 ± 0.8	29 ± 3	20 ± 1
TR350-1hr	15.1	29 ± 1	17 ± 1	28 ± 1	15.6 ± 0.7
TR400-1hr	16.3	21 ± 1	10.8 ± 0.7	20 ± 2	10.2 ± 0.9
TR450-30m	19.6	18 ± 1	8.8 ± 0.8	15.5 ± 0.9	5.5 ± 0.9
Matrimid[a]	15.7	43.4	17.3	30.4	27.1
6FDA-TAB[b]	17.4[c]	28.9	--	23.0	13.0
PIM-1[d]	25	27.9	12.4	20.4	9.8
PTMSP[e]	32[f]	4.9	2.5	5.0	0.4

[a]: [25], pressure not reported, [b]: [14], [c]: [15], [d]: [16], [e]: [17], 1 atm, [f]: [18]

Interestingly, the order of values of E_D differs from the expected order for the TR polymers (e.g., E_D is lower for CO_2 than for H_2). This effect becomes more significant at higher TR conversions where there is a significant increase in free volume. Diffusivity and, therefore, E_D have some pressure dependence [9], and E_D has a stronger pressure dependence in polymers with high FFV such as PIM-1 and PTMSP [16, 17]. In high FFV polymers, increasing pressure has the effect of decreasing the activation energy of diffusion [16]. The activation energies and enthalpies reported here are at 10 atm, and a

corresponding decrease in E_D is seen due to pressure (cf., Figure 5.18). The decrease in E_D with increasing pressure can be seen below 10 atm in our studies, similar to that seen in PIM-1 [16], and more substantial decreases are expected below the pressures presented in Figure 5.18. In PTMSP, the highest FFV polymer, the decrease in E_D due to this effect is even observed at pressures of 1 atm [17].

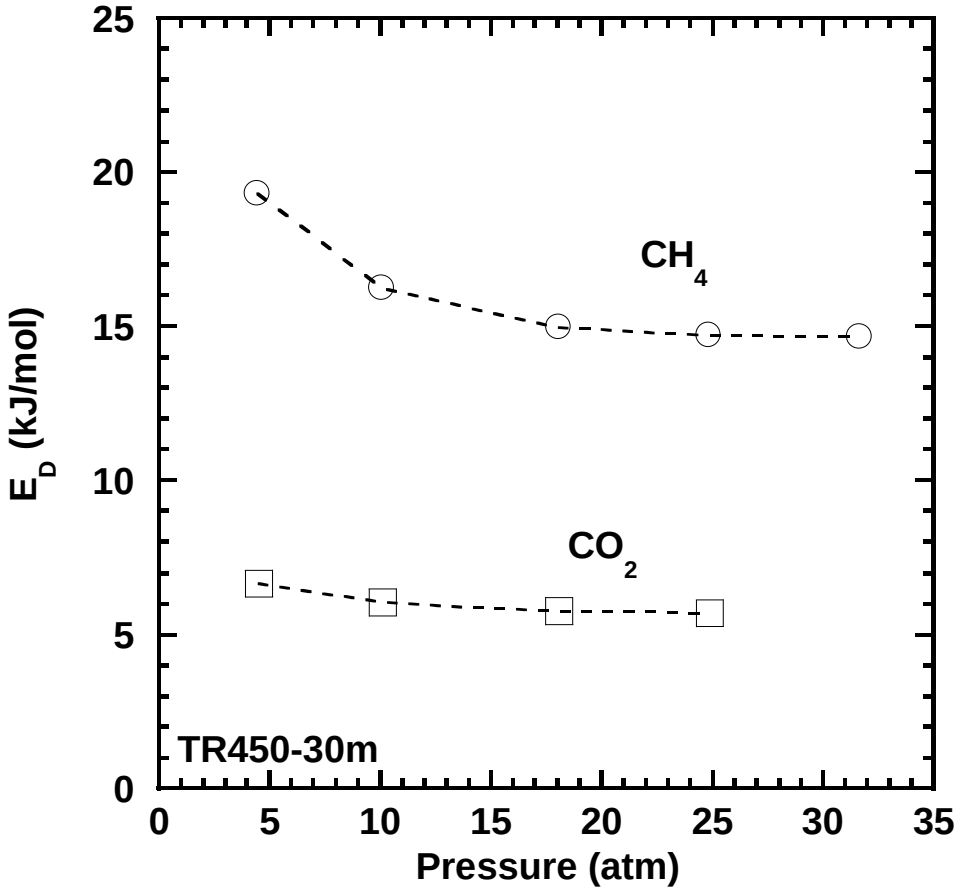

Figure 5.18. Effect of pressure on activation energy of diffusion in TR450-30m.

As TR conversion increases, FFV increases [5, 26], which yields lower energy barriers to diffusion and, therefore, lowers values of E_D as shown in Figure 5.19. In the simplest case, E_D would decrease approximately linearly as 1/FFV decreases [27].

However, in HAB-6FDA and its TR polymer analogs, E_D does not decrease linearly with 1/FFV. As is often observed for high free volume glassy polymers [28, 29], TR polymers can display bimodal distributions of free volume element sizes [30]. Free volume distribution changing as a function of TR conversion may be the source of nonlinear behavior of E_D versus 1/FFV [30].

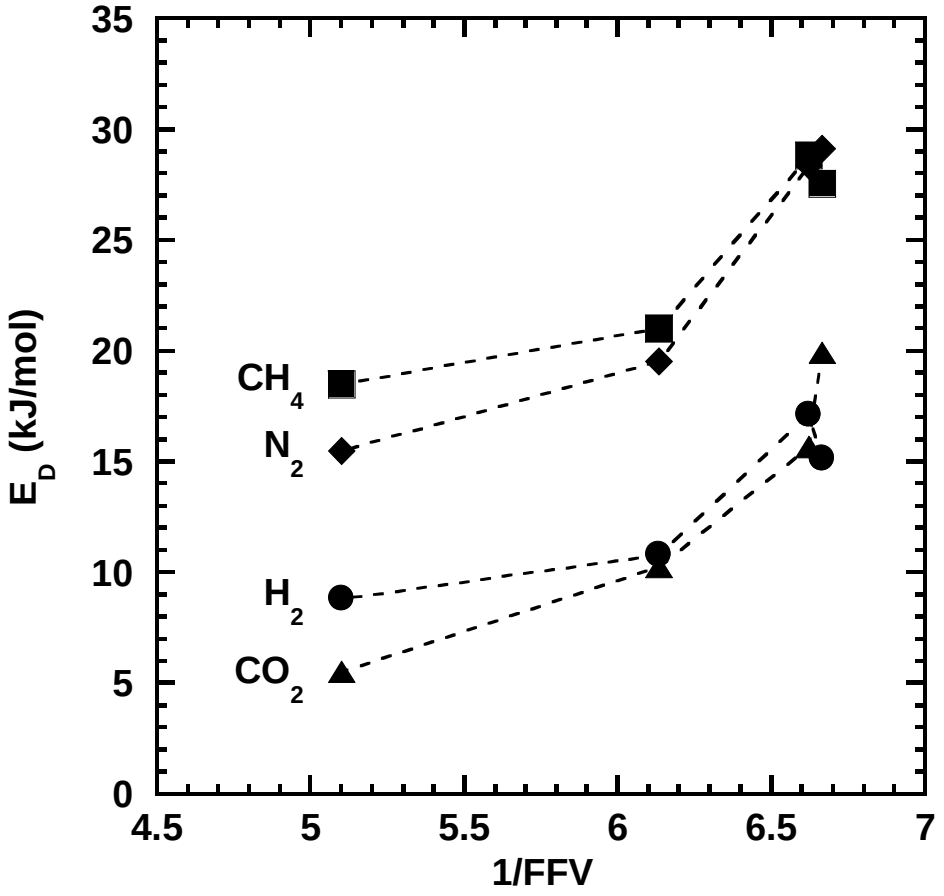

Figure 5.19. Activation energy of diffusion as a function of inverse free volume.

5.3 REFERENCES

[1] P.R. Bevington, D.K. Robinson, Data reduction and error analysis for the physical sciences, McGraw Hill, Boston, 2003.

[2] A. Bos, I.G.M. Pünt, M. Wessling, H. Strathmann, CO_2-induced plasticization phenomena in glassy polymers, Journal of Membrane Science, 155 (1999) 67-78.

[3] N.R. Horn, D.R. Paul, Carbon dioxide plasticization and conditioning effects in thick vs. thin glassy polymer films, Polymer, 52 (2011) 1619-1627.

[4] J.S. Chiou, J.W. Barlow, D.R. Paul, Plasticization of glassy polymers by CO_2, Journal of Applied Polymer Science, 30 (1985) 2633-2642.

[5] D.F. Sanders, Z.P. Smith, C.P. Ribeiro, R. Guo, J.E. McGrath, D.R. Paul, B.D. Freeman, Gas permeability, diffusivity, and free volume of thermally rearranged polymers based on 3,3′-dihydroxy-4,4′-diamino-biphenyl (HAB) and 2,2′-bis-(3,4-dicarboxyphenyl) hexafluoropropane dianhydride (6FDA), Journal of Membrane Science, 409-410 (2012) 232-241.

[6] D.F. Sanders, R. Guo, Z.P. Smith, K.A. Stevens, Q. Liu, J.E. McGrath, D.R. Paul, B.D. Freeman, Influence of polyimide precursor synthesis route and ortho-position functional group on thermally rearranged (TR) polymer properties: Pure gas permeability and selectivity, Journal of Membrane Science, 463 (2014) 73-81.

[7] H.B. Park, C.H. Jung, Y.M. Lee, A.J. Hill, S.J. Pas, S.T. Mudie, E. Van Wagner, B.D. Freeman, D.J. Cookson, Polymers with cavities tuned for fast selective transport of small molecules and ions, Science, 318 (2007) 254-258.

[8] Z.P. Smith, D.F. Sanders, C.P. Ribeiro, R. Guo, B.D. Freeman, D.R. Paul, J.E. McGrath, S. Swinnea, Gas sorption and characterization of thermally rearranged polyimides based on 3,3′-dihydroxy-4,4′-diamino-biphenyl (HAB) and 2,2′-bis-(3,4-dicarboxyphenyl) hexafluoropropane dianhydride (6FDA), Journal of Membrane Science, 415-416 (2012) 558-567.

[9] S. Matteucci, Y. Yampolskii, B.D. Freeman, I. Pinnau, Transport of gases and vapors in glassy and rubbery polymers, in: Y. Yampolskii, I. Pinnau, B. Freeman (Eds.) Materials science of membranes for gas and vapor separation, John Wiley & Sons, Ltd, Chichester, UK, 2006, pp. 1-47.

[10] K.A. Stevens, Z.P. Smith, K.L. Gleason, M. Galizia, D.R. Paul, B.D. Freeman, Influence of temperature on gas solubility in thermally rearranged (TR) polymers, Journal of Membrane Science, *Submitted*.

[11] Z.P. Smith, R.R. Tiwari, T.M. Murphy, D.F. Sanders, K.L. Gleason, D.R. Paul, B.D. Freeman, Hydrogen sorption in polymers for membrane applications, Polymer, 54 (2013) 3026-3037.

[12] L.M. Robeson, Z.P. Smith, B.D. Freeman, D.R. Paul, Contributions of diffusion and solubility selectivity to the upper bound analysis for glassy gas separation membranes, Journal of Membrane Science, 453 (2014) 71-83.

[13] L. Ansaloni, M. Minelli, M. Giacinti Baschetti, G.C. Sarti, Effect of relative humidity and temperature on gas transport in Matrimid®: Experimental study and modeling, Journal of Membrane Science, 471 (2014) 392-401.

[14] C.M. Zimmerman, W.J. Koros, Polypyrrolones for membrane gas separations. II. Activation energies and heats of sorption, Journal of Polymer Science Part B: Polymer Physics, 37 (1999) 1251-1265.

[15] C.M. Zimmerman, W.J. Koros, Polypyrrolones for membrane gas separations. I. Structural comparison of gas transport and sorption properties, Journal of Polymer Science Part B: Polymer Physics, 37 (1999) 1235-1249.

[16] P. Li, T.S. Chung, D.R. Paul, Temperature dependence of gas sorption and permeation in PIM-1, Journal of Membrane Science, 450 (2014) 380-388.

[17] T. Masuda, Y. Iguchi, B.-Z. Tang, T. Higashimura, Diffusion and solution of gases in substituted polyacetylene membranes, Polymer, 29 (1988) 2041-2049.

[18] D.S. Pope, W.J. Koros, H.B. Hopfenberg, Sorption and dilation of poly(1-(trimethylsilyl)-1-propyne) by carbon dioxide and methane, Macromolecules, 27 (1994) 5839-5844.

[19] L.M. Robeson, Correlation of separation factor versus permeability for polymeric membranes, Journal of Membrane Science, 62 (1991) 165-185.

[20] L.M. Robeson, The upper bound revisited, Journal of Membrane Science, 320 (2008) 390-400.

[21] B.W. Rowe, L.M. Robeson, B.D. Freeman, D.R. Paul, Influence of temperature on the upper bound: Theoretical considerations and comparison with experimental results, Journal of Membrane Science, 360 (2010) 58-69.

[22] T.-S. Chung, C. Cao, R. Wang, Pressure and temperature dependence of the gas-transport properties of dense poly[2,6-toluene-2,2-bis(3,4-dicarboxylphenyl)hexafluoropropane diimide] membranes, Journal of Polymer Science Part B: Polymer Physics, 42 (2004) 354-364.

[23] S.H. Han, J.E. Lee, K.-J. Lee, H.B. Park, Y.M. Lee, Highly gas permeable and microporous polybenzimidazole membrane by thermal rearrangement, Journal of Membrane Science, 357 (2010) 143-151.

[24] T.C. Merkel, V. Bondar, K. Nagai, B.D. Freeman, Y.P. Yampolskii, Gas sorption, diffusion, and permeation in poly(2,2-bis(trifluoromethyl)-4,5-difluoro-1,3-dioxole-co-tetrafluoroethylene), Macromolecules, 32 (1999) 8427-8440.

[25] S. Shishatskiy, C. Nistor, M. Popa, S.P. Nunes, K.V. Peinemann, Polyimide asymmetric membranes for hydrogen separation: Influence of formation conditions on gas transport properties, Advanced Engineering Materials, 8 (2006) 390-397.

[26] D.F. Sanders, R. Guo, Z.P. Smith, Q. Liu, K.A. Stevens, J.E. McGrath, D.R. Paul, B.D. Freeman, Influence of polyimide precursor synthesis route and ortho-position functional group on thermally rearranged (TR) polymer properties: Conversion and free volume, Polymer, 55 (2014) 1636-1647.

[27] H. Lin, B.D. Freeman, Gas permeation and diffusion in cross-linked poly(ethylene glycol diacrylate), Macromolecules, 39 (2006) 3568-3580.

[28] K. Nagai, B.D. Freeman, A.J. Hill, Effect of physical aging of poly(1-trimethylsilyl-1-propyne) films synthesized with $TaCl_5$ and $NbCl_5$ on gas permeability, fractional free volume, and positron annihilation lifetime spectroscopy parameters, Journal of Polymer Science Part B: Polymer Physics, 38 (2000) 1222-1239.

[29] D. Hofmann, M. Entrialgo-Castano, A. Lerbret, M. Heuchel, Y. Yampolskii, Molecular modeling investigation of free volume distributions in stiff chain polymers with conventional and ultrahigh free volume: Comparison between molecular modeling and positron lifetime studies, Macromolecules, 36 (2003) 8528-8538.

[30] S. Kim, Y.M. Lee, Rigid and microporous polymers for gas separation membranes, Progress in Polymer Science, 43 (2015) 1-32.

Chapter 6: Influence of temperature on gas transport properties of tetraaminodiphenylsulfone (TADPS) based polybenzimidazoles

6.1 SUMMARY

Polybenzimidazoles have been the focus of increasing study due to their good H_2/CO_2 separation properties and high thermal stability. Gas transport properties of a novel series of polybenzimidazoles based on a new tetraaminodiphenylsulfone (TADPS) monomer have been characterized at temperatures from 35 to 190 °C. Permeability increases with increasing temperature for all gases, and the activation energies of permeation increase in the order of increasing gas size with the exception of CO_2. CO_2 exhibits a lower activation energy of permeation than for H_2 and He, presumably due to strong sorption effects. Separations with TADPS-based PBIs are strongly size selective, with CO_2/N_2, CO_2/CH_4, and N_2/CH_4 selectivities decreasing with increasing temperature. However, H_2/CO_2 selectivities increase with increasing temperature due to a lower activation energy of permeation for CO_2 than for H_2. All samples move towards the upper right on the H_2/CO_2 upper bound as temperature increases. Estimated diffusivities increase significantly with temperature, which is indicative of high activation energies of diffusion and consistent with the strongly size-sieving nature of these materials.

6.2 RESULTS AND DISCUSSION

6.2.1 Gas permeability measurements

Permeabilities of H_2, He, N_2, CH_4, and CO_2 were measured at several temperatures in three TADPS-based PBIs and *m*-PBI. The structures of these polymers are presented in Table 6.1. Over the range of temperatures tested, the permeabilities of H_2 and He in TADPS-based PBIs and *m*-PBI were invariant with upstream pressure, within the uncertainty of the measurements. The more condensable gases (e.g., CO_2) exhibited

some decrease in permeability with increasing pressure at lower temperatures, consistent with normal glassy polymer behavior (i.e., dual mode behavior [1] was observed for CO_2 at lower temperatures). The permeability versus pressure data is shown in Figures 6.1 through 6.5. In general, permeability for a given gas increased in the order of *m*-PBI < TADPS-IPA < TADPS-TPA < TADPS-OBA.

Table 6.1. Structures of *m*-PBI and tetraaminodiphenylsulfone-based polybenzimidazoles.

Name	Structure	T_g (°C)	Ref.
TADPS-TPA	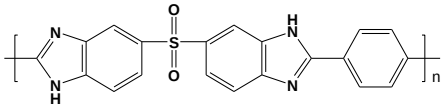	480	[2]
TADPS-IPA	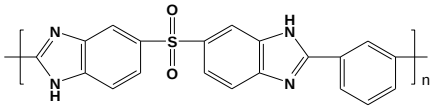	447	[2]
TADPS-OBA	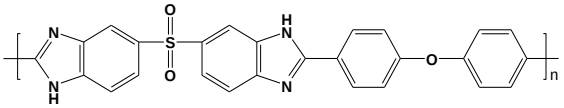	428	[2]
m-PBI	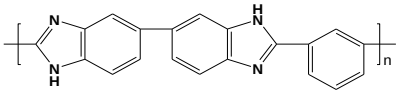	416	[3]

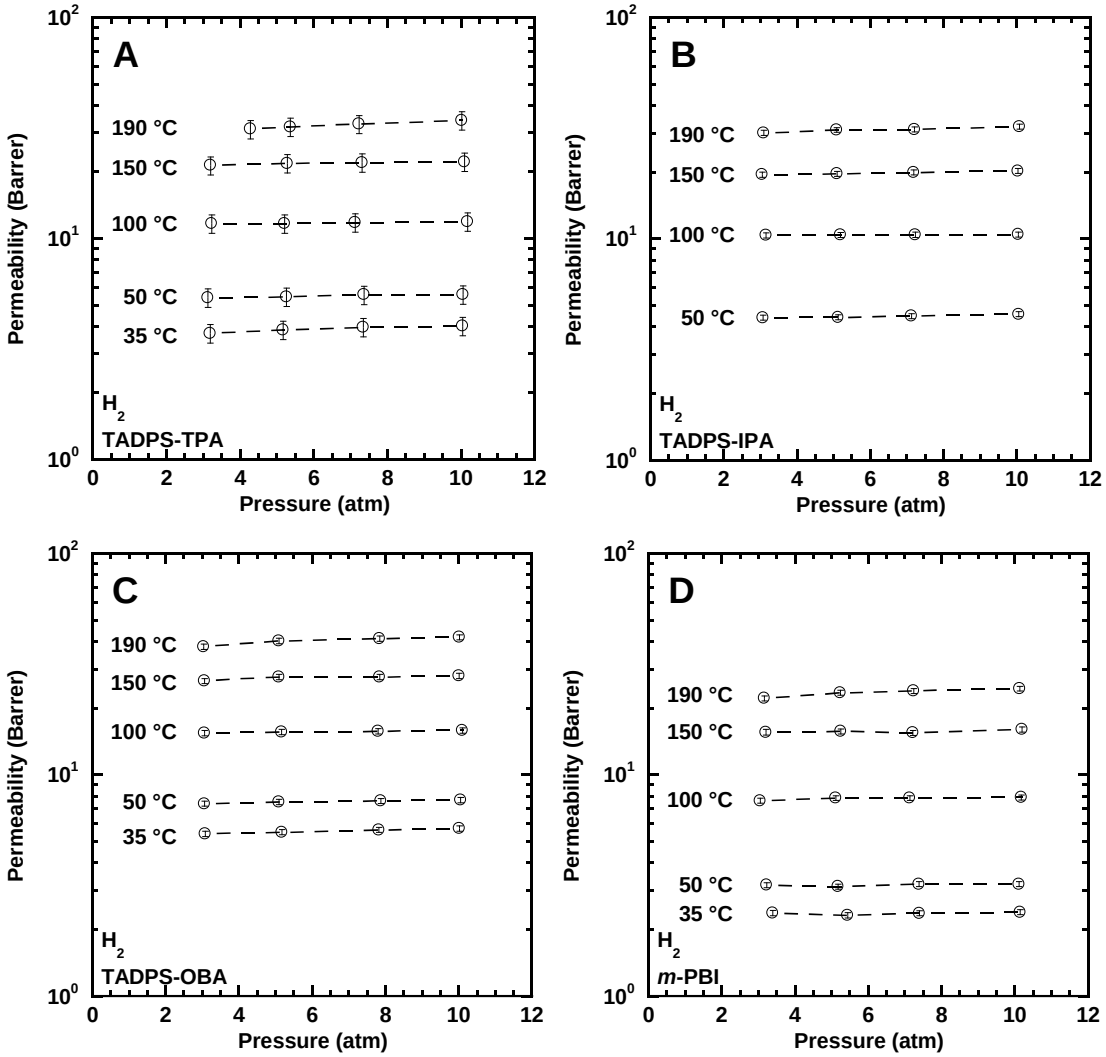

Figure 6.1. The effect of upstream pressure on H_2 permeability at multiple temperatures in: A) TADPS-TPA, B) TADPS-IPA, C) TADPS-OBA, and D) *m*-PBI. Dashed lines are guides for the eye.

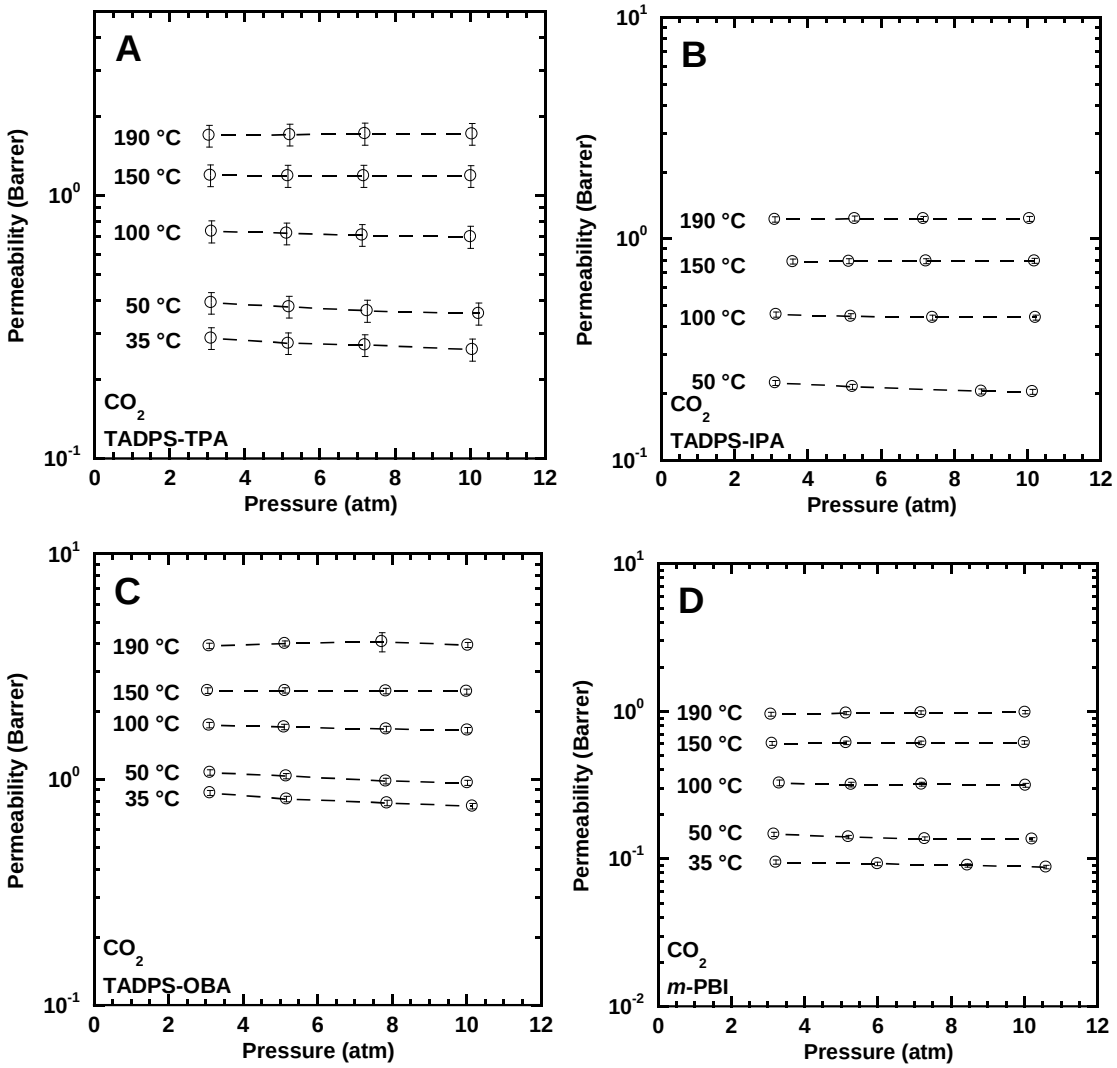

Figure 6.2. The effect of upstream pressure on CO_2 permeability at multiple temperatures in: A) TADPS-TPA, B) TADPS-IPA, C) TADPS-OBA, and D) *m*-PBI. Dashed lines are guides for the eye.

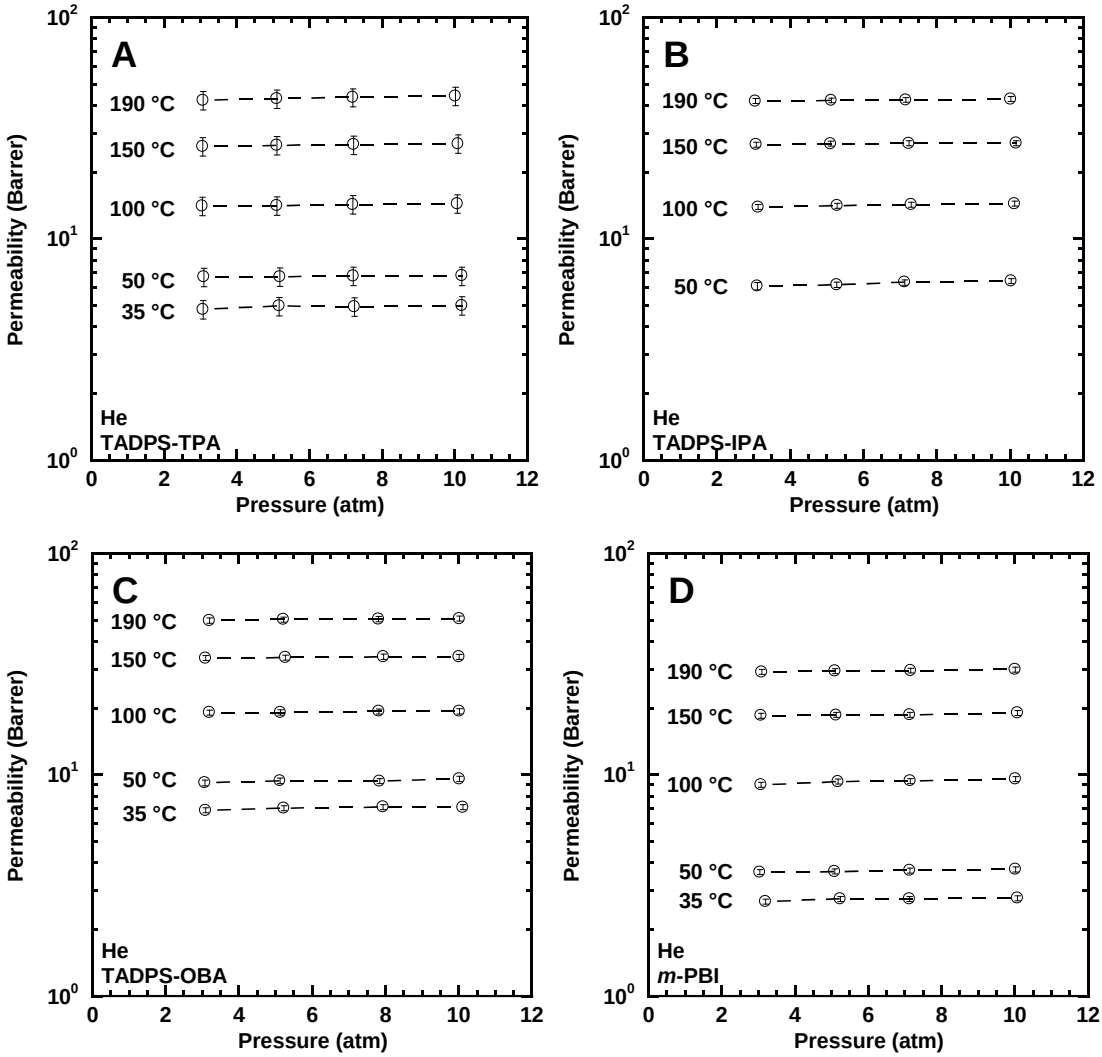

Figure 6.3. The effect of upstream pressure on He permeability at multiple temperatures in: A) TADPS-TPA, B) TADPS-IPA, C) TADPS-OBA, and D) *m*-PBI. Dashed lines are guides for the eye.

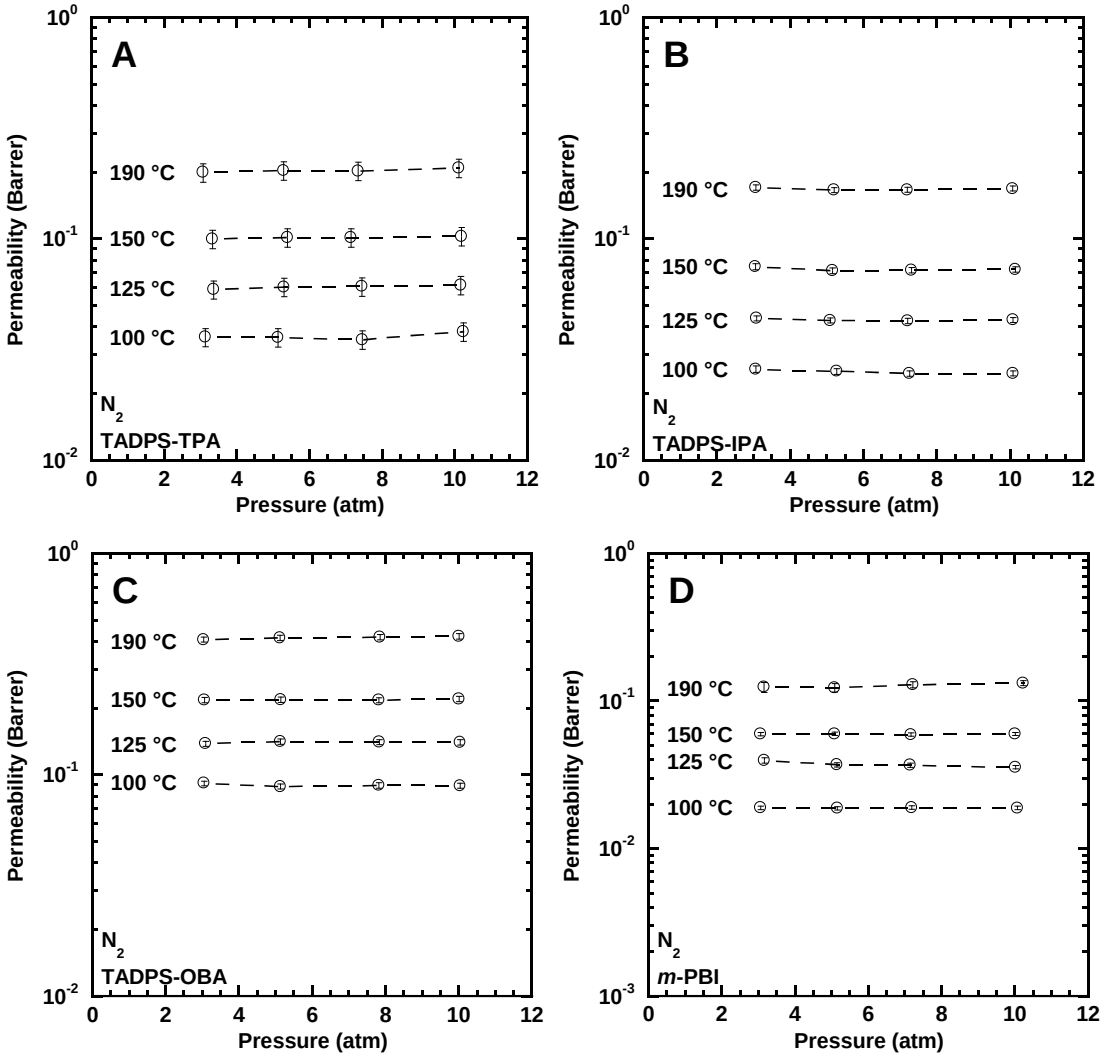

Figure 6.4. The effect of upstream pressure on N_2 permeability at multiple temperatures in: A) TADPS-TPA, B) TADPS-IPA, C) TADPS-OBA, and D) *m*-PBI. Dashed lines are guides for the eye.

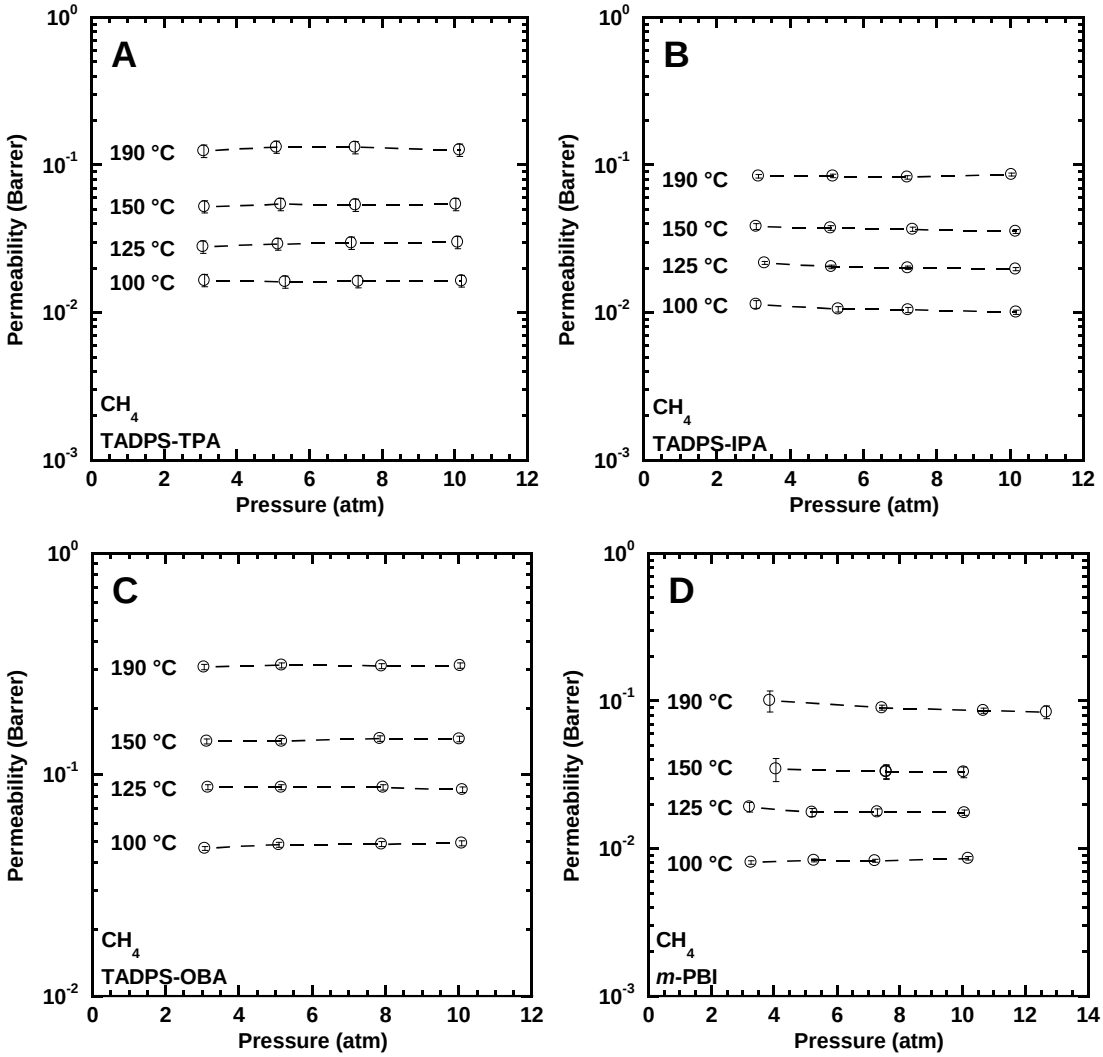

Figure 6.5. The effect of upstream pressure on CH_4 permeability at multiple temperatures in: A) TADPS-TPA, B) TADPS-IPA, C) TADPS-OBA, and D) *m*-PBI. Dashed lines are guides for the eye.

The permeabilities at 35 °C and 3 atm are presented in Table 6.2. The permeabilities at 35 °C of the TADPS-based PBIs measured in this study were reported previously [2]. The method of measuring permeabilities in this study differed from the approach of Borjigin et al., and the permeabilities at 35 °C reported here differ from those of Borjigin et al. [2]. H_2 and He permeabilities are approximately 30% lower in this study

than previously reported for TADPS-TPA (cf., Table 6.2) and 10% lower for TADPS-IPA while CO_2 permeabilities in this study were higher, resulting in lower selectivities. The protocol for measuring permeabilities in this study included a degassing step at the initial temperature (i.e., 190 °C) prior to measurements, which would remove some residual water [4] and, consequently, impact the transport behavior of PBIs. For comparison, the Borjigin et al. study [2] did not include this high temperature drying step in the permeation system prior to beginning the permeability measurements, which likely leaves some residual water in the samples. Additionally, due to the change in drying protocol, the Borjigin et al. samples had a different thermal history than those in this study, and such differences in thermal history are known to influence permeation properties of glassy polymers [5]. These effects are being investigated further and will be reported in a future publication.

Table 6.2. Permeabilities at 35 °C for TADPS-based PBIs and *m*-PBI.

Polymer	Permeabilities at 35 °C (Barrer) and 3 atm				
	He	H_2	N_2	CH_4	CO_2
TADPS-TPA [2]	6.7 ± 0.2	5.5 ± 0.3	---	---	0.56 ± 0.02
TADPS-TPA	4.8 ± 0.5	3.7 ± 0.7	0.0054[a]	0.0017[a]	0.29 ± 0.03
TADPS-IPA	4.4[a]	3.2[a]	0.0031[a]	0.0013[a]	0.17[a]
TADPS-OBA	6.9 ± 0.2	5.4 ± 0.1	0.018*	0.0061[a]	0.87 ± 0.02
m-PBI	2.67 ± 0.07	2.4 ± 0.1	0.0025[a]	0.00052[a]	0.100 ± 0.003
m-PBI [3]	1.05	0.6	0.0048[b]	0.0018[b]	0.16[b]
m-PBI [6]	--	3.4[c]	0.0095[c]	--	0.22[c]

[a]: Extrapolated from higher temperature data using Equation [2-4].
[b]: Estimated using solubility and an estimated density based on gas size.
[c]: Calculated from activation energies of permeation and data at 250 °C.
NOTE: Uncertainties calculated using propagation of errors [7].

The permeabilities at 190 °C and 3 atm are presented in Table 6.3. Permeabilities of several gases in *m*-PBI have been reported previously [3, 6]. Li et al. calculated permeabilities based on high-temperature permeances for hollow fibers utilizing SEM imaging for selective layer thickness [6]. Li also reported activation energies of permeation [6], which can be used to estimate permeabilities at 190 °C. The permeabilities from these previous studies were different from those reported in this, perhaps due to differences in thermal history, experimental methodology, or estimation techniques. Permeabilities for *m*-PBI were lower in this study than those in Li et al. [6], and selectivities are higher for H_2/CO_2 and H_2/N_2 (cf., Table 6.4). The difference in selectivities and permeabilities could also be associated with differences in film preparation and thermal history as well as testing conditions. Without additional studies,

it is impossible to definitely identify the source of the wide variation in the literature permeability results.

Table 6.3. Permeabilities at 190 °C for TADPS-based PBIs and *m*-PBI.

Polymer	Permeabilities at 190 °C (Barrer) and 3 atm				
	He	H_2	N_2	CH_4	CO_2
TADPS-TPA	42 ± 4	31 ± 3	0.20 ± 0.02	0.12 ± 0.01	1.7 ± 0.2
TADPS-IPA	42 ± 1	30.1 ± 0.8	0.170 ± 0.005	0.084 ± 0.002	1.22 ± 0.03
TADPS-OBA	50 ± 1	38 ± 1	0.41 ± 0.01	0.307 ± 0.008	3.9 ± 0.1
m-PBI	29.1 ± 0.8	22.1 ± 0.6	0.12 ± 0.01	0.10 ± 0.02	0.95 ± 0.03
m-PBI (190 °C) [6]	--	43.2[a]	0.345[a]	--	2.01[a]
m-PBI (250 °C) [6]	--	76.81	0.7812	--	3.335

[a]: Estimated from activation energies of permeation and data at 250 °C.
NOTE: Uncertainties calculated using propagation of errors [7].

Table 6.4. Permeability selectivities at 190 °C for TADPS-based PBIs and *m*-PBI.

Polymer	Permeability selectivities at 190 °C and 3 atm		
	CO_2/CH_4	H_2/CO_2	H_2/N_2
TADPS-TPA	14 ± 2	18 ± 2	160 ± 20
TADPS-IPA	14.6 ± 0.6	24.6 ± 0.9	178 ± 7
TADPS-OBA	12.8 ± 0.5	9.7 ± 0.4	93 ± 4
m-PBI	9 ± 2	23.3 ± 0.9	180 ± 10
m-PBI (190 °C) [6]	--	21.5	125

[a]: Estimated from activation energies of permeation and data at 250 °C.

The permeabilities of TADPS-IPA and TADPS-TPA exhibit *meta*/*para* relationships common to aromatic polymers [1]. That is, *meta* isomers often exhibit higher selectivities but lower permeabilities than their *para* analogs [1]. Here, the same is true. TADPS-IPA, the *meta* isomer, exhibits lower permeabilities, especially at lower temperatures (cf., Table 6.2) and higher selectivities than the *para* isomer, TADPS-TPA. TADPS-OBA exhibits the highest permeabilities and lowest selectivities, presumably due to its ether oxygen moiety, which often increases polymer chain flexibility and lowers T_g [1], which is consistent with the T_g data in Table 6.1. TADPS-OBA also exhibits the lowest selectivities measured in this study.

As shown in Figure 6.6, for all samples and temperatures, permeability increased in the following order: $CH_4 < N_2 < CO_2 < H_2 < He$. The temperature dependence of gas permeabilities in these materials will be analyzed in more detail below. As presented in Figure 6.7, the permeabilities were reasonably correlated with gas size, as expected in strongly size-sieving materials [1]. In Figure 6.7, the log of permeabilities at 190 °C in the four PBIs tested are plotted as a function of diffusion diameter squared [8]. Permeability decreases strongly with increasing gas size. The slope of the line in Figure 6.7A, for TADPS-TPA, is -0.78, and the other PBIs have similar slopes. Commonly used polymers such as polysulfone (PSF) [9] and Matrimid® [10] have slopes of -0.6 and -0.7, respectively, at 35 °C. The strong dependence of permeability on gas size in these polybenzimidazoles is indicative of strong size-sieving behavior at temperatures as high as 190 °C.

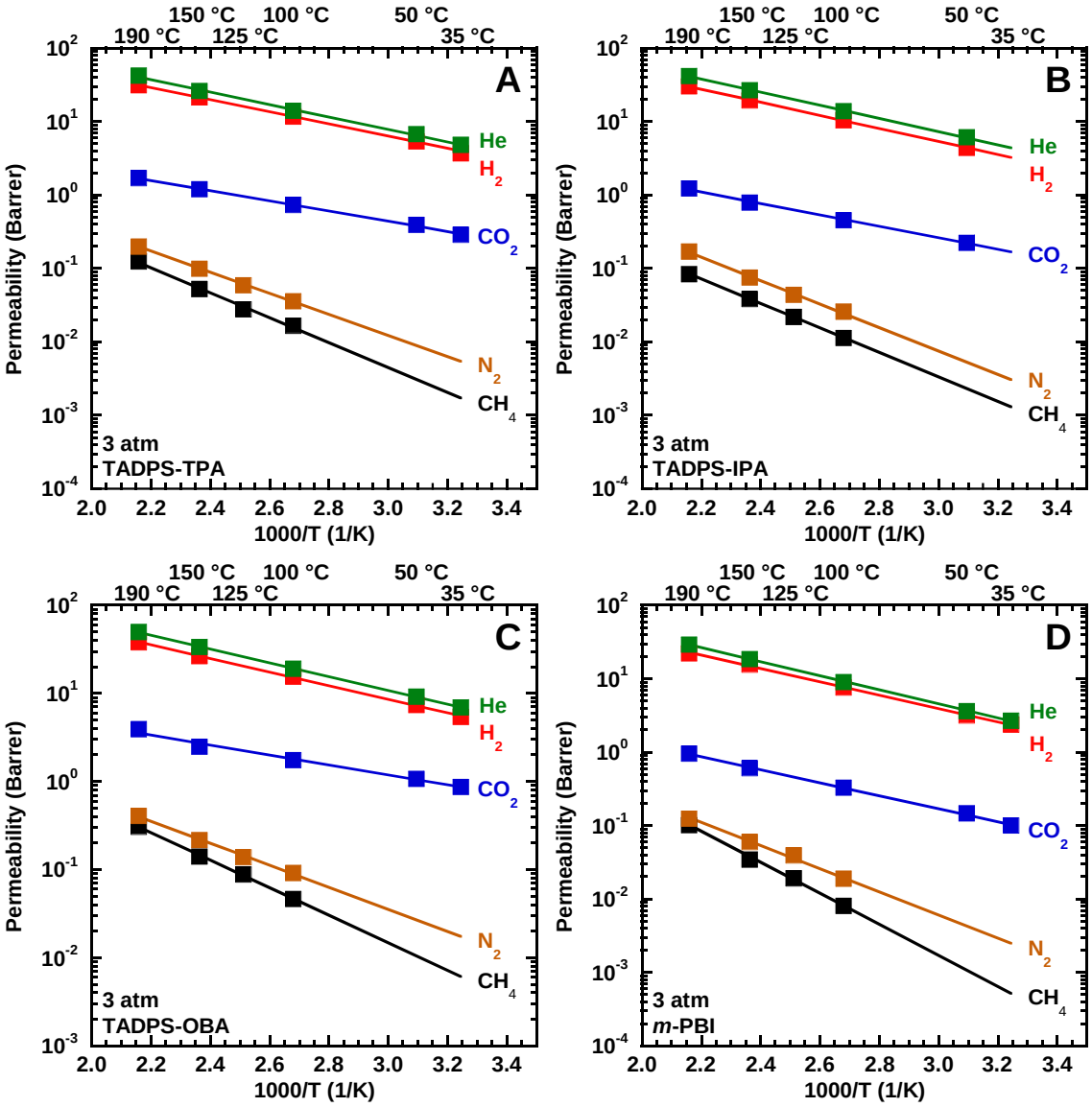

Figure 6.6. The effect of temperature on permeability in: A) TADPS-TPA, B) TADPS-IPA, C) TADPS-OBA, and D) *m*-PBI. Solid lines represent fits to the Arrhenius model. All data reported in this figure are at a feed pressure of 3 atm.

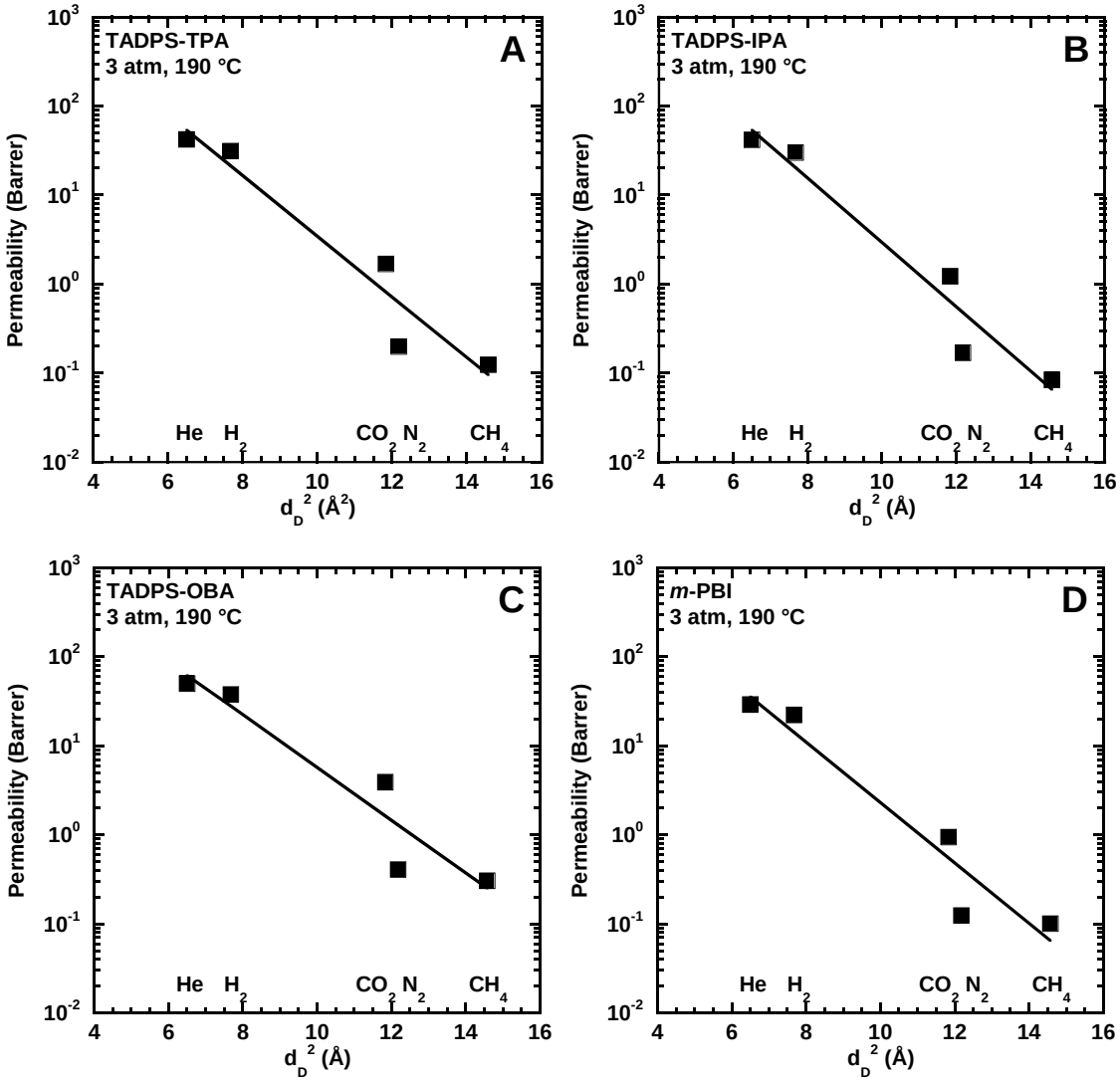

Figure 6.7. Gas permeability at 190 °C as a function of gas diffusion diameter, d_D in: A) TADPS-TPA, B) TADPS-IPA, C) TADPS-OBA, and D) *m*-PBI. The solid lines are best-fits.

6.2.2 Effect of temperature on gas permeation

Permeabilities of CH_4, N_2, CO_2, H_2, and He in TADPS-TPA, TADPS-IPA, TADPS-OBA, and *m*-PBI at 3 atm from 35 to 190 °C (100 to 190 °C for CH_4 and N_2) were presented in Figure 6.6. Permeabilities followed an Arrhenius relationship (i.e.,

Equation [2-4]). CO_2 exhibited the weakest temperature dependence for each sample, while CH_4 displayed the strongest temperature dependence. CH_4 and N_2 permeabilities were not measured below 100 °C, because the permeabilities were too low to be accurately measured. Therefore, Arrhenius fits using Equation [2-4] were used to extrapolate permeability and selectivity values below 100 °C.

Activation energies of permeation were calculated (cf., Equation [2-4]) from the data in Figure 6.6 and are presented in Table 6.5. All activation energies of permeation were positive, and the largest gases exhibited the highest activation energies of permeation. Activation energies of permeation generally decreased in the order of $CH_4 > N_2 > H_2 \approx He > CO_2$. For TADPS-based PBIs, helium and hydrogen activation energies are essentially the same within the uncertainty of the measurements. CO_2 exhibited the lowest activation energy in these materials, except for *m*-PBI, where it is within uncertainty of the activation energy for hydrogen. The addition of the SO_2 moiety into the polymer backbone (i.e., comparing *m*-PBI to TADPS-IPA) results in minimal or no decreases in the activation energy of permeation for most gases. E_P for N_2 does not substantially change upon addition of the sulfonyl group, but E_P for CH_4 decreases significantly. Two possible explanations are proposed for this behavior. First, CH_4 would have the least number of free volume elements available to it due to its large size, so any changes to the size distribution of free volume elements due to changing the polymer structure would have a more significant effect on CH_4 than on N_2. The addition of the SO_2 moiety may disrupt chain packing [2] and modify the size distribution of free volume elements, allowing CH_4 more access to free volume and lowering energy barriers for its diffusion and permeation. Additionally, CH_4 is typically more soluble than N_2, and sorption effects due to changing chemical structure may contribute to this effect [1]. Further analysis of these samples by techniques such as positron annihilation lifetime

spectroscopy or temperature-dependent sorption would be beneficial for fully explaining these effects.

Table 6.5. Activation energies of permeation for TADPS-based PBIs, *m*-PBI, and other materials.

Polymer	Activation energies of permeation (kJ/mol)				
	He	H_2	CO_2	N_2	CH_4
Gas Diffusion Diameter (Å)	2.55	2.77	3.44	3.49	3.817
TADPS-TPA	16.2 ± 0.9	16 ± 1	13.3 ± 0.9	28 ± 2	33 ± 2
TADPS-IPA	17.1 ± 0.3	17.0 ± 0.3	14.9 ± 0.3	30.5 ± 0.6	31.9 ± 0.8
TADPS-OBA	15.0 ± 0.2	14.8 ± 0.2	10.8 ± 0.2	23.9 ± 0.6	29.9 ± 0.5
m-PBI	18.3 ± 0.3	17.4 ± 0.3	17.0 ± 0.3	30.2 ± 0.9	40 ± 2
m-PBI [6]	--	19.4	17.1	27.5	--
6F-PBI [6]	--	8.36	0.391	11.02	--
TR-PBI [11]	--	-1.48	-4.93	3.29	8.73
Matrimid® [12]	14	--	9.8	21	26

Activation energies in kJ/mol. Diffusion diameters from Robeson et al. [8]. Uncertainties from propagation of errors [7].

Table 6.5 also includes other materials of interest. Li et al. studied a range of polybenzimidazoles by varying the diacid monomer [6]. Their base polymer, *m*-PBI, had similar activation energies of permeation to those of *m*-PBI our measurements. Li et al. incorporated a 6F (i.e., hexafluoroisopropylidene) moiety into the polymer backbone [6], which typically disrupts chain packing and increases permeability [1]. The inclusion of 6F resulted in higher permeabilities due to the more open polymer structure and significant decreases in activation energies of permeation [6]. Han et al. examined

polybenzimidazoles created by a thermal rearrangement method [11]. This method typically results in an open polymer structure with high permeabilities, moderate selectivities, and low activation energies of permeation [13-18]. The resultant TR-PBI structure had very high permeability (1779 Barrer for H_2 at 25 °C) with low and even negative activation energies of permeation for small (i.e., H_2) and condensable (i.e., CO_2) gases [11]. Activation energies for TADPS-based PBIs have activation energies below those of *m*-PBI, but E_P values for all gases are still higher than those of 6F-PBI, TR-PBI, and common polyimides such as Matrimid®.

Pure-gas selectivities for several pairs of gases in TADPS-TPA at 3 atm were calculated and are reported in Figure 6.8 as a function of temperature. Similar trends are seen for the three other samples considered (cf., Figures 6.9-6.11). Selectivities for many, but not all, gas pairs decrease as temperature increases. N_2/CH_4 selectivity decreases from 2.2 at 100 °C to 1.6 at 190 °C. CO_2 selectivity over other gases (e.g., CO_2/CH_4 and CO_2/N_2) also decreases as temperature increases. CO_2 is both smaller and more soluble than N_2 and CH_4, so both diffusivity selectivity and solubility selectivity may contribute to these selectivity decreases [8]. In contrast, He/H_2 selectivity was approximately constant at values from 1.2 to 1.3 over the entire temperature range considered due to similar activation energies of permeation, as shown in Table 6.5.

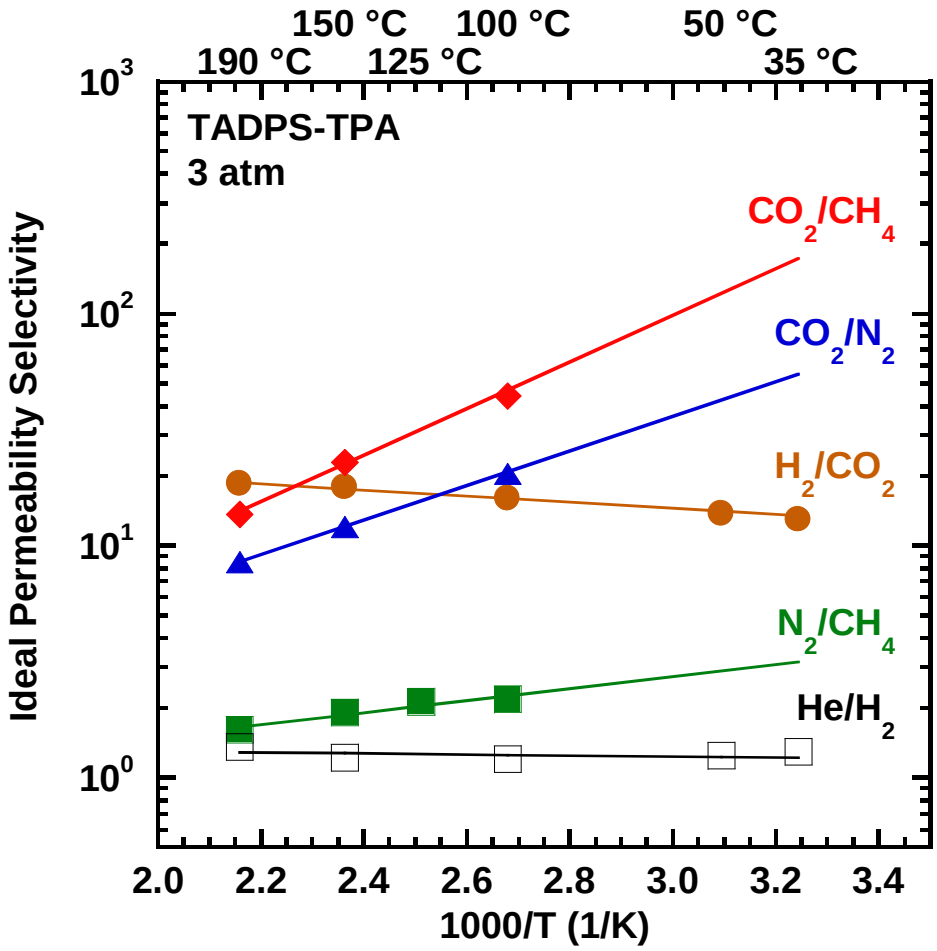

Figure 6.8. Ideal (pure-gas) permeability selectivities for various gas pairs at 3 atm in TADPS-TPA as a function of temperature. Solid lines were calculated from Arrhenius fits of the data in Figure 6.6.

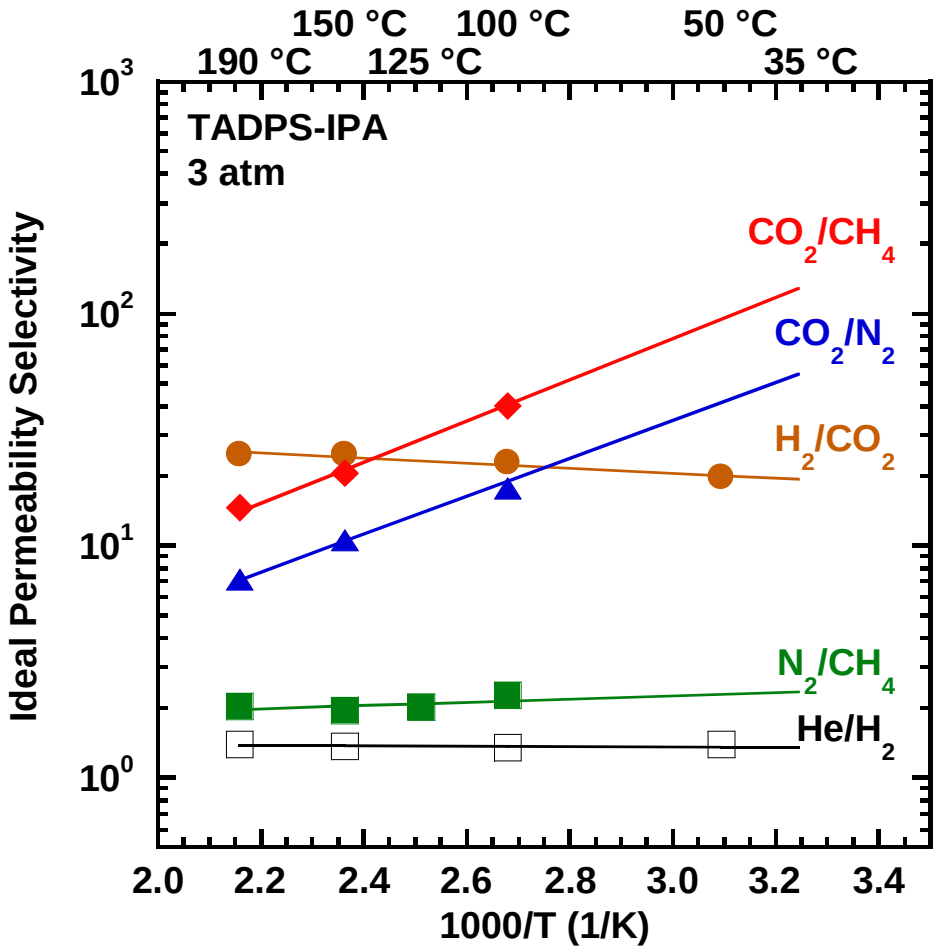

Figure 6.9. Ideal (pure-gas) permeability selectivities for various gas pairs at 3 atm in TADPS-IPA as a function of temperature. Solid lines were calculated from Arrhenius fits of the data in Figure 6.6.

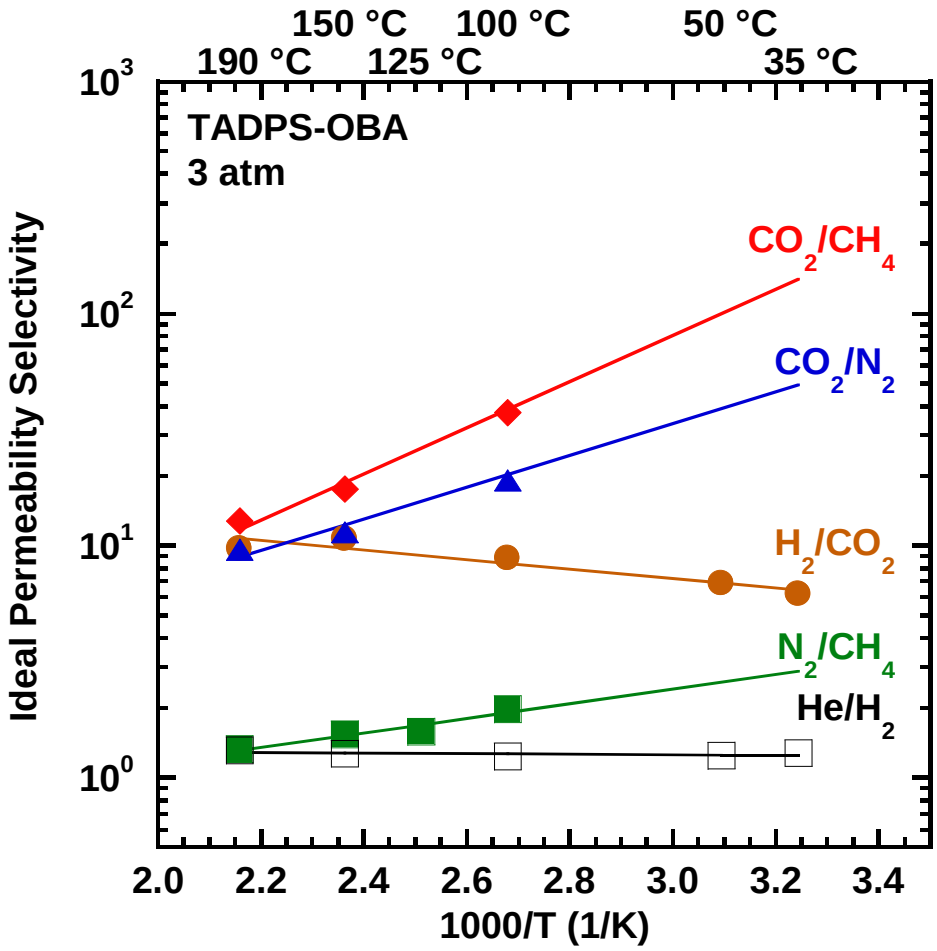

Figure 6.10. Ideal (pure-gas) permeability selectivities for various gas pairs at 3 atm in TADPS-OBA as a function of temperature. Solid lines were calculated from Arrhenius fits of the data in Figure 6.6.

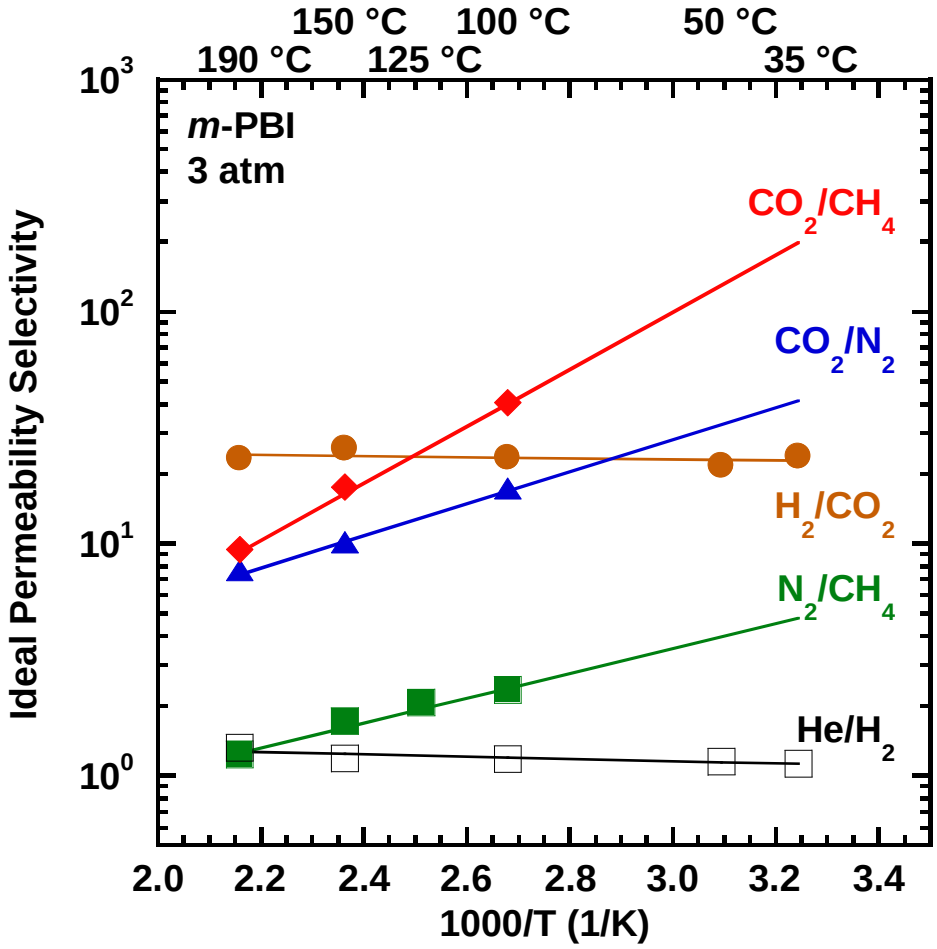

Figure 6.11. Ideal (pure-gas) permeability selectivities for various gas pairs at 3 atm in *m*-PBI as a function of temperature. Solid lines were calculated from Arrhenius fits of the data in Figure 6.6.

H_2/CO_2 selectivity increased with temperature. H_2/CO_2 pure gas selectivity for each sample is presented versus H_2 permeability and the Robeson upper bound in Figure 6.12. As temperature increases from 35 °C (i.e., the leftmost data points for each sample) to 190 °C (i.e., the rightmost data points for each sample), H_2 permeability and H_2/CO_2 selectivity simultaneously increase. There is some scatter in the permeability and selectivity for some samples, but general trends are evident. TADPS-OBA exhibits the greatest increase in selectivity over the 155 °C range considered, indicating the largest

difference between activation energies of permeation for H_2 and CO_2, and *m*-PBI exhibited the least change in selectivity, due to similar activation energies of permeation of H_2 and CO_2. Permeability-selectivity combinations for a range of other PBIs studied by Li et al. at 250 °C [6] are included for comparison. The samples considered here are in the lower permeability/higher selectivity range of PBIs, but extrapolations to 250 °C would yield combinations of permeability and selectivity in the region expected based on variations of chemical structure such as those reported by Li et al. [6] (i.e., combinations of permeability and selectivity that follow the trade-off between permeability and selectivity and approximately follow the slope of the upper bound). The behavior shown here of high H_2/CO_2 selectivities and simultaneously increasing H_2/CO_2 selectivity and gas permeabilities with increasing temperature is due to both the size-sieving behavior of these polymers coupled with an E_P for CO_2 that is lower than might be expected based on its size, presumably due to potential polymer-penetrant interactions. Upper bound plots for CO_2/CH_4, H_2/N_2, and He/H_2 gas pairs are included in Figure 6.13. CO_2/CH_4 moves away from the upper bound as temperature increases, H_2/N_2 moves approximately parallel to the upper bound, and He/H_2 moves horizontally on the upper bound plot.

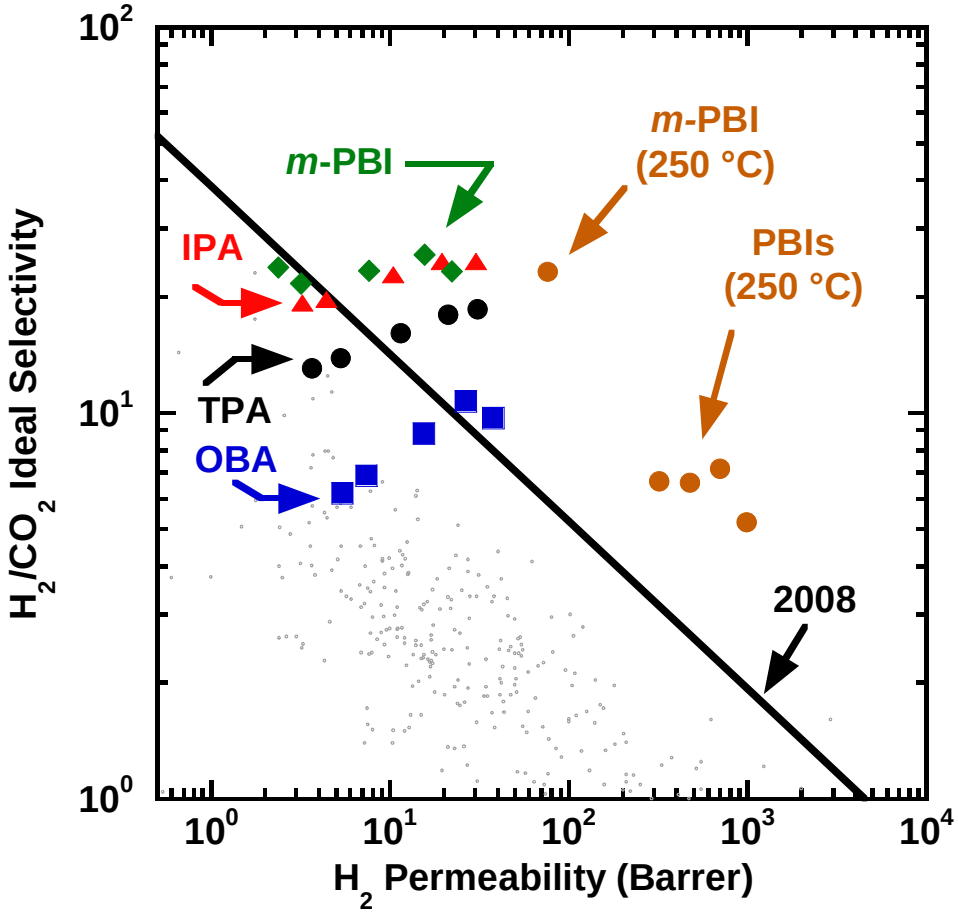

Figure 6.12. H_2/CO_2 ideal selectivity plotted versus H_2 permeability for TADPS-IPA (red triangles), TADPS-TPA (black circles), TADPS-OBA (blue squares), *m*-PBI (green diamonds), and other PBIs [6] at 250 °C (dark orange circles). Temperature of the materials measured in this study increases from left to right (35, 50, 100, 150, 190 °C). The 35 °C data point for IPA is extrapolated using Equation [2-4].

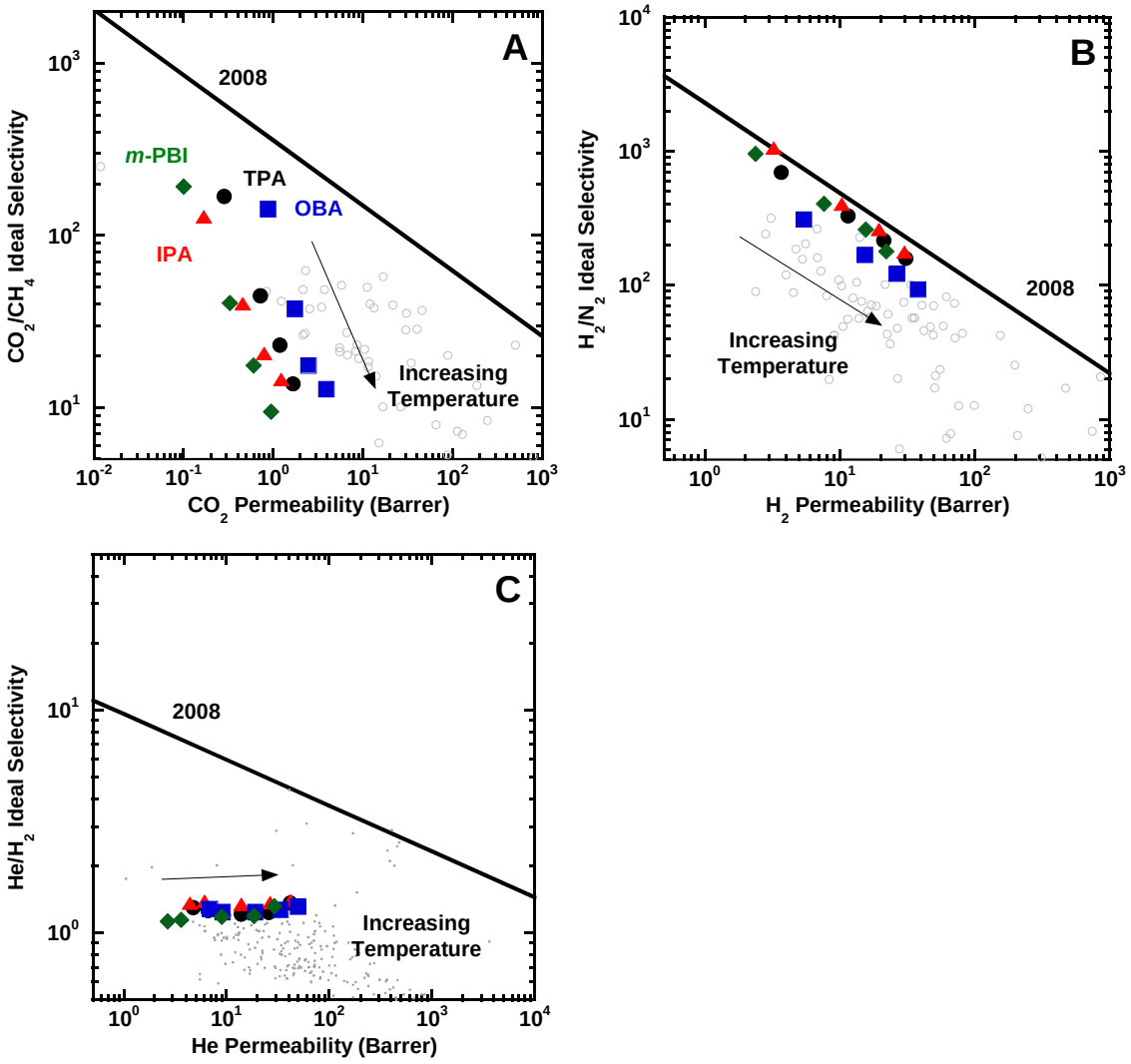

Figure 6.13. A) CO_2/CH_4 selectivity versus CO_2 permeability at 35, 100, 150, and 190 °C, B) H_2/N_2 selectivity versus H_2 permeability at 35, 100, 150, and 190 °C, and C) He/H_2 selectivity versus He permeability at 35, 50, 100, 150, and 190 °C for TADPS-IPA (red triangles), TADPS-TPA (black circles), TADPS-OBA (blue squares), and *m*-PBI (green diamonds). Temperature of the materials measured in this study increases from left to right (35, 50, 100, 150, 190 °C). The 35 °C data points for IPA and for gas pairs involving CH_4 or N_2 are extrapolated using Equation [2-4]. The line represents the 2008 upper bound [19], and the light gray data points are representative of many different polymers and are taken from the literature [19].

Gas diffusivities (and activation energies of diffusion) typically scale with gas size [1, 20, 21]. In the absence of diffusivity data, activation energies of permeation may be analyzed to draw some conclusions. Activation energies of permeation for the gases and samples in this study are presented as a function of gas size in Figure 6.14. As gas size increases, the energy required for a gas molecule to diffuse through a polymer increases, and the data in Figure 6.14 are consistent with this behavior, with the exception of CO_2. CO_2 is the most condensable and soluble gas considered, and it would be anticipated to have the most exothermic (i.e., negative) enthalpy of sorption. Additionally, favorable interactions between CO_2 and polar groups in these polymers may occur, further contributing to more exothermic sorption. Therefore, some depression in the E_P values for CO_2 is expected. CO_2 exhibits the lowest activation energy of permeation for each of the TADPS-based PBIs as well as *m*-PBI. The significant increase in activation energy of permeation for most gases (except CO_2) with gas size indicates strong size-sieving behavior of these polymers [1, 20, 21].

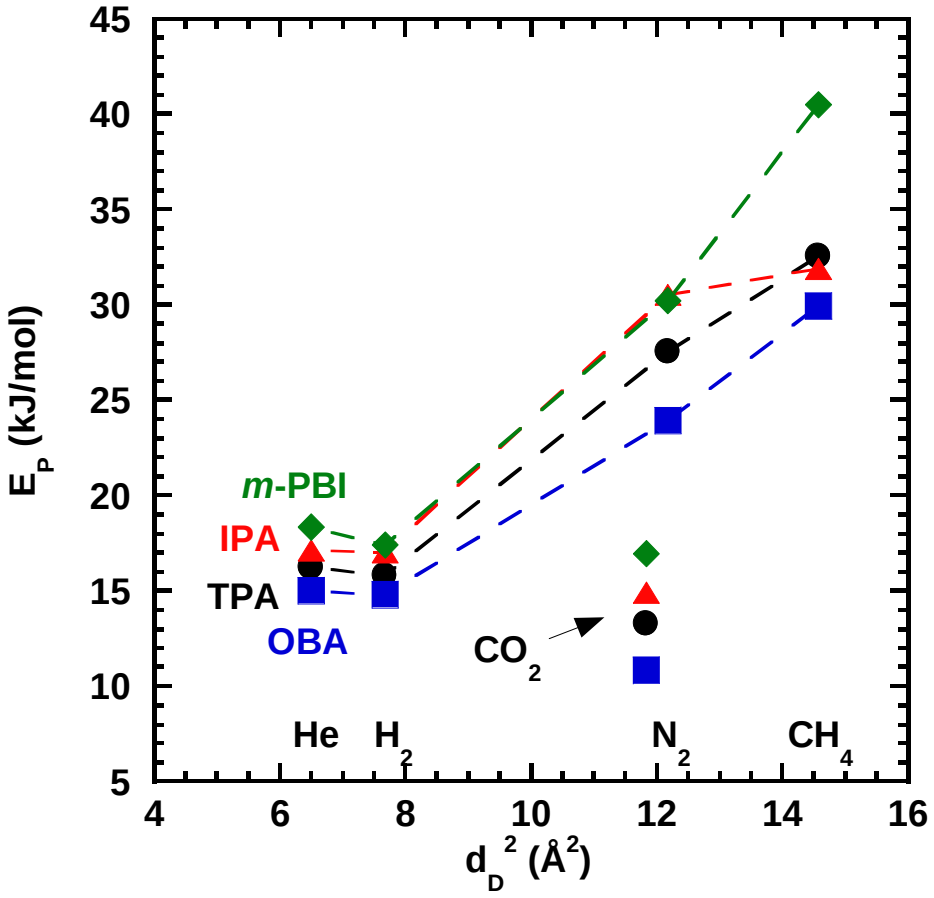

Figure 6.14. Activation energy of permeation versus diffusion diameter, d_D, squared. Dashed lines are guides for the eye.

6.2.3 Temperature dependence of diffusivity

The temperature dependence of diffusion coefficients can provide more detail about the transport behavior of PBIs. The diffusion coefficients of faster gases (i.e., He and H_2) were too fast to be measured reliably. Diffusivities of CO_2, N_2, and CH_4 were estimated in TADPS-TPA by using the method reported by De Angelis et al. [22] and are presented in Figure 6.15 as a function of inverse temperature. (Similar calculations can be

performed for other PBIs, but any variation in upstream pressure before steady state permeation was reached complicated the fitting procedure. TADPS-TPA provided the most complete data set and was considered here.) As temperature increases, diffusion coefficients increase significantly. Gas size also plays a significant role in diffusivity. For example, CH_4, with a diffusion diameter of 3.817 Å, displays an order of magnitude lower diffusivity at 100 °C than nitrogen, which has a diffusion diameter of 3.49 Å [8]. CO_2, the smallest gas considered for these estimations, displays the highest diffusivities.

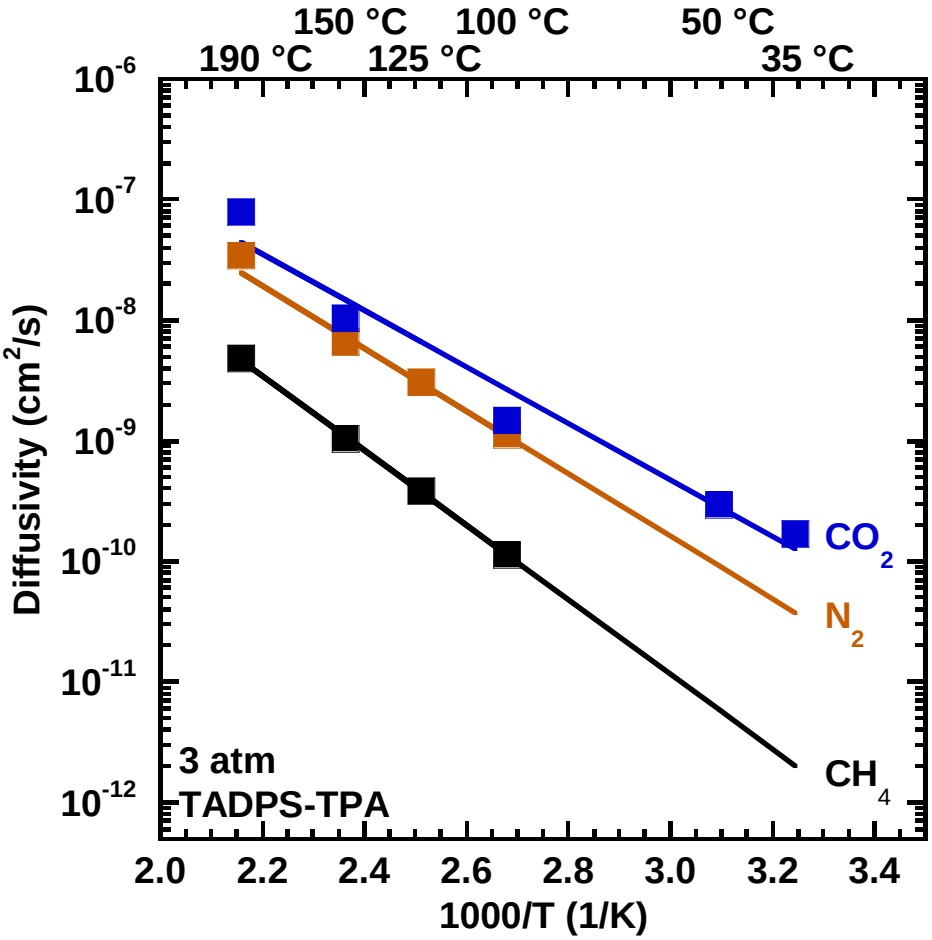

Figure 6.15. Estimated diffusivity in TADPS-TPA at approximately 3 atm. Diffusivities were estimated using the method reported by De Angelis [22], and the solid lines represent Arrhenius fits.

Activation energies of diffusion can be calculated based on the data in Figure 6.15. Gas size, as expected (cf., Equation [2-9]), impacts the activation energies of diffusion. Methane exhibits an activation energy of diffusion of 59 ± 4 kJ/mol where CO_2 has activation energy of 45 ± 1 kJ/mol. The enthalpies of sorption, calculated using Equation [2-7], increase with penetrant condensability (i.e., critical temperature), where CO_2, the most condensable penetrant, exhibits the most exothermic enthalpy of sorption,

as might be expected based on its high T_c value [1] and potential to interact with polar groups [23] in these polymers.

Table 6.6. Activation energies of permeation, activation energy of diffusion, and enthalpy of sorption in TADPS-TPA at 3 atm.

Gas	Diffusion diameter [8]	Critical temperature (K) [1]	E_P	E_D	ΔH_S
CO_2	3.44	304.2	13 ± 1	45 ± 1	-32 ± 1
N_2	3.49	126.2	28 ± 2	50 ± 5	-22 ± 6
CH_4	3.817	190.6	33 ± 2	59 ± 4	-27 ± 4

Activation energies and enthalpies reported at 3 atm in kJ/mol.

6.3 REFERENCES

[1] S. Matteucci, Y. Yampolskii, B.D. Freeman, I. Pinnau, Transport of gases and vapors in glassy and rubbery polymers, in: Y. Yampolskii, I. Pinnau, B. Freeman (Eds.) Materials science of membranes for gas and vapor separation, John Wiley & Sons, Ltd, Chichester, UK, 2006, pp. 1-47.

[2] H. Borjigin, K.A. Stevens, R. Liu, J.D. Moon, A.T. Shaver, S. Swinnea, B.D. Freeman, J.S. Riffle, J.E. McGrath, Synthesis and characterization of polybenzimidazoles derived from tetraaminodiphenylsulfone for high temperature gas separation membranes, Polymer, 71 (2015) 135-142.

[3] S.C. Kumbharkar, P.B. Karadkar, U.K. Kharul, Enhancement of gas permeation properties of polybenzimidazoles by systematic structure architecture, Journal of Membrane Science, 286 (2006) 161-169.

[4] T.-S. Chung, A critical review of polybenzimidazoles, Journal of Macromolecular Science, Part C, 37 (1997) 277-301.

[5] A.H. Chan, D.R. Paul, Effect of sub-Tg annealing on gas transport in polycarbonate, Journal of Applied Polymer Science, 25 (1980) 971-974.

[6] X. Li, R.P. Singh, K.W. Dudeck, K.A. Berchtold, B.C. Benicewicz, Influence of polybenzimidazole main chain structure on H_2/CO_2 separation at elevated temperatures, Journal of Membrane Science, 461 (2014) 59-68.

[7] P.R. Bevington, D.K. Robinson, Data reduction and error analysis for the physical sciences, McGraw Hill, Boston, 2003.

[8] L.M. Robeson, Z.P. Smith, B.D. Freeman, D.R. Paul, Contributions of diffusion and solubility selectivity to the upper bound analysis for glassy gas separation membranes, Journal of Membrane Science, 453 (2014) 71-83.

[9] J.S. McHattie, W.J. Koros, D.R. Paul, Gas transport properties of polysulphones: 1. Role of symmetry of methyl group placement on bisphenol rings, Polymer, 32 (1991) 840-850.

[10] H. Zhao, Y. Cao, X. Ding, M. Zhou, Q. Yuan, Effects of cross-linkers with different molecular weights in cross-linked Matrimid 5218 and test temperature on gas transport properties, Journal of Membrane Science, 323 (2008) 176-184.

[11] S.H. Han, J.E. Lee, K.-J. Lee, H.B. Park, Y.M. Lee, Highly gas permeable and microporous polybenzimidazole membrane by thermal rearrangement, Journal of Membrane Science, 357 (2010) 143-151.

[12] L. Ansaloni, M. Minelli, M. Giacinti Baschetti, G.C. Sarti, Effect of relative humidity and temperature on gas transport in Matrimid®: Experimental study and modeling, Journal of Membrane Science, 471 (2014) 392-401.

[13] H.B. Park, C.H. Jung, Y.M. Lee, A.J. Hill, S.J. Pas, S.T. Mudie, E. Van Wagner, B.D. Freeman, D.J. Cookson, Polymers with cavities tuned for fast selective transport of small molecules and ions, Science, 318 (2007) 254-258.

[14] D.F. Sanders, R. Guo, Z.P. Smith, K.A. Stevens, Q. Liu, J.E. McGrath, D.R. Paul, B.D. Freeman, Influence of polyimide precursor synthesis route and ortho-position functional group on thermally rearranged (TR) polymer properties: Pure gas permeability and selectivity, Journal of Membrane Science, 463 (2014) 73-81.

[15] D.F. Sanders, R. Guo, Z.P. Smith, Q. Liu, K.A. Stevens, J.E. McGrath, D.R. Paul, B.D. Freeman, Influence of polyimide precursor synthesis route and ortho-position functional group on thermally rearranged (TR) polymer properties: Conversion and free volume, Polymer, 55 (2014) 1636-1647.

[16] D.F. Sanders, Z.P. Smith, C.P. Ribeiro, R. Guo, J.E. McGrath, D.R. Paul, B.D. Freeman, Gas permeability, diffusivity, and free volume of thermally rearranged polymers based on 3,3′-dihydroxy-4,4′-diamino-biphenyl (HAB) and 2,2′-bis-(3,4-dicarboxyphenyl) hexafluoropropane dianhydride (6FDA), Journal of Membrane Science, 409-410 (2012) 232-241.

[17] Z.P. Smith, D.F. Sanders, C.P. Ribeiro, R. Guo, B.D. Freeman, D.R. Paul, J.E. McGrath, S. Swinnea, Gas sorption and characterization of thermally rearranged polyimides based on 3,3′-dihydroxy-4,4′-diamino-biphenyl (HAB) and 2,2′-bis-(3,4-dicarboxyphenyl) hexafluoropropane dianhydride (6FDA), Journal of Membrane Science, 415-416 (2012) 558-567.

[18] K.A. Stevens, M. Galizia, D.R. Paul, B.D. Freeman, Influence of temperature on gas permeability and diffusivity in thermally rearranged (TR) polymers, Journal of Membrane Science, *In preparation*.

[19] L.M. Robeson, The upper bound revisited, Journal of Membrane Science, 320 (2008) 390-400.

[20] D.W. van Krevelen, Properties of polymers, 3rd ed., Elsevier, Amsterdam, 1997.

[21] P. Meares, The Diffusion of Gases Through Polyvinyl Acetate, Journal of the American Chemical Society, 76 (1954) 3415-3422.

[22] M.G. De Angelis, G.C. Sarti, A. Sanguineti, P. Maccone, Permeation, diffusion, and sorption of dimethyl ether in fluoroelastomers, Journal of Polymer Science Part B: Polymer Physics, 42 (2004) 1987-2006.

[23] K. Ghosal, R.T. Chern, B.D. Freeman, W.H. Daly, I.I. Negulescu, Effect of Basic Substituents on Gas Sorption and Permeation in Polysulfone, Macromolecules, 29 (1996) 4360-4369.

Chapter 7: Conclusions and recommendations

7.1 CONCLUSIONS

The solubilities of N_2, CH_4, and CO_2 were measured in HAB-6FDA polyimide and three of its TR analogs at pressures up to 27 atm and temperatures from -10 °C to 50 °C. Solubility increased with increasing TR conversion, and enthalpies of sorption became less exothermic upon initial TR conversion. However, further TR conversion had a small impact on the enthalpies of sorption. The endothermic shift in enthalpies of sorption at low levels of TR conversion is hypothesized to be related to the presence of hydrogen bonding, which would tend to increase the energetic penalty to create Henry's law sorption sites, and by cross-links formed during thermal rearrangement. Solubility selectivity decreased with increasing TR conversion but only changed slightly with temperature due to similar enthalpies of sorption for CH_4 and CO_2. Infinite dilution solubilities correlated well with penetrant critical temperature.

The effect of temperature on H_2, N_2, CH_4, and CO_2 permeability and diffusivity in HAB-6FDA polyimide and TR polymer analogs were studied. Permeability generally increased as temperature increased, though CO_2 exhibited the opposite trend in the most highly converted TR sample considered, TR450-30m. Significant plasticization by CO_2 was observed at low temperatures in the polyimide precursor, while no detectable plasticization was observed in highly converted TR polymers. Activation energies of permeation initially increased slightly for all gases except CO_2, and then all activation energies of permeation decreased significantly with TR conversion until, at the highest TR conversion, E_P for CO_2 decreased below zero. At the highest TR conversion, CO_2 permeability and CO_2/CH_4 selectivity both increase with decreasing temperature, resulting in a trend toward the upper right on the upper bound, which is consistent with the temperature-dependent behavior observed for other high FFV polymers. Diffusivities

increased with increasing temperature, and the largest increases were seen in the TR350-1hr sample with the largest gas (e.g., CH_4). By combining activation energies of permeation with previous sorption measurements, the activation energies of diffusion were calculated. E_P and E_D exhibited similar trends with TR conversion, which is consistent with the observed increase in FFV in TR samples. The order of activation energies of diffusion differed from the expected trend with gas size, particularly in higher-converted samples.

The temperature dependence of He, H_2, N_2, CH_4, and CO_2 permeability in TADPS-IPA, TADPS-TPA, TADPS-OBA, and *m*-PBI polybenzimidazoles was measured. Permeabilities increased with increasing temperature, and the activation energies of permeation increased with increasing gas size except for CO_2, which had the lowest activation energy of permeation for the TADPS-based PBIs. CO_2/N_2, CO_2/CH_4, and N_2/CH_4 selectivities decreased with increasing temperature, while H_2/CO_2 selectivities increased. All TADPS-based PBI samples moved towards the upper right on the H_2/CO_2 upper bound as temperature increased. Estimated diffusivities in TADPS-TPA increased significantly with temperature due to high activation energies of diffusion, consistent with the strongly size-sieving behavior of polybenzimidazoles.

7.2 RECOMMENDATIONS

7.2.1 Lattice fluid modeling for gas sorption and permeation in TR polymers

The dual mode model is widely accepted and used to describe gas sorption in glassy polymers [1]. This model was used as a function of temperature in the study described in Chapter 4. There, the model was adapted using Arrhenius-van't Hoff relationships to describe gas sorption as a function of temperature [1, 2]. While the dual mode model is adequate to describe gas sorption, it lacks predictive capability. Other

models, such as the Non-Equilibrium Lattice Fluid (NELF) model [3], are capable of predictive calculations. In the NELF model, the Sanchez-Lacombe lattice fluid parameters are used with polymer density to accurately calculate gas sorption after accounting for any polymer swelling effects [3]. Lattice fluid parameters are typically determined in the rubbery state [3], which is inaccessible for TR polymers. An alternative method [4] has been developed to determine lattice fluid parameters by regression of gas sorption data. This approach can be used to model gas sorption in TR polymers. An extension of this model could be derived to combine sorption calculations with penetrant mobility and diffusion to fully describe gas permeation in TR polymers from a theoretical approach.

7.2.2 The effect of humidity on the transport properties of PBIs

Chapter 6 describes the temperature dependence of gas permeation in TADPS-based PBIs. The permeation sample preparation procedure includes steps that involve film exposure to humidity: removal from the oven after drying and after curing the epoxy used to mount the permeation sample to its support but before the sample is loaded into a permeation system. The water content due to ambient humidity can reach several percent, and the equilibrium uptake in liquid water is near or above 15% by weight [5]. This process necessitates a drying step to avoid apparent permeabilities changing during measurements. The effect of the presence of water on other polymer systems, such as Matrimid® [6] and Nafion® 117 [7, 8], have been studied as a function of relative humidity. Glassy polymers such as Matrimid® exhibit depression of gas permeability due to the competitive sorption of water [6] while Nafion® 117 exhibits strong increases in the permeability of gases due in part to swelling of the polymer matrix [7]. Initial measurements indicate that TADPS-based PBIs film thicknesses can increase by

approximately 4% while exposed to ambient humidity as compared to a dry state. Competitive sorption will act to reduce permeability while swelling of the polymer matrix due to hydrophilicity will act to increase permeabilities. The contributions of these effects to permeability can be separated by a combination of water sorption and permeation measurements, humidified mixed-gas permeation, and humidified gas sorption measurements.

The presence of water and its effect on the polymer matrix also complicates the measurement of densities, which are typically measured using Archimedes' principle at ambient conditions or in a density gradient column with aqueous salt solution. The use of a density gradient column is complicated by potential interaction of the salt with the polymer backbone due to its strongly polar nature in combination with hydrophilicity. The measurement of density as a function of relative humidity can be achieved more simply by measurements using Archimedes' principle in a humidity-controlled atmosphere. The effects of humidity on polymer density and, therefore, fractional free volume would greatly benefit the study of transport of gases in highly hydrophilic glassy polymers, such as these PBIs.

7.3 REFERENCES

[1] K. Ghosal, B.D. Freeman, Gas separation using polymer membranes: an overview, Polymers for Advanced Technologies, 5 (1994) 673-697.

[2] W.J. Koros, D.R. Paul, G.S. Huvard, Energetics of gas sorption in glassy polymers, Polymer, 20 (1979) 956-960.

[3] F. Doghieri, G.C. Sarti, Nonequilibrium Lattice Fluids: A Predictive Model for the Solubility in Glassy Polymers, Macromolecules, 29 (1996) 7885-7896.

[4] M. Galizia, M.G. De Angelis, G.C. Sarti, Sorption of hydrocarbons and alcohols in addition-type poly(trimethyl silyl norbornene) and other high free volume glassy

polymers. II: NELF model predictions, Journal of Membrane Science, 405-406 (2012) 201-211.

[5] H. Borjigin, K.A. Stevens, R. Liu, J.D. Moon, A.T. Shaver, S. Swinnea, B.D. Freeman, J.S. Riffle, J.E. McGrath, Synthesis and characterization of polybenzimidazoles derived from tetraaminodiphenylsulfone for high temperature gas separation membranes, Polymer, 71 (2015) 135-142.

[6] L. Ansaloni, M. Minelli, M. Giacinti Baschetti, G.C. Sarti, Effect of relative humidity and temperature on gas transport in Matrimid®: Experimental study and modeling, Journal of Membrane Science, 471 (2014) 392-401.

[7] J. Catalano, T. Myezwa, M.G. De Angelis, M.G. Baschetti, G.C. Sarti, The effect of relative humidity on the gas permeability and swelling in PFSI membranes, International Journal of Hydrogen Energy, 37 (2012) 6308-6316.

[8] S. Ban, C. Huang, X.-Z. Yuan, H. Wang, Molecular simulation of gas adsorption, diffusion, and permeation in hydrated Nafion membranes, The Journal of Physical Chemistry B, 115 (2011) 11352-11358.

References

A. Bos, I.G.M. Pünt, M. Wessling, H. Strathmann, CO_2-induced plasticization phenomena in glassy polymers, Journal of Membrane Science, 155 (1999) 67-78.

A. Morisato, B.D. Freeman, I. Pinnau, C.G. Casillas, Pure hydrocarbon sorption properties of poly(1-trimethylsilyl-1-propyne) (PTMSP), poly(1-phenyl-1-propyne) (PPP), and PTMSP/PPP blends, Journal of Polymer Science Part B: Polymer Physics, 34 (1996) 1925-1934.

A.G. Wonders, D.R. Paul, Effect of CO_2 exposure history on sorption and transport in polycarbonate, Journal of Membrane Science, 5 (1979) 63-75.

A.H. Chan, D.R. Paul, Effect of sub-Tg annealing on gas transport in polycarbonate, Journal of Applied Polymer Science, 25 (1980) 971-974.

B.D. Freeman, Basis of permeability/selectivity tradeoff relations in polymeric gas separation membranes, Macromolecules, 32 (1999) 375-380.

B.W. Rowe, B.D. Freeman, D.R. Paul, Effect of Sorbed Water and Temperature on the Optical Properties and Density of Thin Glassy Polymer Films on a Silicon Substrate, Macromolecules, 40 (2007) 2806-2813.

B.W. Rowe, L.M. Robeson, B.D. Freeman, D.R. Paul, Influence of temperature on the upper bound: Theoretical considerations and comparison with experimental results, Journal of Membrane Science, 360 (2010) 58-69.

C.M. Zimmerman, W.J. Koros, Polypyrrolones for membrane gas separations. I. Structural comparison of gas transport and sorption properties, Journal of Polymer Science Part B: Polymer Physics, 37 (1999) 1235-1249.

C.M. Zimmerman, W.J. Koros, Polypyrrolones for membrane gas separations. II. Activation energies and heats of sorption, Journal of Polymer Science Part B: Polymer Physics, 37 (1999) 1251-1265.

D. Hofmann, M. Entrialgo-Castano, A. Lerbret, M. Heuchel, Y. Yampolskii, Molecular modeling investigation of free volume distributions in stiff chain polymers with conventional and ultrahigh free volume: Comparison between molecular modeling and positron lifetime studies, Macromolecules, 36 (2003) 8528-8538.

D.F. Sanders, R. Guo, Z.P. Smith, K.A. Stevens, Q. Liu, J.E. McGrath, D.R. Paul, B.D. Freeman, Influence of polyimide precursor synthesis route and ortho-position functional group on thermally rearranged (TR) polymer properties: Pure gas permeability and selectivity, Journal of Membrane Science, 463 (2014) 73-81.

D.F. Sanders, R. Guo, Z.P. Smith, Q. Liu, K.A. Stevens, J.E. McGrath, D.R. Paul, B.D. Freeman, Influence of polyimide precursor synthesis route and ortho-position functional group on thermally rearranged (TR) polymer properties: Conversion and free volume, Polymer, 55 (2014) 1636-1647.

D.F. Sanders, Z.P. Smith, C.P. Ribeiro, R. Guo, J.E. McGrath, D.R. Paul, B.D. Freeman, Gas permeability, diffusivity, and free volume of thermally rearranged polymers based on 3,3′-dihydroxy-4,4′-diamino-biphenyl (HAB) and 2,2′-bis-(3,4-dicarboxyphenyl) hexafluoropropane dianhydride (6FDA), Journal of Membrane Science, 409-410 (2012) 232-241.

D.F. Sanders, Z.P. Smith, R. Guo, L.M. Robeson, J.E. McGrath, D.R. Paul, B.D. Freeman, Energy-efficient polymeric gas separation membranes for a sustainable future: A review, Polymer, 54 (2013) 4729-4761.

D.R. Pesiri, B. Jorgensen, R.C. Dye, Thermal optimization of polybenzimidazole meniscus membranes for the separation of hydrogen, methane, and carbon dioxide, Journal of Membrane Science, 218 (2003) 11-18.

D.S. Pope, W.J. Koros, H.B. Hopfenberg, Sorption and dilation of poly(1-(trimethylsilyl)-1-propyne) by carbon dioxide and methane, Macromolecules, 27 (1994) 5839-5844.

D.W. van Krevelen, Properties of polymers, 3rd ed., Elsevier, Amsterdam, 1997.

E.S. Sanders, High-pressure sorption of pure and mixed gases in glassy polymers (Ph.D. Dissertation), North Carolina State University, Raleigh, 1983.

G.E. Serad, B.D. Freeman, M.E. Stewart, A.J. Hill, Gas and vapor sorption and diffusion in poly(ethylene terephthalate), Polymer, 42 (2001) 6929-6943.

G.J. van Amerongen, The Permeability of Different Rubbers to Gases and Its Relation to Diffusivity and Solubility, Journal of Applied Physics, 17 (1946) 972-972.

H. Borjigin, K.A. Stevens, R. Liu, J.D. Moon, A.T. Shaver, S. Swinnea, B.D. Freeman, J.S. Riffle, J.E. McGrath, Synthesis and characterization of polybenzimidazoles derived from tetraaminodiphenylsulfone for high temperature gas separation membranes, Polymer, 71 (2015) 135-142.

H. Czichos, T. Saito, L. Smith, Springer handbook of materials measurement methods, Springer Verlag, 2006.

H. Lin, B.D. Freeman, Gas permeation and diffusion in cross-linked poly(ethylene glycol diacrylate), Macromolecules, 39 (2006) 3568-3580.

H. Zhao, Y. Cao, X. Ding, M. Zhou, Q. Yuan, Effects of cross-linkers with different molecular weights in cross-linked Matrimid 5218 and test temperature on gas transport properties, Journal of Membrane Science, 323 (2008) 176-184.

H.B. Park, C.H. Jung, Y.M. Lee, A.J. Hill, S.J. Pas, S.T. Mudie, E. Van Wagner, B.D. Freeman, D.J. Cookson, Polymers with cavities tuned for fast selective transport of small molecules and ions, Science, 318 (2007) 254-258.

J. Sánchez-Laínez, B. Zornoza, S. Friebe, J. Caro, S. Cao, A. Sabetghadam, B. Seoane, J. Gascon, F. Kapteijn, C. Le Guillouzer, G. Clet, M. Daturi, C. Téllez, J. Coronas,

Influence of ZIF-8 particle size in the performance of polybenzimidazole mixed matrix membranes for pre-combustion CO_2 capture and its validation through interlaboratory test, Journal of Membrane Science, 515 (2016) 45-53.

J.G. Wijmans, R.W. Baker, The solution-diffusion model: a review, Journal of Membrane Science, 107 (1995) 1-21.

J.M. Smith, H.C. Van Ness, M.M. Abbott, Introduction to chemical engineering thermodynamics, McGraw-Hill, Boston, 2005.

J.S. Chiou, J.W. Barlow, D.R. Paul, Plasticization of glassy polymers by CO_2, Journal of Applied Polymer Science, 30 (1985) 2633-2642.

J.S. McHattie, W.J. Koros, D.R. Paul, Gas transport properties of polysulphones: 1. Role of symmetry of methyl group placement on bisphenol rings, Polymer, 32 (1991) 840-850.

K. Ghosal, B.D. Freeman, Gas separation using polymer membranes: an overview, Polymers for Advanced Technologies, 5 (1994) 673-697.

K. Ghosal, R.T. Chern, B.D. Freeman, W.H. Daly, I.I. Negulescu, Effect of Basic Substituents on Gas Sorption and Permeation in Polysulfone, Macromolecules, 29 (1996) 4360-4369.

K. Nagai, B.D. Freeman, A.J. Hill, Effect of physical aging of poly(1-trimethylsilyl-1-propyne) films synthesized with $TaCl_5$ and $NbCl_5$ on gas permeability, fractional free volume, and positron annihilation lifetime spectroscopy parameters, Journal of Polymer Science Part B: Polymer Physics, 38 (2000) 1222-1239.

K.A. Berchtold, R.P. Singh, J.S. Young, K.W. Dudeck, Polybenzimidazole composite membranes for high temperature synthesis gas separations, Journal of Membrane Science, 415-416 (2012) 265-270.

K.A. Stevens, M. Galizia, D.R. Paul, B.D. Freeman, Influence of temperature on gas permeability and diffusivity in thermally rearranged (TR) polymers, Journal of Membrane Science, *In preparation*.

K.A. Stevens, Z.P. Smith, K.L. Gleason, M. Galizia, D.R. Paul, B.D. Freeman, Influence of temperature on gas solubility in thermally rearranged (TR) polymers, Journal of Membrane Science, *Submitted*.

K.C. O'Brien, G. Krishnan, K.A. Berchtold, S. Blum, R. Callahan, W. Johnson, D.L. Roberts, D. Steele, D. Byard, J. Figueroa, Towards a pilot-scale membrane system for pre-combustion CO_2 separation, Energy Procedia, 1 (2009) 287-294.

K.L. Gleason, Z.P. Smith, Q. Liu, D.R. Paul, B.D. Freeman, Pure- and mixed-gas permeation of CO_2 and CH_4 in thermally rearranged polymers based on 3,3'-dihydroxy-4,4'-diamino-biphenyl (HAB) and 2,2'-bis-(3,4-dicarboxyphenyl) hexafluoropropane dianhydride (6FDA), Journal of Membrane Science, 475 (2015) 204-214.

L. Ansaloni, M. Minelli, M. Giacinti Baschetti, G.C. Sarti, Effect of relative humidity and temperature on gas transport in Matrimid®: Experimental study and modeling, Journal of Membrane Science, 471 (2014) 392-401.

L.M. Costello, W.J. Koros, Thermally stable polyimide isomers for membrane-based gas separations at elevated temperatures, Journal of Polymer Science Part B: Polymer Physics, 33 (1995) 135-146.

L.M. Robeson, Correlation of separation factor versus permeability for polymeric membranes, Journal of Membrane Science, 62 (1991) 165-185.

L.M. Robeson, The upper bound revisited, Journal of Membrane Science, 320 (2008) 390-400.

L.M. Robeson, Z.P. Smith, B.D. Freeman, D.R. Paul, Contributions of diffusion and solubility selectivity to the upper bound analysis for glassy gas separation membranes, Journal of Membrane Science, 453 (2014) 71-83.

M.G. De Angelis, G.C. Sarti, A. Sanguineti, P. Maccone, Permeation, diffusion, and sorption of dimethyl ether in fluoroelastomers, Journal of Polymer Science Part B: Polymer Physics, 42 (2004) 1987-2006.

N.R. Horn, D.R. Paul, Carbon dioxide plasticization and conditioning effects in thick vs. thin glassy polymer films, Polymer, 52 (2011) 1619-1627.

P. Li, T.S. Chung, D.R. Paul, Temperature dependence of gas sorption and permeation in PIM-1, Journal of Membrane Science, 450 (2014) 380-388.

P. Meares, The Diffusion of Gases Through Polyvinyl Acetate, Journal of the American Chemical Society, 76 (1954) 3415-3422.

P.R. Bevington, D.K. Robinson, Data reduction and error analysis for the physical sciences, McGraw Hill, Boston, 2003.

R.P. Singh, G.J. Dahe, K.W. Dudeck, C.F. Welch, K.A. Berchtold, High temperature polybenzimidazole hollow fiber membranes for hydrogen separation and carbon dioxide capture from synthesis gas, Energy Procedia, 63 (2014) 153-159.

R.S. Prabhakar, B.D. Freeman, I. Roman, Gas and vapor sorption and permeation in poly(2,2,4-trifluoro-5-trifluoromethoxy-1,3-dioxole-co-tetrafluoroethylene), Macromolecules, 37 (2004) 7688-7697.

R.S. Prabhakar, T.C. Merkel, B.D. Freeman, T. Imizu, A. Higuchi, Sorption and transport properties of propane and perfluoropropane in poly(dimethylsiloxane) and poly(1-trimethylsilyl-1-propyne), Macromolecules, 38 (2005) 1899-1910.

R.W. Baker, K. Lokhandwala, Natural gas processing with membranes: an overview, Industrial & Engineering Chemistry Research, 47 (2008) 2109-2121.

S. Kim, J.G. Seong, Y.S. Do, Y.M. Lee, Gas sorption and transport in thermally rearranged polybenzoxazole membranes derived from polyhydroxylamides, Journal of Membrane Science, 474 (2015) 122-131.

S. Kim, Y.M. Lee, Rigid and microporous polymers for gas separation membranes, Progress in Polymer Science, 43 (2015) 1-32.

S. Matteucci, Y. Yampolskii, B.D. Freeman, I. Pinnau, Transport of gases and vapors in glassy and rubbery polymers, in: Y. Yampolskii, I. Pinnau, B. Freeman (Eds.) Materials science of membranes for gas and vapor separation, John Wiley & Sons, Ltd, Chichester, UK, 2006, pp. 1-47.

S. Mazumdar, Monte Carlo methods for confidence bands in nonlinear regression (M.S. Thesis), University of North Florida, Jacksonville, 1995.

S. Shishatskiy, C. Nistor, M. Popa, S.P. Nunes, K.V. Peinemann, Polyimide asymmetric membranes for hydrogen separation: Influence of formation conditions on gas transport properties, Advanced Engineering Materials, 8 (2006) 390-397.

S.C. Kumbharkar, P.B. Karadkar, U.K. Kharul, Enhancement of gas permeation properties of polybenzimidazoles by systematic structure architecture, Journal of Membrane Science, 286 (2006) 161-169.

S.C. Kumbharkar, U.K. Kharul, Investigation of gas permeation properties of systematically modified polybenzimidazoles by N-substitution, Journal of Membrane Science, 357 (2010) 134-142.

S.C. Kumbharkar, U.K. Kharul, N-substitution of polybenzimidazoles: Synthesis and evaluation of physical properties, European Polymer Journal, 45 (2009) 3363-3371.

S.C. Kumbharkar, Y. Liu, K. Li, High performance polybenzimidazole based asymmetric hollow fibre membranes for H_2/CO_2 separation, Journal of Membrane Science, 375 (2011) 231-240.

S.H. Han, J.E. Lee, K.-J. Lee, H.B. Park, Y.M. Lee, Highly gas permeable and microporous polybenzimidazole membrane by thermal rearrangement, Journal of Membrane Science, 357 (2010) 143-151.

T. Masuda, Y. Iguchi, B.-Z. Tang, T. Higashimura, Diffusion and solution of gases in substituted polyacetylene membranes, Polymer, 29 (1988) 2041-2049.

T.C. Merkel, H. Lin, X. Wei, R. Baker, Power plant post-combustion carbon dioxide capture: An opportunity for membranes, Journal of Membrane Science, 359 (2010) 126-139.

T.C. Merkel, M. Zhou, R.W. Baker, Carbon dioxide capture with membranes at an IGCC power plant, Journal of Membrane Science, 389 (2012) 441-450.

T.C. Merkel, V. Bondar, K. Nagai, B.D. Freeman, Sorption and transport of hydrocarbon and perfluorocarbon gases in poly(1-trimethylsilyl-1-propyne), Journal of Polymer Science Part B: Polymer Physics, 38 (2000) 273-296.

T.C. Merkel, V. Bondar, K. Nagai, B.D. Freeman, Y.P. Yampolskii, Gas sorption, diffusion, and permeation in poly(2,2-bis(trifluoromethyl)-4,5-difluoro-1,3-dioxole-co-tetrafluoroethylene), Macromolecules, 32 (1999) 8427-8440.

T.C. Merkel, V.I. Bondar, K. Nagai, B.D. Freeman, I. Pinnau, Gas sorption, diffusion, and permeation in poly(dimethylsiloxane), Journal of Polymer Science Part B: Polymer Physics, 38 (2000) 415-434.

T.-S. Chung, A critical review of polybenzimidazoles, Journal of Macromolecular Science, Part C, 37 (1997) 277-301.

T.-S. Chung, C. Cao, R. Wang, Pressure and temperature dependence of the gas-transport properties of dense poly[2,6-toluene-2,2-bis(3,4-dicarboxylphenyl)hexafluoropropane diimide] membranes, Journal of Polymer Science Part B: Polymer Physics, 42 (2004) 354-364.

T.T. Moore, W.J. Koros, Gas sorption in polymers, molecular sieves, and mixed matrix membranes, Journal of Applied Polymer Science, 104 (2007) 4053-4059.

V.I. Bondar, Y. Kamiya, Y.P. Yampol'skii, On pressure dependence of the parameters of the dual-mode sorption model, Journal of Polymer Science Part B: Polymer Physics, 34 (1996) 369-378.

V.M. Shah, B.J. Hardy, S.A. Stern, Solubility of carbon dioxide, methane, and propane in silicone polymers: Effect of polymer side chains, Journal of Polymer Science Part B: Polymer Physics, 24 (1986) 2033-2047.

W.J. Koros, A.H. Chan, D.R. Paul, Sorption and transport of various gases in polycarbonate, Journal of Membrane Science, 2 (1977) 165-190.

W.J. Koros, D.R. Paul, A.A. Rocha, Carbon dioxide sorption and transport in polycarbonate, Journal of Polymer Science: Polymer Physics Edition, 14 (1976) 687-702.

W.J. Koros, D.R. Paul, CO_2 sorption in poly(ethylene terephthalate) above and below the glass transition, Journal of Polymer Science: Polymer Physics Edition, 16 (1978) 1947-1963.

W.J. Koros, D.R. Paul, G.S. Huvard, Energetics of gas sorption in glassy polymers, Polymer, 20 (1979) 956-960.

W.J. Koros, D.R. Paul, Observations concerning the temperature dependence of the langmuir sorption capacity of glassy polymers, Journal of Polymer Science: Polymer Physics Edition, 19 (1981) 1655-1656.

W.J. Koros, G.K. Fleming, Membrane-based gas separation, Journal of Membrane Science, 83 (1993) 1-80.

W.S. Lyoo, J.H. Choi, S.S. Han, W.S. Yoon, M.S. Park, B.C. Ji, J. Cho, Preparation of organo-soluble poly[(2,2′-m-phenylene)-5,5′-bibenzimidazole] with high yield by homogeneous nitration reaction, Journal of Applied Polymer Science, 78 (2000) 438-445.

X. Li, R.P. Singh, K.W. Dudeck, K.A. Berchtold, B.C. Benicewicz, Influence of polybenzimidazole main chain structure on H_2/CO_2 separation at elevated temperatures, Journal of Membrane Science, 461 (2014) 59-68.

Y. Yampolskii, S. Shishatskii, A. Alentiev, K. Loza, Correlations with and prediction of activation energies of gas permeation and diffusion in glassy polymers, Journal of Membrane Science, 148 (1998) 59-69.

Z.P. Smith, D.F. Sanders, C.P. Ribeiro, R. Guo, B.D. Freeman, D.R. Paul, J.E. McGrath, S. Swinnea, Gas sorption and characterization of thermally rearranged polyimides based on 3,3′-dihydroxy-4,4′-diamino-biphenyl (HAB) and 2,2′-bis-(3,4-dicarboxyphenyl) hexafluoropropane dianhydride (6FDA), Journal of Membrane Science, 415-416 (2012) 558-567.

Z.P. Smith, K. Czenkusch, S. Wi, K.L. Gleason, G. Hernández, C.M. Doherty, K. Konstas, T.J. Bastow, C. Álvarez, A.J. Hill, A.E. Lozano, D.R. Paul, B.D. Freeman, Investigation of the chemical and morphological structure of thermally rearranged polymers, Polymer, (2014) 1-9.

Z.P. Smith, R.R. Tiwari, T.M. Murphy, D.F. Sanders, K.L. Gleason, D.R. Paul, B.D. Freeman, Hydrogen sorption in polymers for membrane applications, Polymer, 54 (2013) 3026-3037.

Vita

Kevin Anthony Stevens was born in Beaumont, Texas and raised in Winnie, Texas, where he attended East Chambers High School. He attended Lamar University and graduated with a bachelor's degree in Chemical Engineering in May 2010. He entered the graduate program at the University of Texas at Austin and pursued his graduate degree under Dr. Benny D. Freeman. He earned his Ph.D. in Chemical Engineering in December, 2016.

Permanent email: k.stevens.ut "at" gmail.com

This dissertation was typed by Kevin Stevens.